A Hybrid Prognostic Approach for Battery Health Monitoring and Remaining-Useful-Life Prediction

by

Mohamed Ahwiadi

A thesis

presented to the Lakehead University

in fulfillment of the

thesis requirement for the degree of

Doctor of Philosophy

in

Electrical and Computer Engineering

Lakehead University, Thunder Bay, Ontario, Canada

2020

AUTHOR'S DECLARATION

I hereby declare that I am the sole author of this thesis. This is a true copy of the thesis, including any required final revisions, as accepted by my examiners.

I understand that my thesis may be made electronically available to the public.

Abstract

Lithium-ion (Li-ion) batteries are commonly used in various industrial and domestic applications, such as portable communication devices, medical equipment, and electric vehicles. However, the Li-ion battery performance degrades over time due to the aging phenomenon, which may lead to system performance degradation or even safety issues, especially in vehicle and industrial applications. Reliable battery health monitoring and prognostics systems are extremely useful for improving battery performance, to diagnose the battery's state-of-health (SOH), and to predict its remaining-useful-life (RUL). In general, it is challenging to accurately track the battery's nonlinear degradation features as battery degradation parameters are almost inaccessible to measure using general sensors. In addition, a battery is an electro-chemical system whose properties vary with variations in environmental and operating conditions. Although there are some techniques proposed in the literature for battery SOH estimation and RUL analysis, these techniques have clear limitations in applications, due to reasons such as lack of proper representation of the posterior probability density functions to capture and model the nonlinear dynamic system of Li-ion batteries. In addition, these techniques cannot effectively deal with the time-varying system properties, especially for long-term predictions.

To tackle these problems, a novel hybrid prognostic framework has been developed in this PhD work for battery SOH monitoring and RUL prediction. It integrates two new models: the model-based filtering method and the evolving fuzzy rule-based prediction technique. The strategy is to propose and use more efficient techniques in each module to improve processing, accuracy and reliability. Firstly, a newly enhanced mutated particle filter technique is proposed to enhance the performance of particle filter technique and improve the modeling accuracy of the battery system's degradation process. It consists of three novel aspects: an enhanced mutation approach, a selection scheme, and an outlier detection method. Secondly, an adaptive evolving fuzzy technique is suggested for long-term time series forecasting. It has a novel error-assessment method to control the fuzzy cluster/rule generation process—also, a new optimization technique to enhance incremental learning and improve modeling efficiency. Finally, a new hybrid prognostic framework integrates the merits of both proposed techniques to capture the underlying physics of the battery systems for its SOH estimation, and improve the prognosis of dynamic system for long-term prediction of Li-ion battery RUL. The effectiveness of the proposed techniques is verified through simulation tests using some commonly used-benchmark models and battery databases in this field, such as the one from the National Aeronautics and Space Administration (NASA) Ames Prognostic Center of Excellence. Test results have shown that the proposed hybrid prognostics framework can effectively capture the battery SOH degradation process, and can accurately predict its RUL.

ACKNOWLEDGMENTS

Firstly, I want to take this opportunity to extend a sincere thank you to my advisor, Prof. Wilson Wang, for his continuous support and guidance, and for his invaluable leadership and patience. I am also truly grateful for his financial assistance. Prof. Wang is an invaluable source of knowledge, advice, and encouragement, and I cannot imagine having a greater advisor for my PhD study. You helped and motivated me to overcome many challenges during my PhD journey -- thank you so much.

I also want to extend my profound gratitude to Prof. Abdelhamid Tayebi, Graduate Coordinator, for his assistance and motivation to successfully complete my PhD.

I would also like to acknowledge the members of my committee, Prof. Sriram Narasimhan (external examiner), along with Prof. Salama Ikki and Prof. Rachid Benlamri (internal members), for taking the time to review my work, and for providing insightful comments and constructive suggestions that helped improve the quality of this research. Your feedback was always greatly valued and appreciated.

Finally, a heartfelt thank you to my wife and lovely children Shatha, Salem, Roaa, and Hala, as well as to my brothers and sisters, for their unending love, support and understanding throughout this process. Thank you for believing in me -- this accomplishment would not have been possible without you.

TABLE OF CONTENTS

LIST OF FIGURES

LIST OF TABLES

CHAPTER 1

INTRODUCTION AND LITERATURE REVIEW

1.1 Motivation of the Proposed Research

The Lithium-ion (Li-ion) battery is one of the greatest advances in energy-storage technology, in which the anode chemistry is lithium-based. Compared to other existing rechargeable batteries such as nickel-metal hydride and lead-acid types, the Li-ion battery has advantages such as being lightweight, with high energy density, as well as having a long lifespan and low self-discharge [1,2]. Nowadays, Li-ion batteries have become the core component of many machines, ranging from cell phones and small medical devices, to large aircraft and electric vehicles (EVs). For example, with the increasing awareness about climate change, EVs are now increasingly popular, whose performance is highly dependent on battery functionality and reliability [3,4]. Batteries are expected to provide the necessary power to ensure sufficient energy availability in EV operation. However, regardless of the quality of the Li-ion battery, its overall performance will degrade over time due to its repetitive cycles of discharge and charge, which is known as the aging phenomenon [3,5].

Battery aging is considered to be the main disadvantage of a Li-ion battery that limits its performance. The two major effects of battery aging are capacity decrease and impedance growth, which depend on load conditions and working environment [2,6]. In general, failure will occur when the performance exceeds a threshold at an unsatisfactory level, which could result in system performance degradation, breakdowns, or even serious safety issues in applications such as EVs [3,7-9]. Thus, a reliable technology for Li-ion battery health monitoring and prognostics is urgently needed to improve battery functionality and reliability, to diagnose the battery's state-of-health (SOH), to schedule battery recharging operations, and to accurately predict the remaining-useful-life (RUL) for battery replacement and preventive maintenance.

In recent years, the health assessment and prognostics for machinery have received significant attention in the research community whereby several methods, tools, and practical applications have been proposed [5,9]. However, the electro-chemical behaviours of the Li-ion battery system are different from those of mechanical systems, mainly because the data from a

battery's internal electro-chemical reaction is practically inaccessible using common sensor technologies. Other differences include the fact that the operation profiles of a Li-ion battery are much more dynamic than mechanical systems; its monitoring data collected is value-typed, whereas the machinery data is waveform [2,3,5,10]. Therefore, the uniqueness of a Li-ion battery system should be considered when developing or identifying a battery prognostic method to ensure high reliability for providing power sources and avoiding battery failures.

1.2 Li-ion Battery Aging and Degradation Mechanisms

In general, a Li-ion battery cell consists of four primary components: anode, cathode, electrolyte, and separator: 1) Anode: known as the negative electrode, and commonly constructed from graphite and other carbon materials; 2) Cathode: the active source of all the Li-ions known as the positive electrode, built from lithium metal; 3) Electrolyte: constructed from lithium salts and organic solvents; 4) Separator: a microporous sheet constructed of a polymer material, and contains a safety feature to prevent contact between the cathode and the anode in case the cell accidentally heats up. Its working process can be summarized as shown in Fig. 1.1. The Li-ion moves between the anode and the cathode during the charging and discharging processes, creating electricity flow to be used for electronic applications [6,10-13].

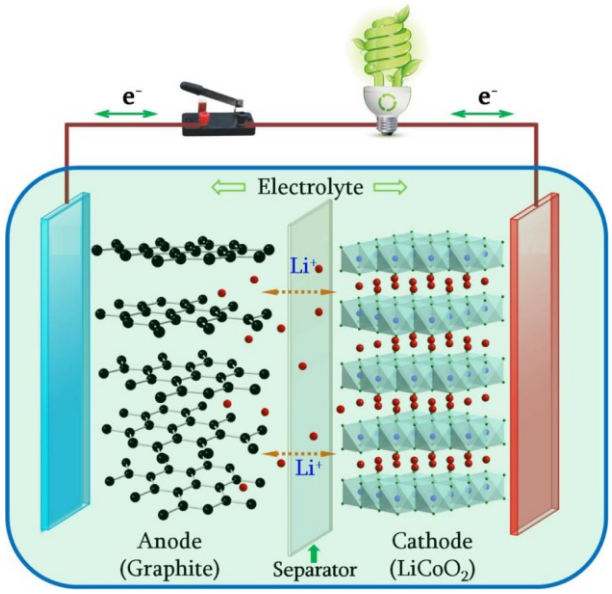

Fig. 1.1 Work mechanism of a Li-ion battery [13].

Overall, the performance of a Li-ion battery relies on material development and other components of its cells, where degradation occurs throughout the battery's entire life in many proportions related to its utilization mode and environmental conditions [6,9,10,14]. However, it is difficult to identify degradation activities because multiple variations are involved in the entire process, whereby a number of factors, such as environment and its operating mode, interact to provoke different aging effects [2]. In general, aging first occurs in the chemical composition of the Li-ion battery electrolyte because cell component degradation is usually caused by a change of the electrolyte chemical composition, or waste of active material such as lithium, graphite, and carbon [6,8,9,11,14]. For example, research in [15] shows that the degradation is tied to the loss of recyclable lithium, a phenomenon manifested via the formation of a solid electrolyte interface that occurs by electrolyte decomposition. In addition, the side reaction of lithium with decomposed electrolytes will heighten the degree of degradation.

As stated in [16], the chemical composition of a battery's electrolyte might also explain the aging process, whereby both negative and positive electrodes vary considerably during degradation. The composition of these electrodes strongly influences the mechanical and chemical aging mechanisms. In addition, throughout the aging period, the degradation of the cell components influences other processes including the variation of the electrolyte chemical composition, alteration of the structural properties, and dissolution of the material in the electrolyte, all of which result in the loss of active materials [16,14]. To identify the extent of battery aging, some indicators/notions have been used in battery management systems to quantify the battery's health state. The most commonly-used indicators in the literature include the state of charge (SOC), state of health (SOH), and remaining-useful-life (RUL), which can be computed based on some extracted battery features [10,16].

1.3 Literature Review of Technical Approaches for Li-ion Battery Health Monitoring and RUL Prediction

General approaches to estimate the SOC and SOH, and to predict the RUL of Li-ion batteries, can be grouped into three main categories: model-based filtering methods, data-driven techniques and hybrid approaches [2,7], whose performance relies upon accurate tracking of the nonlinear degradation feature of a battery's system. The following will describe the related techniques in each category, followed by the research objectives of this work.

1.3.1 Model-based filtering methods:

Model-based filtering methods usually combine mathematical models and filtering techniques to characterize the system's degradation for system state tracking and prediction [2,9]. In general, the Li-ion battery is a nonlinear dynamic system that requires a precise model to represent its electro-chemical characteristics, and to adaptively describe the system's degradation process [1,17]. With respect to battery aging/degradation characteristics, several diagnosis models have been proposed in literature to describe battery performance evolution during its lifetime, and to characterize the degradation trend [10,9,16]. Where a proper filtering/estimation technique can be used to identify the model parameters that represent the hidden state (e.g., damage state, degradation behavior, etc.), the following models are considered to be the commonly used in this field:

a) Equivalent circuit-based models:

These models simulate the battery's running process based on equivalent circuit theory, whose model parameters are estimated using some estimation methods [16,18]. For estimating battery aging/degradation, the model parameters represent the internal battery parameters such as current, voltage and impedance, which can be identified directly from measurements, or by using certain equivalent circuit models [2,10]. However, the main limitation of these models is related to the extraction accuracy of model parameters.

b) Performance-based models:

These models are constructed using the correlation between stress factors and capacity decline/impedance increase, whereby such a correlation can be identified from battery aging tests conducted under different operating conditions. The purpose is to quantify the impact of aging factors and define physical equations to model different aging states over a battery's lifetime, where modeling accuracy depends on testing experience under several conditions [2,16].

c) Electrochemical models:

Electrochemical models can provide physical and chemical information during battery operation based on its performance and conditions (e.g., current, voltage, temperature, electrolyte concentration, and corrosion) [2]. However, they usually require precise knowledge about the battery's physical and chemical properties of the battery, such as electrolyte volume, density and

porosity of the active materials. Even though these models can provide the internal battery behavior parameters that are necessary for monitoring the battery health condition, it is challenging to develop a reliable and precise model considering the fact that several factors that impact performance degradation interact with each other. Thus, these models use only one or two factors in tracking the aging phenomenon in real battery monitoring applications [16,19].

d) Analytical model with empirical fitting:

Such a model is identified based on historical experimental data, and can be used to evaluate or predict the estimator values [10]. In modeling, estimation techniques utilize certain battery measurements to estimate the aging model parameters. The parameter estimation is a process used to adjust a model from observations in order to minimize errors. The well-accepted methods are the Coulomb counting approach, in which the SOH is estimated through the integration of the current over time, and the electrochemical impedance spectroscopy (EIS), in which the SOH is predicted by using battery impedance to characterize its dynamic behavior [16,20].

In general, the reliability of these diagnosis models to analyze the processes of battery aging/degradation mechanism relies on the accuracy of the used estimation methods to identify the model failure parameters using the available battery features [9,21]. For a complex electro-chemical dynamic system of a Li-ion battery, its internal electrochemical process and degradation features are almost inaccessible, and therefore cannot be measure using common sensor technologies. Advanced estimation/filtering techniques such as Kalman filter (KF) and particle filter (PF) are the most estimation techniques in this field, as they can identify the model parameters in the monitoring process and make inferences about hidden states in the dynamic system [21,22]. The KF and PF conduct state estimation based on system model and noisy measurements using the Bayesian inference to estimate the posterior probability density function (PDF).

These filtering methods consist of two steps: prediction and correction. The dynamic state-space models consist of a transition model for system state prediction, and a measurement (sensor) model to associate the predicted states to the noisy measurements [23,24]. The goal is to propagate the posterior PDF of the current state (i.e., initial PDF) to project the future state distribution (i.e., predicted PDF); when the measured data become available, the posterior PDF

will be formed/corrected based on the likelihood of given the incoming data [2,5]. KF can make inferences about hidden states in a dynamic system based on available system models and noisy measurements, which could provide the optimal solution for linear-Gaussian estimation problems [25]. In KF, the dynamic state-space models consist of a transition model for system state prediction, and a measurement (sensor) model that associates the predicted states to the noisy measurements [10]. The aim is to compute the posterior PDF for state estimation by updating finite-dimensional parameters recursively so as to minimize the state error covariance. Although KF has been applied in various applications such as communication, inertial navigation, robotics and control, it cannot model systems properly with nonlinear/non-Gaussian properties [25,26]. This is because KF is derived based on the assumption that transition and measurement models are linear-Gaussian, which makes it unreliable to be used for nonlinear estimation problems [5].

Improved KF techniques have been suggested in several studies to overcome the related non-linear Gaussian problem by linearizing the nonlinear models. For instance, Extended KF (EKF) performs linear approximation of the nonlinear dynamic state-space models using a first-order Taylor series expansion, then applies the standard KF to the resulting linear estimation problem [26]. The aim is to linearize the nonlinear state and/or the measurement models around the current estimate in each time step. The related parameters of the EKF can be adjusted to deal with different application conditions, including the factorization of the covariance matrix, Taylor series order, and process noise tuning. Many research papers have concluded that the EKF can provide more accurate estimation result than KF [3,5], however, EKF cannot deal with highly non-linear systems since the Taylor series expansion has limited adaptation to nonlinearities. Also, this linearization approach approximates the posterior PDF to be Gaussian, which can degrade the estimation accuracy if the true density is non-Gaussian [5,7,9].

The unscented KF (UKF) has been suggested to reduce linearization errors in the EKF; it employs an unscented transform function to improve the posterior PDF representation [26]. The aim is to generate a number of sampling points (Sigma points) around the current state estimate, which then are propagated through the non-linear models to represent the state distribution. Therefore, these sample points would have a higher probability to capture the true mean and covariance of the true posterior PDF, resulting in a better performance than the EKF [25]. However, this improvement comes with an increased computational cost, which could prevent

UKF from being used for real-time monitoring applications [5]. Also, the UKF is only an approximate nonlinear estimator and can diverge when the system or measurement nonlinearities become too high [7,8,25].

In contrast, the PF can model dynamic systems with nonlinear and non-Gaussian characteristics, and has outperformed EKF and UKF in many applications [3,25,35,44]. In general, PF has become a state-of-the-art estimator in prognostics of engineering systems [1,9], including system state tracking [27,28] and prediction applications [7,22,29]. It numerically implements the recursive Bayesian function via the Monte Carlo simulation to perform inferences in the state-space from observations. The posterior PDF is represented by a set of random samples (i.e., particles), and their associated weights are computed by the conditional likelihood of each particle based on the observations at that moment [23,25]. The PF can represent the uncertainty in the estimated state (e.g., RUL prediction result) with its posterior PDF instead of a single value like other prognostic methods (e.g., data-driven techniques); it is also less affected by the level of noise and model complexity [1,5,25,26].

PF-based techniques have been applied to battery RUL prediction and health monitoring in several studies. For example, Saha *et al*. [30], in the Prognostics Center of Excellence of NASA's Ames Center, have investigated the use of PF for system state estimation and RUL prediction in Li-ion batteries. PF is utilized to estimate the coefficients of an exponential growth model for both electrolyte and charge transfer resistances from EIS measurements. According to the relationship between resistance and capacity, capacity is derived for use in RUL prediction. Also, Saha *et al*. [31] have constructed an empirical capacity model by using the coulombic efficiency factor and relaxation effect. PF is applied to estimate the model parameters, where the future capacity value is extrapolated to estimate the RUL. Walker *et al*. [32] have investigated the performance of PF for Li-ion batteries' prognostics in comparison to two estimation methods. Test results show that PF is more accurate than the non-linear least squares and UKF methods for predicting the RUL of Li-ion batteries. Xing *et al*. [33] have proposed a PF-based model to fuse the principles of the polynomial regression and the empirical exponential models to estimate the RUL of Li-ion batteries, whereas PF is used to adjust the model parameters online. Furthermore, Wang *et al*. [34] have proposed a discharge-rate-dependent prognostic model to assess the RUL of a battery at different rates of discharge by using PF to posteriorly estimate the parameter distribution of the model. In other similar work conducted by Dong *et al*. [35], PF is used to

estimate the parameters of the Brownian motion degradation model for Li-ion batteries SOH estimation and RUL prediction.

However, PF has suffered from two long-standing problems: sample degeneracy and impoverishment, which limit its capability to accurately capture the electro-chemical behaviors in system state estimation of battery systems [1,7,10,21,36]. Some PF techniques have been suggested in the literature to improve its performance. For example, Liu *et al*. [37] have proposed a regularized auxiliary PF technique for system state estimation and forecasting, which can be used to predict the RUL of Li-ion batteries. Test results have revealed that the regularized auxiliary PF technique can provide more accurate state estimation and RUL prediction than the standard and auxiliary PFs. In a parallel study, Miao *et al*. [38] have utilized the unscented PF, which is combined the unscented KF and the linear re-sampling algorithm to generate the particles proposal distribution in order to reduce particle diversity deficiency in predicting the RUL of Li-ion batteries; that method could predict the RUL more accurately than using the standard PF. Dong *et al*. [39] have implemented the support vector regression PF to calculate the battery's SOH and RUL; their investigation has concluded that this algorithm could monitor the SOH and predict the RUL more effectively than using the standard PF.

Another type of PF-based prognostic technique is the artificial fish swarm algorithm proposed by Tian *et al*. [40], which could outperform the PF approach in predicting the Li-ion battery's RUL. Peng *et al*. [41] have proposed a support vector regression-unscented PF to predict the RUL of a battery, which could provide more favorable results in comparison to the unscented PF and standard PF methods. Wang *et al*. [42] have introduced a spherical cubature PF to predict the RUL of Li-ion batteries, which has outperformed the standard PF for this purpose. Yu *et al*. have used a quantum particle swarm optimization-based PF in [43] because it requires fewer parameters to control; it performs better in global searching than the particle swarm optimization technique to predict the RUL of a Li-ion battery. Li *et al*. [7] have proposed a mutation approach with a particle selection scheme to deal with PF limitations in estimating system state and predicting the RUL of a Li-ion battery. Test results have revealed that the proposed mutated PF could outperform the standard PF and regularized auxiliary PF technique.

Although these PF techniques claim to outperform the standard PF for system state estimating and for predicting the RUL of Li-ion batteries, they usually suffer from problems related to parameters setting and noise sensitivity [36]. In addition, they require a large number

of particles to represent the posterior space, which could lead to high computational costs, and therefore could not be used for real-time monitoring applications. Furthermore, these PF methods rely on the normalized weights to detect and process low-weight particles (sample degeneracy), which may not be a robust measurement when all particles are located in low probability regions of the posterior space. This could lead to misrepresentation of the high-likelihood area of the estimated posterior PDF, and degradation of the estimation accuracy for several iterations. Aside from these PFs limitations, the model-based filtering methods may be suitable only in short-term prognostics, as the pattern of the battery degradation state remains unchanged or with minimal change. This is because the posterior PDF can not be updated in the absence of future measurements in order to capture the new variation of the battery degradation process, resulting in fixed model parameters during the prediction period. This degrades the prognostic performance of model-based filtering methods and could lead to considerable propagated uncertainty when the prediction horizon becomes longer [17,22,44].

1.3.2 Data-driven approaches:

Data-driven approaches utilize extracted features (e.g., voltage, current and impedance) from the battery performance data (training data) to identify the characteristics of the battery system in order to predict the system degradation behavior for RUL predictions. Learning algorithms are applied in these methods to improve modeling accuracy and minimize training errors [1,45,46]. Data-driven approaches include these statistical methods and soft-computing tools. The most commonly-used statistical methods consist of relevance/support vector machine, Gaussian process regression and least squares regression, while soft-computing tools include neural networks (NN), fuzzy logic and neural fuzzy (NF) techniques [2,3].

a) Statistical methods:

Statistical methods conduct predictions based on a large number of datasets that represent different health states of a battery system [10,47]. Wang *et al.* [48] have applied the relevance vector machine method for battery SOH estimation and RUL prediction using a three-parameter capacity degradation model to fit the predictive values at the cycles of the relevance vectors. In a parallel study, Nuhic *et al*. [49] have used the support vector machine method to estimate the SOH and predict the RUL of Li-ion cells; a specific data processing method is applied to reduce the influence of noise in environmental and load conditions. However, these methods are time-

consuming due to the very high computation load, and the final model could be difficult to interpret for error analysis [50]. To overcome these problems, Liu *et al.* [51] have proposed a least squares support vector machine method for battery capacity prediction based on the charging/discharging rate and temperature. Although it could converge quickly during training to reach a global solution, this method is sensitive to the outliers and noise with non-Gaussian distributions.

Yang *et al.* [52] have used the Gaussian process regression for battery SOH estimation, whereby four parameters are extracted from the charging curves to represent the battery aging. Richardson *et al.* [53] also have utilized Gaussian process regression for forecasting a battery's SOH, whereby kernel functions are used to capture the battery degradation behavior. Compared to relevance/support vector machine methods, although Gaussian process regression has the advantages of probability interpretation and self-adaptive acquisition of hyper-parameters, it has high computational training costs and poor performance in long-term forecasting, as well as a wider confidence interval. In addition, most of the aforementioned methods rely on the assumption that the data is noise-free, or that the noise is Gaussian with a zero mean [54]. Although some statistical methods require less training data, they may also suffer from uncertainty representation. In addition, it may be difficult to obtain sufficient datasets that are proportional to different battery health stages for training the models [5].

b) Soft-computing tools:

Soft-computing tools use battery performance data to recognize the mapping relationship between the battery system characteristics and its health condition so as to fit degradation models to estimate the SOC, SOH and RUL of a battery [2,55]. For example, Yang *et al*. [56] have suggested a three-layer back propagation NN to estimate a Li-ion battery SOH using the data sets generated from a first-order equivalent circuit model for NN training. Eddahech *et al*. [57] have built a recurrent NN to monitor the SOH of a high-power-density Li-ion cell, where the EIS measurements are used to model the Li-ion cell's behavior. In a parallel study, Liu *et al*. [58] have proposed an adaptive recurrent NN for system dynamic state predicting of Li-ion batteries, where its NN weights are adaptively optimized using the recursive Levenberg-Marquardt algorithm. However, a NN has "black box" reasoning, whereby it is difficult to explain the recognized reasoning mechanism. In addition, the NN training phase requires large amounts of

data, which may lead to over-fitting in battery RUL prediction and can become time-consuming [9,59].

Fuzzy logic can deal with uncertainty and nonlinearity through the use of a series of fuzzy IF-THEN rules for reasoning operations [3]. Singh *et al*. [60] have pre-processed the measurements and modeled EIS data of a Li-ion battery to select suitable parameters, which are used as inputs to the fuzzy predictor for battery SOH and SOC. Landi *et al.* [61] have used two exponential functions to identify the index of battery SOH from battery datasets; fuzzy logic technique is then used to estimate the battery health index based on the fitting curve. There are only a few studies involving pure fuzzy logic in this field, as it would be difficult to optimize the fuzzy system parameters, where any change in a membership function requires a change in fuzzy rules, and vice versa. This is because fuzzy logic technique lacks the capability of machine-learning that NNs have, therefore it does not have proper adaptive capability to accommodate varying system dynamic conditions.

To overcome the limitations of both NNs and fuzzy logic and take advantage of their strengths, their synergetic schemes (e.g., NF techniques) have been suggested, which have both adaptive learning mechanism and semantic transparency [10]. In general, the adaptive NF inference system (ANFIS) is well-known for modeling non-linear systems, and has been used in several studies to model battery dynamic characteristics and predict the RUL. For example, Tsai *et al*. [62] have run a new Li-ion battery until it has reached the end of its life in order to collect data from the extracted charge, internal resistance and no-load voltage, which are used for training the ANFIS. The trained ANFIS is then used to estimate the SOC of Li-ion batteries, with less training data require during the training phase. Also, Dai *et al*. have used the ANFIS for online battery SOC estimation in [63]. In parallel studies, ANFIS is used in papers [64-66] for Li-ion battery SOH estimation and RUL prediction. Notwithstanding the above, some advanced research papers reported that a properly-trained NF technique can outperform both the stochastic models and the various NN-based models in forecasting applications [66,67,68].

On the other hand, the NF techniques may not have sufficient adaptive capability to accommodate dynamic systems with significant time-varying properties such as the electro-chemical Li-ion batteries under EV operating conditions [68]. In addition, it would be hard to determine the proper number of IF-THEN rules in an electro-chemical system with many inputs

but a fixed reasoning architecture. The number of rules used for the input-output mapping can negatively affect both performance accuracy by under-fitting and over-fitting; as a result, the computation efficiency will be very low in estimation and optimization of the related consequent and antecedent NF parameters [69]. In general, the reliability of these data-driven techniques depends on the quantity and quality of the historical and empirical training data that should be representative of the battery's operation performance; it will be challenging to obtain accurate and representative battery datasets in most real-life applications [5,45,59,69]. Those techniques also usually suffer from limitations related to training efficiency and parameter-setting in real-time monitoring applications. Furthermore, the recognized models could have limited adaptive capability to adapt to new system states, which could adversely affect performance accuracy [7,17, 69,70]. In addition, data-driven approaches cannot be used to model the hidden states in the dynamic system (e.g., degradation state, damage state, etc.), which are either inaccessible to the sensors or hard to measure using general data acquisition systems. Also, it could not properly express uncertainty associated with its predicted future values, which is a critical aspect in prognostics systems to schedule predictive maintenance operations [1,9,55].

1.3.3 Hybrid approaches:

In general, using a single methodology for the prognostic task (e.g., model-based filtering and data-driven) may not provide the expected level of performance due to the complexities of battery system degradation dynamics, uncertainties associated with the prediction horizon, and the amount of available data [9,22]. The main objective of the hybrid approach is to integrate two or more data-driven and model-based methods to strengthen their respective advantages and overcome their limitations [1,45]. In the field of Li-ion battery prognostics, model-based filtering methods could provide more accurate modeling than data-driven techniques due to their advantages such as: 1) modeling the underlying physics of battery SOH degradation processes, 2) making inferences about hidden states in a dynamic system, and 3) being able to characterize and represent the uncertainty in the estimated results, which is a key element in prognostics systems [1,10].

However, since there are no measurements accessible during the prediction period of the RUL, the model-based filtering method cannot update its degradation-prediction model parameters in order to capture the new characteristics of battery degradation process during that

period, which can essentially degrade prediction accuracy and result in large propagated uncertainty, especially for long-term prediction [71]. To overcome these shortcomings, some hybrid approaches have been suggested in the literature to enhance modeling accuracy during the prognostic process, such as integrating a data-driven method to provide (predict) the degradation measurements to the model-based method during the prediction period. For example, Liu *et al*. [67] have proposed a data-model fusion framework to improve prediction performance. Three data-driven models (i.e., NN, NF, and the recurrent NF) are used to track the system degradation trend from historical data, and to predict the future measurement values. The model-based PF then used those predicted measurements to update the prediction model parameters. Test results demonstrate that the fusion framework can provide more accurate RUL prediction than using a single method (i.e., model-based PF, and the recurrent NF).

In parallel work, Yang *et al*. have proposed a hybrid prognostic method in [44], which combines the data-model PF and relevance vector machine for battery RUL prediction. Test results have shown that it can outperform the data-model PF for battery RUL prediction under different testing conditions. Linxia *et al.* [17] have introduced a hybrid framework for battery RUL prediction; it has integrated the model-based PF with two data-driven methods (i.e., support vector regression and ANFIS), which are trained offline to build a measurement model and to predict the future degradation measurements in order to guide the model-based PF during the prediction process. Test results have shown that the hybrid framework can provide more accurate RUL prediction than using individual methods (i.e., model-based PF, support vector regression, and ANFIS). Another similar framework is suggested by Yuchen *et al.* in [72], which combines the nonlinear degradation-autoregressive model with a regularized PF. The nonlinear degradation-autoregressive model estimates the observations using long-term degradation trends, and the processing results are then used as inputs in the regularized PF for RUL prediction.

Although test results have shown that these proposed frameworks could improve prognostic accuracy in comparison to the results by using individual methods, the previously-discussed limitations of PF and data-driven methods could still affect the reliability of the framework. In general, the reliability of a hybrid prognostic framework depends on the processing accuracy of each unit. For example, the PF might not provide accurate state estimation when the posterior PDF is inaccurately characterized. On the other hand, if the data-

driven predictor generates poor measurement prediction, it will degrade the upcoming prognostic accuracy. Thus, it is extremely important that each model (data-driven approach and model-based filtering) operates efficiently in order to reach the expected goal of a hybrid approach for reliability and robustness.

1.4 Research Objectives

To tackle the related limitations of the aforementioned approaches, a new hybrid prognostic framework will be proposed in this PhD work for Li-ion battery health monitoring and RUL prediction. The approach is to apply more efficient technique(s) in each processing module to improve overall prognostics accuracy. Specific objectives are as follows:

1) A model-based enhanced mutated particle filter (EMPF) technique will be proposed to tackle some of the current PF methods limitations related to sample degeneracy and impoverishment. The innovative aspects include the following:

a) A novel mutation method is proposed to explore the posterior PDF space more efficiently by taking into account the prior knowledge about the high-likelihood areas. The goal is to generate mutated particles from those particles with low weights to represent the high-likelihood area of the posterior PDF more sufficiently.

b) A new selection mechanism is suggested to detect and process low-weight particles in order to improve particles diversity. The new mechanism uses the unnormalizing particle weights to tackle the problem of using the current normalizing weights, especially when all particles are located in low-likelihood areas with negligible weights.

c) An outlier detection method is proposed to monitor the posterior PDF distribution and to identify and process outlier particles. A new measure is suggested to monitor the overall pattern, and to characterize the skew properties of the posterior PDF distribution.

2) An adaptive evolving fuzzy (AEF) technique for long-term time series prediction will be developed to improve forecasting accuracy and to deal with some limitations of soft-computing tools in long-term forecasting such as the fixed reasoning architectures, high number of fuzzy clusters/rules, and limited adaptive capability. The new predictor has the following unique aspects:

a) An error-assessment method is suggested to monitor the trend of cumulative training errors and to control the fuzzy cluster evolving process.

b) An adaptive particle filter (aPF) technique is proposed to optimize the fuzzy clusters in order to enhance incremental learning and improve modeling efficiency.

3) A new prognostic framework will be developed to integrate the merits of the model-based EMPF method and AEF technique (predictor) in order to deal with the lack of battery measurements during the prognostic processing to further improve battery prognostics accuracy. In this framework, the model-based MPF method will characterize the underlying physics of the battery system degradation process for SOH estimation, and the AEF technique will gradually evolve using the available battery degradation information in order to forecast degradation indicator values beyond the available window. The model-based MPF will then carry out RUL prediction, and its posterior PDF can be updated using these predicted indicator values to reduce modeling uncertainty and improve the accuracy of SOH and RUL prediction.

The effectiveness of the proposed techniques will be verified by simulation tests using some commonly used benchmark models and battery databases in this field, such as the one from the National Aeronautics and Space Administration (NASA) Ames Prognostic Center of Excellence.

1.5 Contributions List

[1] M. Ahwiadi and W. Wang, "An Enhanced Mutated Particle Filter Technique for System State Estimation and Battery Life Prediction," IEEE Transaction on Instrumentation and Measurement, vol. 68, no. 3, pp. 923-935, 2019.

[2] M. Ahwiadi and W. Wang, "An Adaptive Particle Filter Technique for System State Estimation and Prognosis," IEEE Transaction on Instrumentation and Measurement, vol. 69, no. 9, pp. 6756-6765, 2020.

[3] M. Ahwiadi and W. Wang, "An Adaptive Evolving Fuzzy Technique for Prognosis of Dynamic Systems," IEEE Transaction on Fuzzy Systems, (under review), 2020.

[4] Received the Graduate Student Research Excellence (GSRE) Award, 2019, Lakehead University.

1.6 Thesis Outline

After the introduction and literature review as described in Chapter 1, the remainder of this thesis is organized as follows:

Chapter 2 introduces the proposed EMPF technique and demonstrates its effectiveness in system state estimation. In this Chapter, a detailed review of the general PF will be provided to highlight the exciting problems, and then the EMPF technique will be proposed to deal with these limitations. Also, the effectiveness of the proposed EMPF technique will be evaluated in this Chapter by simulation tests under different testing conditions, using a common benchmark model in this field for state estimation.

Chapter 3 discusses the model-based EMPF technique and demonstrates its effectiveness for battery SOH estimation and RUL prediction. In this Chapter, the Li-ion battery prognostic data from the NASA Ames Prognostic Center of Excellence will be described. Also, the EMPF technique will be implemented for battery SOH estimation and RUL prediction, using two well-accepted degradation models to describe battery degradation in terms of impedance growth and capacity degradation.

Chapter 4 focuses on the discussion of the proposed AEF technique and demonstrates its effectiveness in long-term forecasting. An overview of the evolving fuzzy system will be provided in this Chapter to highlight its advantages compared to the classical data-driven techniques, also its shortcomings in long-term forecasting operations of nonlinear systems. The AEF technique will be proposed to control the fuzzy cluster/rule generation and to enhance incremental learning for improving modeling efficiency for long-term time series forecasting.

Chapter 5 includes the proposed hybrid prognosis framework for Li-ion battery SOH monitoring and RUL prediction, and demonstrates its effectiveness.

Chapter 6 summarizes the conclusion remarks and suggestions for future research.

CHAPTER 2

ENHANCED MUTATED PARTICLE FILTER TECHNIQUE

2.1 Overview

Battery state estimation and RUL prediction are the key issues in battery health monitoring and management systems. Among the various types of estimation methods, PF technique can be used to model dynamic systems with nonlinear and non-Gaussian properties. In general, PF is a Bayesian estimation method based on the Monte Carlo simulation, which can be applied to make inferences about hidden states in a dynamic system, and to identify the model parameters in the prognostic process [73,74]. PF has been employed for battery health monitoring and RUL prediction in several studies due to its ability to model the nonlinear degradation feature of battery aging mechanisms; It also can represents uncertainty in the estimated state (e.g., RUL prediction result) in the form of PDF, and is less affected by the level of noise and model complexity [1,5,25,27].

However, PF has some limitations in real-world applications, such as sample degeneracy and impoverishment, which are considered as long-standing challenges in this R&D field [7,21,36,74]. Although several techniques have been proposed in literature to tackle these two problems, they also have limitations; for example, they cannot effectively represent the entire posterior PDF, and are usually unable to deal effectively with sample degeneracy and impoverishment. In this Chapter, an enhanced mutated particle filter (EMPF) technique will be proposed to improve the performance of PFs. Firstly, a novel enhanced mutation approach is proposed in the EMPF technique to actively explore the posterior PDF to locate the high-likelihood area. Secondly, a new selection scheme is suggested to process low-weight particles for optimizing the posterior distribution and tackling sample degeneracy. Thirdly, an outlier assessment method is adopted to monitor the overall pattern of the posterior distribution based on interquartile range statistical analysis in order to detect and block outlier particle(s) from participating in the state estimation.

To facilitate illustration of the proposed EMPF, a review of a general PF will first be provided using a sequential importance sampling PF algorithm, which is the main approach in PFs.

2.2 Particle Filter Algorithm

As stated in Subsection 1.3.1, PF numerically implements the recursive Bayesian function via the Monte Carlo simulation to perform inference in the state space [23,25]. It conducts state estimation based on state transition and measurement (observation) models. The system state model in Eq. (2.1) defines the evolution of the system state with time, which is modeled as a Markov process. The measurement or observation model in Eq. (2.2) correlates the noisy measurements to the hidden state [24]:

$$x_k = f_k(x_{k-1}, u_k) \tag{2.1}$$

$$y_k = h_k(x_k, v_k) \tag{2.2}$$

where x_k is the hidden state to be estimated; y_k is the measurement at k^{th} time instant; u_k and v_k are Gaussian white noise signals with zero mean, which denote the process and measurement noise, respectively.

The Markov process in the system state model is with the initial distribution $p(\chi_0)$, and the transition equation $p(x_k \mid x_{k-1})$. The posterior PDF $p(\chi_k|y_{1:k})$ is represented by a set of N random samples (particles) $\{\chi_k^i\}_{i=1}^N$ and their associated weights $\{\pi_k^i\}_{i=1}^N$ computed by the conditional likelihood of each particle, given the observation y_k at that time moment. The posterior density at the k^{th} time instant can be approximated as [26]:

$$p(\chi_k|y_{1:k}) \approx \sum_{i=1}^{N} \pi_k^i \delta(\chi_k - \chi_k^i) \tag{2.3}$$

where $\delta(\cdot)$ is the Dirac function [26], and $y_{1:k} = \{y_1, y_2, ..., y_k\}$ is the sequence of noisy measurements. The weight π_k^i can be recursively updated using methods such as the principle importance sampling with important density [75]. The particle set is drawn from the prior PDF, which is usually selected as the proposal distribution:

$$q(x_k^i \mid x_{k-1}^i, y_{1:k}) = p(x_k^i \mid x_{k-1}^i) \tag{2.4}$$

where $q(x_k^i \mid x_{k-1}^i, y_k)$ is the importance density to generate the particles.

When a new measurement becomes available, the particle weights are updated according to the importance of corresponding particles. With the calculated likelihood $p\left(y_k \middle| \chi_k^i\right)$, the weight will be more significant as the error between the prediction value and the observation becomes smaller [25,26]. The particle importance weight can be recursively updated by:

$$\pi_k^i \propto \pi_{k-1}^i \frac{p(y_k \mid x_k^i) p(x_k^i \mid x_{k-1}^i)}{q(x_k^i \mid x_{k-1}^i, y_k)} \tag{2.5}$$

The weights π_k^i of these N particles can be normalized such that:

$$\tilde{\pi}_k^i = \frac{\pi_k^i}{\Sigma_{j=1}^N \pi_k^j} \tag{2.6}$$

In general, the PF algorithm has two phases: 1) the prediction phase: the particles are randomly generated/propagated from the information obtained in the previous step (i.e., prior PDF); and 2) the update or correction phase: when a new measurement becomes available, each estimated particle from the prediction phase is then compared to the measurement using the state model and the measurement model of the system. The weight is updated according to the importance of the related measurement, or the weight will become more significant if the error between the prediction value and the observation becomes smaller. However, after a number of iterations in particle propagation, the weight will concentrate on only a few particles, and other particles will have negligible weight, resulting in the problem of sample degeneracy [25,36].

2.2.1 Sample degeneracy:

The common problem with the sequential importance sampling PF algorithm is degeneracy; after some iterations, the variance of the importance weight gradually becomes skewed. In other words, weight concentrates on only a few particles, and the remaining particles will have negligible weights. Due to the degeneracy issue, these few particles with high weights cannot usually capture the entire posterior PDF, resulting in a poor approximation of the target posterior distribution. Moreover, significant computational effort is required to update these particles with negligible weights, whose contribution to the target distribution is almost zero [26,36].

To address sample degeneracy, Gordon *et al*. introduced a sampling importance resampling PF (SIR-PF) algorithm in [26], in which resampling is performed at each iteration to reduce sample degeneracy. Resampling is a process to replicate these high weight particles to replace those having low weights at every iteration in order to force the particles to shift to areas of high-likelihood. This, however, may cause another problem, namely sample impoverishment.

2.2.2 Sample impoverishment

Due to the resampling process, particles with high weights could be selected multiple times, which leads to degraded diversity among the particles on the resulting distribution. Fig. 2.1 illustrates the relationship between sample degeneracy and impoverishment, in which the circle's size represents the weight of the particles. The sample degeneracy problem is illustrated in the top row, where weight concentrates on a few particles (green circles). After resampling, only those particles with high weights are sampled, and the low-weighted particles (red circles) are abandoned (as illustrated in the bottom row), resulting in sample impoverishment as particles are over-concentrated in few points [26,36].

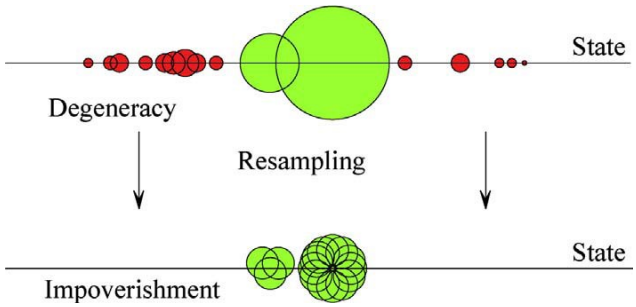

Fig. 2.1. Illustration of the relationship between sample degeneracy and impoverishment [36].

Several techniques have been proposed in literature to tackle these two challenges: the sample degeneracy and impoverishment. For example, an auxiliary PF method is suggested in [24] to characterize transition density using statistical indicators to guide resampling and improve the particles' diversity. An unscented PF method is proposed in [76] to integrate the unscented KF into the Markov chain, Monte Carlo stage, in the PF process to improve the proposal distribution and increase estimation accuracy. However, particle diversity in these methods may deteriorate due to even minimal process noise, as the resampled particles are generated based on a discrete distribution rather than on a continuous one. To improve particle

diversity, some techniques have been proposed in the literature, such as the regularized PF (RPF) [77], regularized auxiliary PF [37], and mixture regulated rao-blackwellized PF [78], to smooth the posterior PDF density and conduct resampling based on continuous distribution. However, if the posterior PDF cannot precisely represent the high-likelihood region, continuous distribution may not be reliable.

Intelligent PFs employ soft-computing tools such as artificial intelligence (e.g., swarm optimization, genetic algorithm and clustering), which have been suggested to locate the high-likelihood area and optimize the distribution of particles [36,40,43]. However, these PF techniques usually suffer from problems related to parameter-setting and noise level, as well as from gaps that may occur in the high-likelihood regions of the estimated posterior PDF [36]. For example, an intelligent PF in [79] is divided the prior particles into large-weight and small-weight particles. Crossover and mutation operations are then performed on the small-weight particles to improve particle diversity. A mutated PF in [7] has conducted a mutation operation to the prior particles to improve the posterior PDF space representation. However, these crossover and mutation operations blindly generated the new particles without providing necessary feedback information about the high-likelihood area to guide the generating process [10]. In addition, these methods relied on the normalized weights to identify and process the low-weight particles, which may not have reflected the real importance to the actual state when all particles fell into the low probability regions. As a result, gaps may have been generated in the high-likelihood area of the estimated posterior PDF, which can degrade estimation accuracy in both the current and subsequent iterations.

To tackle these aforementioned problems, an enhanced mutated PF (EMPF) technique will be proposed in this Chapter to improve the estimation accuracy of PFs. It works to represent the high-likelihood area more efficiently, and enhance the diversity in sampling particles. This is to capture the battery's dynamic characteristics and model its degradation process. The proposed EMPF technique has the following contributions:

1) A novel mutation approach is proposed to explore the posterior PDF space more efficiently by continuously taking into account the prior knowledge about the high-likelihood area.

2) A new selection mechanism is suggested to detect and process low-weight particles in order to locate the high-likelihood area of the posterior PDF and improve particle diversity.

3) An outlier detection method is adopted to monitor posterior distribution to identify and process outlier particles.

2.3. Proposed EMPF Technique

The proposed EMPF technique consists of three innovative steps: a novel mutation mechanism, a selection scheme, and an outlier detection method to combat sample the degeneracy and impoverishment phenomena, which will be discussed in the following subsections.

2.3.1 The enhanced mutation method:

The proposed enhanced mutation method generates mutated particles from prior particles to represent the high-likelihood region more efficiently. The goal is to provide prior knowledge about the best particle location, where the best fitness has been achieved so far. Such feedback information can be used to accelerate the processing time by narrowing down the search region for high probability mass particles, and focusing on areas of high likelihood to generate the mutated particles. For each prior particle in the particle set $\{ \chi_k^1, \chi_k^2, ..., \chi_k^N \}$, the set of mutated particles $\{ \tilde{\chi}_k^1, \tilde{\chi}_k^2, ..., \tilde{\chi}_k^N \}$ are generated using the following steps:

1) Compute the respective upper boundary $U(\tilde{\chi}_k^i)$ and lower boundary $L(\tilde{\chi}_k^i)$:

$$U(\tilde{\chi}_k^i) = \begin{cases} \chi_k^i + \lambda_k, & if\ \chi_k^i \geq \chi_{best} \\ \chi_{best} + \lambda_k, & otherwise \end{cases} \tag{2.7}$$

$$L(\tilde{\chi}_k^i) = \begin{cases} \chi_{best} - \lambda_k, & if\ \chi_k^i \geq \chi_{best} \\ \chi_k^i - \lambda_k, & otherwise \end{cases}, \tag{2.8}$$

where λ_k is a standard deviation of the data, which specifies the extended search area around the original particle; x_{best} is the best fitness particle so far with the highest weight w_{best}; i= {1, 2, …, N} is the index of N particles at the k^{th} time step.

2) Determine the auxiliary position of the original particle using a mutation mechanism [7,80] to generate random numbers over the feasible range with an approximately uniform distribution:

$$q = \frac{U - \chi_k^i}{\chi_k^i - L} \tag{2.9}$$

$$\gamma = \begin{cases} q - q\left(1 - \dfrac{r}{q}\right)^b, & q \geq r \\ q + (1-q)\left(1 + \dfrac{r-q}{1-q}\right)^b, & otherwise \end{cases} \tag{2.10}$$

$$\varphi_k^i = (1-\gamma)L + \gamma U, \tag{2.11}$$

where φ_k^i is the auxiliary position around χ_k^i, and $r \in [0, 1]$ is a random number; $b \in [0.5, 1]$ is the strength factor to describe the variance of the location of mutated particles around the target location; the higher the factor *b*, the broader the area in which the driven particles may appear.

3) Derive the mutated particle from the neighborhood area of the original particle χ_k^i or the highest weight particle:

$$\tilde{\chi}_k^i = U + L - \chi_k^i - \eta(\phi_k^i - \chi_k^i), \tag{2.12}$$

where $\eta \in [0, 1]$ is a random number.

4) Compute the weights w_k^i of the driven particle $\tilde{\chi}_k^i$. If $w_k^i < \xi$, a new particle $\tilde{\chi}_k^i$ will be generated using steps 2) and 3) until $w_k^i \geq \xi$, where ξ is the weight threshold (to be discussed later). In addition, if $w_k^i > w_{best}$, update both χ_{best} and w_{best}, set $\chi_{best} := \tilde{\chi}_k^i$, $w_{best} := w_k^i$.

As an illustration, if the respective lower and upper boundaries are set to be 0 and 1, Eq. (2.9) to (2.11) can be used to randomly generate 10^5 auxiliary particles for a fixed prior particle $\chi_k^i = 0.3$. The distribution of the generated auxiliary particles will have an approximately uniform distribution, as illustrated in Fig. 2.2. The calculated auxiliary position information can then be used to explore the boundary areas in order to find the optimal location to derive the mutated particle.

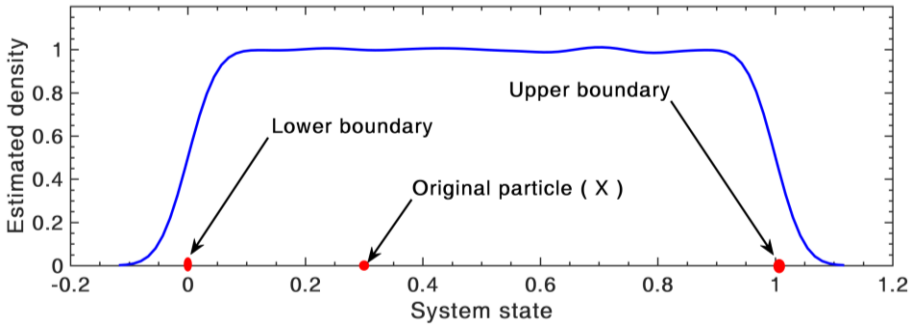

Fig. 2.2. Approximately uniform distribution of the auxiliary particles.

In general, the resulting mutated particles $\{\tilde{\chi}_k^1,\ \tilde{\chi}_k^2,\ ...,\ \tilde{\chi}_k^N\}$ with associated weights $\{w_k^1,\ w_k^2, ...,\ w_k^N\}$ are located in the high probability area, which can result in better system state estimation. Fig. 2.3(a) outlines a typical posterior PDF distribution with the sample degeneracy problem. The weight concentrates only on a few particles, as most particles have very low weights (red crosses). As illustrated in Fig. 2.3(b), the proposed enhanced mutation method can generate high-weight posterior particles from those prior particles with very low weights.

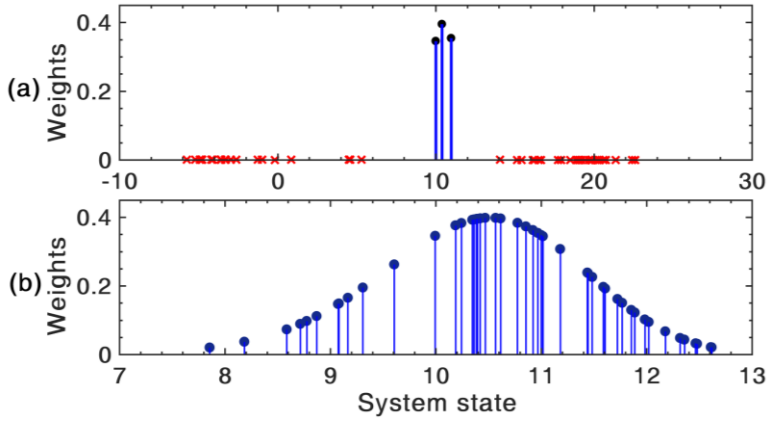

Fig. 2.3. Posterior PDF distribution of system states: (a) without using the enhanced mutation; (b) using the enhanced mutation (red crosses represent particles with low weight factors).

2.3.2. Selection scheme:

It is noticed that the normalized weights cannot effectively reflect the real important weights, especially when all particles are located in the low-likelihood region with negligible weights; normalization is only to render the particles comparable in terms of their values. Furthermore, to carry out weight normalization, all particles must first be generated, and then

normalized, which cannot provide efficient guidance to the mutation process. Fig. 2.4(a) shows a case where all particles on posterior distribution have near-zero weights, as they are located in the low-likelihood area. Nevertheless, some particles still have high weights after normalization, as illustrated in Fig. 2.4(b). Consequently, it may not be appropriate to use the normalized weights as a threshold to determine if the particles are located in the high-likelihood area. As a result, if those particles are selected in the resampling process, gaps will be generated in the high-likelihood region of the approximated posterior PDF, as illustrated in Fig. 2.5; this will degrade the estimation accuracy in both the current and subsequent iterations, as represented by black arrows.

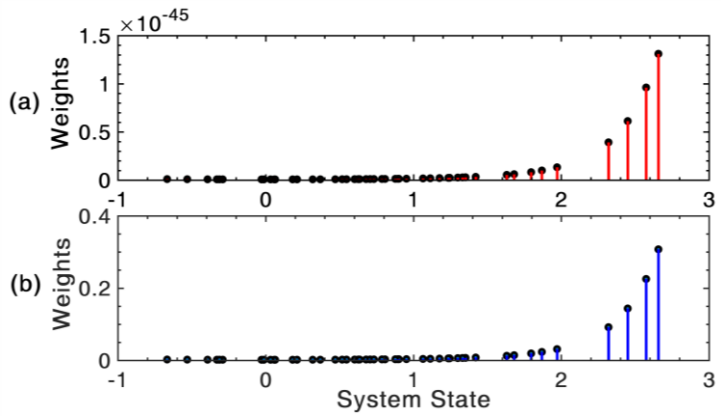

Fig. 2.4. Posterior distribution of a system state: (a) when it is located in the low-likelihood area with very low weights; (b) effects after normalization.

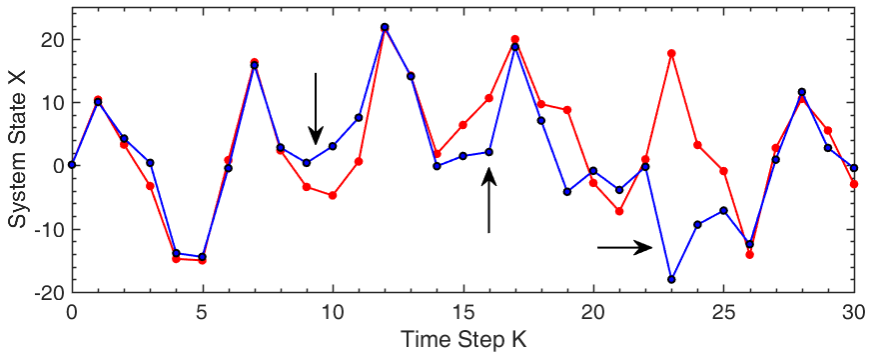

Fig. 2.5. Misleading of the normalized weights (red line: actual states; blue lines: estimated states by the SIR-PF).

In general, the particle degeneracy can be estimated by using an indicator of effective sample size (ESS), which can determine the number of efficiency particles (i.e., having high weights) on the posterior PDF [81, 82]:

$$ESS = \frac{\left(\sum_{i=1}^{N} w_k^i\right)^2}{\sum_{i=1}^{N} (w_k^i)^2} \tag{2.13}$$

where w_k^i denotes the particles' importance weights before normalization; the upper bound of *ESS* is *N*, which is attained when all weights are equal or higher to 1/*N*.

The proposed selection method aims to make the *ESS* achieve and maintain the maximum upper bound. The threshold $\xi = 1/N$ is selected based on the upper bound condition of the *ESS* to assess the contribution of the generated mutated particles to system state estimation. To enhance the posterior PDF representation, the contribution of different particles is characterized by the importance weight, recursively. The new mutated particle is accepted if the weight is $w_k^i \geq \xi$. Otherwise, those particles with $w_k^i < \xi$ will be regenerated over the high-likelihood area using the dynamic feedback mechanism. In addition, the proposed selection scheme ξ can be adaptively adjusted according to the used particle number *N*. This can provide a more accurate representation of the posterior PDF, even with few particles, as the ζ value increases when *N* becomes smaller, and vice versa, to ensure a better representation of the high-likelihood area.

Fig. 2.6(a) demonstrates an example when the posterior distribution is located in the low-likelihood area with very low weights. After using the proposed mutation and selection method, the prior particles with low weights can be replaced by their mutated counterparts in the high-likelihood area, as shown in Fig. 2.6(b).

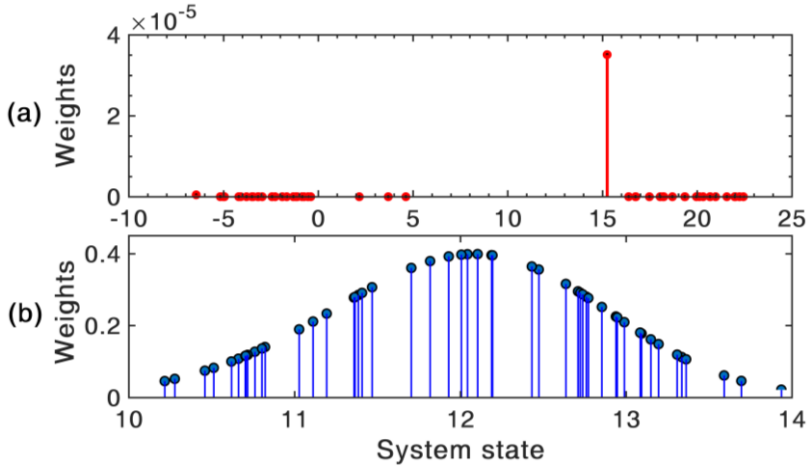

Fig. 2.6. Posterior distribution of a system state: (a) when it is located on the low-likelihood area with very low weight; (b) results after using the proposed mutation and selection method.

To further improve the particle diversity, the samples can be drawn from the following continuous approximation of the posterior density [37,77,83]:

$$p(\tilde{\chi}_k \mid y_{1:k}) \approx \sum_{i=1}^{N} w_k^i \, K_l\left(\chi_k - \tilde{\chi}_k^i\right), \tag{2.14}$$

where $K_l(\cdot)$ is the rescaled kernel function given by:

$$K_l(\chi) = l^{-n} K(\chi / l), \tag{2.15}$$

where $l > 0$ is the scalar kernel bandwidth, and n is the state vector with χ dimension.

The kernel $K_l(\cdot)$ and bandwidth l are chosen to minimize the mean square error between the actual posterior density and the corresponding regularized empirical representation in Eq. (2.14). If all the sample particles have the same weights, the optimal kernel would be the Epanechnikov kernel:

$$K^* = \begin{cases} \dfrac{n+2}{2c_n}\left(1 - \| \chi \|^2\right), & if \; \| \chi \| < 1 \\ 0, & otherwise \end{cases}, \tag{2.16}$$

where c_n is the volume of the n-dimensional unit hypersphere given by:

$$c_n = \begin{cases} 2, & n = 1 \\ \pi, & n = 2 \\ \vdots & \\ 2\pi c_n - 2/n, & n = n \end{cases} \tag{2.17}$$

In general, if the underlying density is Gaussian with a unit covariance matrix [77,83,84], the optimal bandwidth l^* can be determined by:

$$l^* = \left[8c_n^{-1} (n+4) \left(2\sqrt{\pi}\right)^n \right]^{1/(n+4)} N^{1/(n+4)}, \tag{2.18}$$

where N is the number of particles.

As usual, it is assumed that the density is a Gaussian function, whose covariance matrix can be replaced by the empirical covariance matrix [7], such that:

$$MM^T = D, \tag{2.19}$$

where M is the square root matrix of D, the kernel function in Eq. (2.15) will be:

$$K_l(\chi) = (\det M)^{-1} l^{-n} K\left(M^{-1} \chi / l \right), \tag{2.20}$$

where det (M) denotes the determinant of matrix M.

Fig. 2.7 demonstrates the improvement in terms of particle diversity if the samples are drawn from a continuous distribution. It can be seen that the high-likelihood area of the posterior PDF is fully represented.

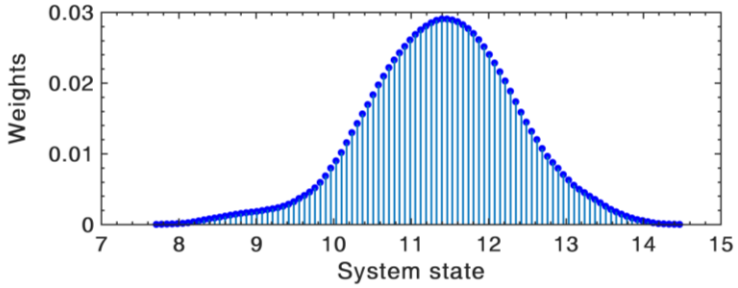

Fig. 2.7. The high-likelihood area of the posterior PDF is represented by sampling from continuous distribution.

2.3.3. Outlier detection for high weight particles:

An outlier can be defined as an observation that numerically deviates from the rest of the data. In general, outliers can occur due to measurement error or noise, or as a result of random variation. Detecting the presence of outliers is important because they could lead to model misspecification and adversely affect the accuracy of parameter estimation and state prediction [85,86].

As previously stated, PF uses a transition model and a measurement (sensor) model to formulate the dynamic state-space model, where the goal is to estimate the conditional PDF of x_k based on measurement y_k; the conditional PDF can be denoted as $p(\chi_k \mid y_k)$.

However, when there is a square operation for the state parameter in the observation model, the PDF of any particle will be the same, no matter if the particle value is positive or negative. Thus, some particles may have high probability even though they are located far from the actual value. This problem occurs when the process or measurement noise exceeds a certain threshold, causing extreme values of the random variables inherent in the distribution. As a result, some outlier particles will appear on the posterior PDF distribution, whose high weights can induce large state estimate errors or even divergence of the filtering operation.

To demonstrate this problem, consider an observation model of a system with square operation state parameters as in Eq. (2.21):

$$y_k = \frac{1}{20}\chi_k^2 + v_k \tag{2.21}$$

Given y_k, the conditional probability of any particle on the set $\{\chi_k^1, \chi_k^2, ..., \chi_k^N\}$ will be the same, whether the particle value is positive or negative. Fig. 2.8 illustrates an example of an outlier located at approximately -10, while the majority of posterior particles with high PDF values are located around +10. The outlier could be caused by noise or random variations that cannot be anticipated. When applying the Bayesian estimator to approximate $P(\chi_k \mid y_k)$, the likelihood of this particle could be misinterpreted as one with a high weight.

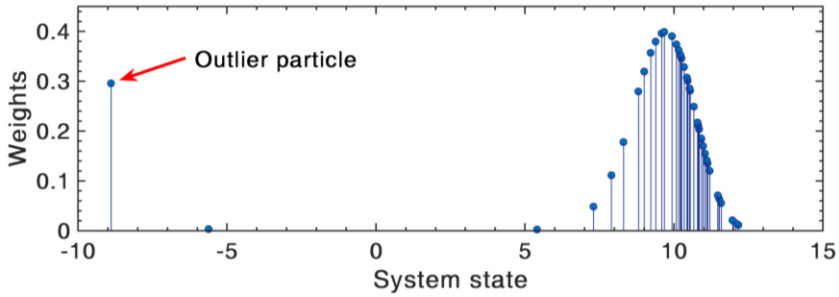

Fig. 2.8. Outlier particle with a high weight.

Directly removing outlier particles may lead to problems such as loose particles diversity on the distribution (i.e., sample degeneracy). The proposed outlier detection method uses a confidence measure to identify outliers based on underlying distribution properties. An outlier with a high weight will modulate statistical distribution properties (e.g., skewed or asymmetrical). An interquartile range (IQR) measure is adopted to characterize the skew properties of the PDF. The IQR does not rely on the standard deviation or mean of the data, which makes no distributional assumptions [86,87].

The IQR can identify an outlier by detecting unusually high or low data points in the distribution. As illustrated in Fig. 2.9, it measures the variables by dividing a rank-ordered dataset into four equal quartiles. The first quartile Q_1 represents the middle value in the first half of the rank-ordered dataset. Q_2 and Q_3 denote the median dataset and the middle value in the second half, respectively. The IQR is computed by:

$$IQR = Q_3 - Q_1 \tag{2.22}$$

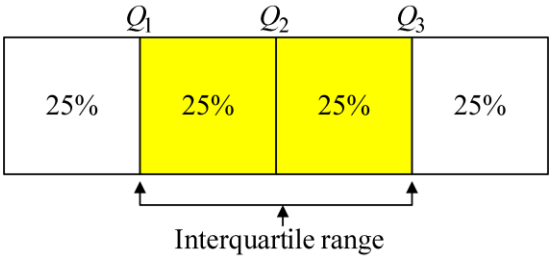

Fig. 2.9. Interquartile range (IQR).

Fig. 2.10 illustrates the measure of an outlier. With respect to the window [Q_1-1.5×(IQR), Q_3+1.5×(IQR)], if a data point falls outside this window, it will be treated as an outlier.

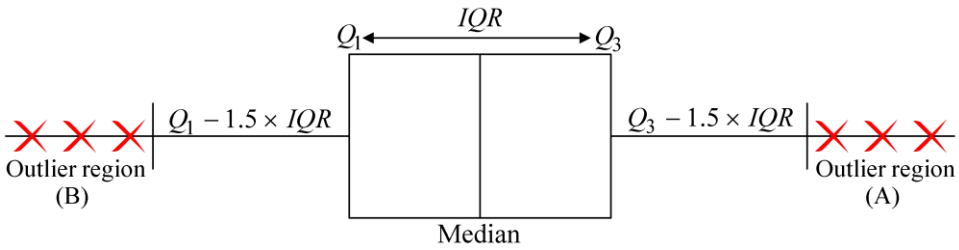

Fig. 2.10. IQR fence edges (regions A and B denote the positive and negative outliers).

The objective of the proposed outlier detection method is to monitor the overall properties of the posterior distribution using the IQR. A particle will be defined as an outlier if it falls either in region *A* (when the mean value of the distribution is negative) or in region *B* (when the mean is positive). Outlier particle(s) is blocked from participating in the current state estimation, without deleting or changing the posterior distribution. Moreover, to accelerate the outlier detection, this algorithm is applied only when the posterior distribution spreads over the positive and negative sides (e.g., ≥75%). The mean value of the majority particles on the posterior distribution should be far from zero, depending on the applications, for example,

$$Outlier = \begin{cases} \chi_k^i < Q_1 - 1.5 \times IQR, & if\ p_m > +\delta_T \\ \chi_k^i > Q_3 + 1.5 \times IQR, & if\ p_m < -\delta_T \end{cases} \tag{2.23}$$

where p_m is the mean of the posterior distribution, and δ_T is the threshold distance from zero.

2.4 Performance Evaluation

The effectiveness of the proposed EMPF technique is evaluated in this section by simulation tests using a commonly used benchmark model for state estimation that has been applied in numerous studies, such as in [7,25-26,37,75,79]. In addition, the related PF techniques for battery RUL prognostic and health monitoring will also be used for comparison, including sampling importance resampling PF (i.e., SIR-PF), regularized PF (i.e., RPF), and mutated PF

(i.e., MPF) techniques. The comparison is in terms of combating sample degeneracy and impoverishment so as to improve system state estimation accuracy.

2.4.1. Performance evaluation of the proposed EMPF technique:

The proposed EMPF technique is examined using a common benchmark model in this field, which has bimodal and highly nonlinear characteristics [25]. The respective state and the measurement equations are:

$$x_k = \frac{1}{2} x_{k-1} + \frac{25 x_{k-1}}{1 + x_{k-1}^2} + 8\cos[1.2(k-1)] + u_k, \tag{2.24}$$

$$y_k = \frac{1}{20} x_k^2 + v_k, \tag{2.25}$$

where u_k and v_k are Gaussian white noise signals with zero means.

The following conditions are used in this testing: the time steps $k = 50$, the variance of the measurement noise $v_k = 1$, the variance of the process noise $u_k = 1$, and the initial state $x_0 = 0.1$ similar to that in [7]. In the proposed EMPF, λ is selected as the standard deviation of the data; the threshold is $\xi = 1/N$, where N is the particle number; the strength factor b is determined by trial-and-error ($b = 0.8$ in this case). To examine the robustness of these four PFs to parameter vairation, four different particle numbers of 25, 50, 100, and 150 are used for simulation tests using Matlab R2017a.

a) Performance evaluation for system state estimation

To evaluate estimation accuracy, the root-mean-squares error (RMSE) between the actual states and the estimated states are calculated over 30 runs. The simulation results are presented in Table 2.1. In general, the more the particles are used, the higher the estimation accuracy of the PFs will become, but the longer time they will take in modeling. Testing has revealed that the average mean of RMSE becomes smaller as the number of particles increases in all four PFs. However, the proposed EMPF performs more accurately (i.e., with the lowest average mean and standard deviation of RMSE) compared to other related PFs. For example, when the particle number is 25, the proposed EMPF is almost 23%, 14%, and 11% more accurate than SIR-PF, RPF, and MPF techniques, respectively, with almost 50% less standard deviation than other PFs. This is because the proposed enhanced mutation method can effectively explore the system state

space, and properly represent the high probability region of the posterior PDF, even with a limited number of particles. In addition, the small averaged standard deviation of the proposed EMPF demonstrates its robustness to maintain a reliable performance over the 30 runs under all testing conditions. This is a result of the selection scheme that can adaptively adjust threshold ξ with the change of particle numbers in order to effectively monitor the particle weights on the posterior PDF, to recognize a low-weight particle, and to process it into a higher-likelihood area.

Table 2.1: Averaged mean and standard deviation of RMSE with different particle numbers

Particle Numbers	**Averaged mean of RMSE**				**Averaged standard deviation of RMSE**			
	SIR-PF	RPF	MPF	EMPF	SIR-PF	RPF	MPF	EMPF
25	4.876	4.364	4.156	3.768	1.488	1.029	1.017	0.681
50	4.613	3.810	3.539	3.346	1.356	0.687	0.589	0.476
100	3.867	3.209	3.107	3.051	0.897	0.672	0.615	0.503
150	3.608	3.336	3.248	2.948	0.729	0.542	0.514	0.477

Table 2.2 summarizes the simulation results of the proposed EMPF with different values of strength factor b when the process noise $u_k = 1$ and the particle number $N = 50$. It is seen that the proposed EMPF has delivered the best performance when $b = 0.8$, in this case.

Table 2.2: Averaged mean and standard deviation of RMSE with a different strength factor

Strength factor *b*	**Averaged mean of RMSE**	**Averaged standard deviation of RMSE**
0.7	3.446	0.505
0.8	3.346	0.476
0.9	3.348	0.589

Fig. 2.11 outlines the test results over 30 random runs using the same observation data generated from the benchmark model with $N = 50$ particles, as the multinomial resampling is implemented at each time step. It can be seen that the proposed EMPF can provide more accurate estimation (i.e., with less variance of the estimation errors) than the other three related PF methods due to its capability to represent the high-likelihood area more effectively. The proposed selection scheme can increase the ESS in the posterior PDF and enrich the particle species.

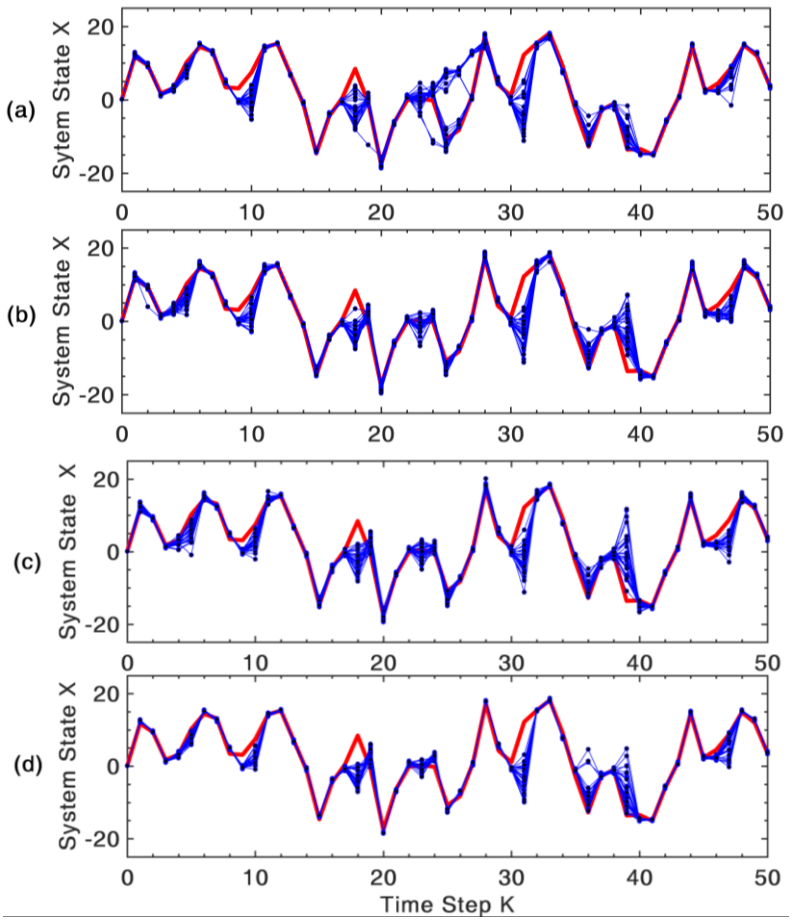

Fig. 2.11. Performance comparison of the related PF techniques over 30 runs by (a) SIR-PF; (b) RPF; (c) MPF; and (d) EMPF (red solid lines: the actual states; blue dotted lines: the estimated states).

b) Performance evaluation in terms of process noise

To further examine the effectiveness of the proposed EMPF, four more test scenarios are undertaken corresponding to different variances of process noise u_k = 1, 5, 10 and 15. In each scenario, 30 datasets are randomly generated using Eq. (2.24) and (2.25). For each dataset, the related PFs are tested over 100 times. The related mean and standard deviation of the RMSE are summarized in Table 2.3. As seen in Fig. 2.12, the RMSE has increased as the process noise is increased. However, the proposed EMPF can adapt itself to these changes and outperforms the other three PFs with the lowest averaged standard deviations; this is due mainly to its enhanced mutation mechanism, and the fact that the selection scheme can explore the distribution more effectively. Moreover, the proposed outlier detection method can monitor the posterior distribution and block outlier particle(s) from participating in state estimation.

Table 2.3: Averaged mean and standard deviation of RMSE with different variance of process noise over 30 datasets tested over 100 times

Noise value	Averaged mean of RMSE				Averaged standard deviation of RMSE			
	SIR-PF	RPF	MPF	EMPF	SIR-PF	RPF	MPF	EMPF
1	4.039	3.652	3.595	3.385	0.962	0.542	0.577	0.520
5	4.727	4.620	4.595	4.362	1.081	0.8253	0.816	0.6162
10	5.836	5.614	5.449	5.114	1.333	1.094	1.068	0.7844
15	6.127	6.062	6.057	5.774	1.385	1.185	1.094	0.897

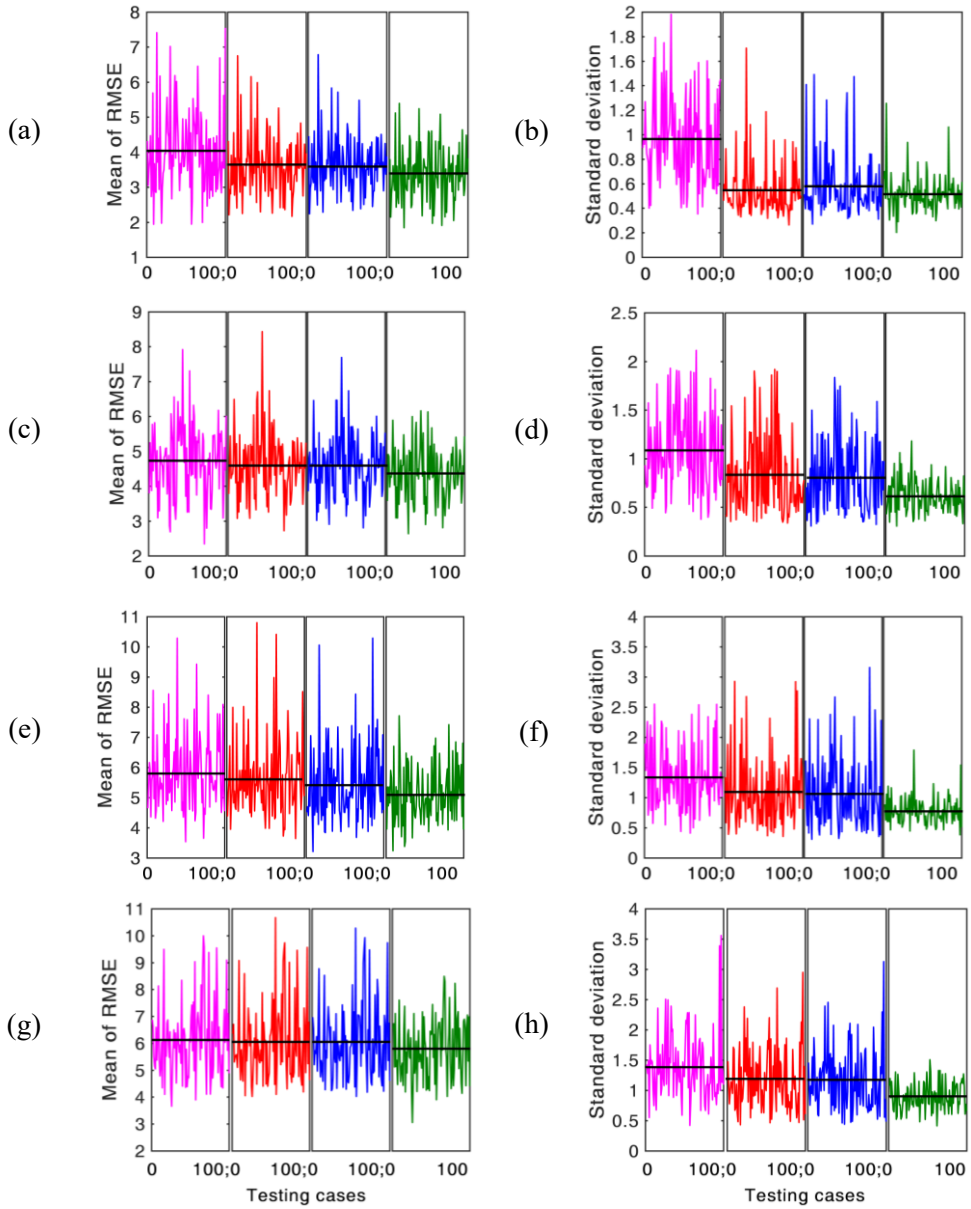

Fig. 2.12. Comparison of the related PFs: (a)(c)(e)(g): means of RMSE with variance = 1, 5, 10, 15 respectively; (b)(d)(f)(h): standard deviations of RMSE with variance = 1, 5, 10, 15, respectively. (pink lines: using SIR-PF; red lines: using RPF; blue lines: using MPF; green lines: using EMPF).

It should be noted that after a few iterations, gaps could occur in the PF high-likelihood area of the estimated posterior PDF due to sample degeneracy and impoverishment. These gaps would degrade the estimation accuracy in the current iteration, which, in turn, would propagate to the subsequent iterations and continue to degrade estimation accuracy. On the contrary, the proposed EMPF can detect and process possible gaps to reduce the effects of these problems by using dynamic feedback and an effective selection scheme. The processing efficiency, or execution time, plays an important role in real-time battery monitoring applications. Test results indicate that the execution time of the related PFs techniques is quite similar, however, given the system state estimation accuracy, the EMPF requires fewer particles, thus, comprehensively, less computation time. This issue will be further discussed in Chapter 3 in terms of the implementation of the Li-ion battery monitoring.

2.4.2. Testing the outlier detection method:

This test is conducted to evaluate the effectiveness of the proposed outlier detection method, since those outlier particles with high weights can induce large state estimate errors, or even divergence of the filtering operation of the PFs. The following tests are conducted with particles of 25, 50, 100, and 150, respectively, with conditions of time steps k = 50, variance of measurement noise v_k = 1, and variance of process noise u_k = 1. The datasets are generated using Eq, (2.24) and (2.25), with the initial state x_0 = 0.1. For each dataset, the three related PF techniques (SIR-PF, RPF, and MPF) are tested in over 1000 runs (i.e., 50,000 values to be estimated). Table 2.4 summarizes the simulation results for the related PFs. In this case, the RMSE is calculated only when an outlier is detected in both scenarios (i.e., using the outlier detection method, and without the detection method). Fig. 2.13 shows the comparison of the three PFs techniques, which shows that the proposed outlier detection method can provides higher modeling accuracy. In addition, the number of iterations where the outliers are detected by the proposed outlier detection method has increased as the particle numbers are increased.

Table 2.4: Summary of the simulation results of the related PF techniques

Particle Numbers	SIR-PF			RPF			MPF		
	RMSE with outliers	RMSE without outliers	Number of iteration	RMSE with outliers	RMSE without outliers	Number of iteration	RMSE with outliers	RMSE without outliers	Number of iterations
25	5.139	4.851	1853	4.989	4.745	2298	4.719	4.488	2193
50	5.023	4.633	3121	4.938	4.439	3866	4.647	4.089	3692
100	4.762	4.411	4713	4.551	3.839	4833	4.439	3.645	4566
150	4.534	4.156	5320	4.416	3.683	5068	4.217	3.355	4743

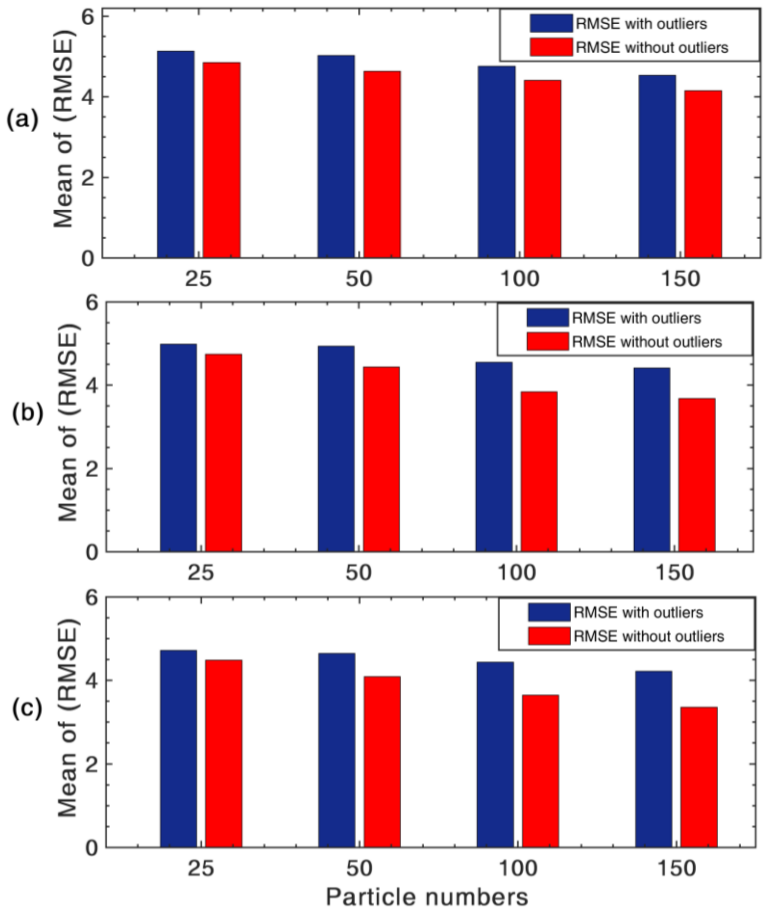

Fig. 2.13. Comparison of the related PFs: (a) SIR-PF, (b) RPF, (c) MPF, with and without using the proposed outlier detection method corresponding to different particle numbers.

2.5 Chapter Conclusion:

In this Chapter, an enhanced mutated particle filter technique (EMPF) has been proposed to improve the performance of PFs for system state estimation. It has generated the mutated particles from prior particles to explore the posterior space and locate the high-likelihood area

with the help of the dynamic feedback mechanism. A selection scheme method is proposed to assess the generated mutated particle based on unnormalized weights. An outlier assessment method is suggested to solve the problem of outlier particles with high weight on the posterior distribution due to the square operation state parameters in the observation model. The effectiveness of the proposed EMPF technique has been verified via simulation tests. Test results have shown that the EMPF technique can effectively enrich the particle species and explore the posterior distribution, even with fewer particles; it has the potential to be used for real-time computations.

In the next Chapter, the EMPF technique will be implemented for battery SOH estimation and RUL prediction.

CHAPTER 3

A MODEL-BASED EMPF TECHNIQUE FOR BATTERY HEALTH MONITORING AND RUL PREDICTION

3.1 Overview

The model-based filtering approach has many advantages over data-driven techniques, including the ability to model the underlying physics of battery degradation processes. It can also make inferences about hidden states in the dynamic system, and represents the uncertainty in its RUL prediction [1,5,10,25,26]. This makes it more attractive to model the electrochemical behaviors in the Li-ion battery system, whose properties change with variations in environmental and operating conditions. The goal is to estimate battery health indicators to evaluate the battery's state of health and predict its RUL. The common indicators in battery health monitoring and management are as follows:

a) State of charge (SOC):

SOC is a measure of the percentage of a battery's remaining usable charge at its current cycle compared to its fully-charged state. The SOC indicates how long a battery can continue to operate before recharging [16]. In reality, knowing the SOC does not usually reflect the battery's health condition. For example, an old battery may run out of power in a short period of time, even though the power indicator SOC might show that it would last for 2 hours, only a half-hour earlier [5,73].

b) State of health (SOH):

SOH is a measure of the current health condition of a battery, compared to its ideal conditions when it is new (100%). This makes it a critical factor in battery prognostics for monitoring the state of battery health, and for quantifying the amount of remaining time before it reaches the failure threshold and loses functionality. In general, a battery's SOH will decrease over time until it reaches the end-of-life criterion (failure threshold), which is commonly set, as it loses 30% of its initial capacity [16, 55,73].

c) Remaining-useful-life (RUL):

RUL is commonly defined as the time from the present SOH until a battery reaches its end-of-life stage, which can be measured in terms of discharge and charge cycles [2,88]. In general, a battery's RUL forecasting represents the prediction of the remaining cycles (time) before battery SOH reaches the predetermined failure threshold.

In this Chapter, the reliability of the proposed Enhanced Mutated Particle Filter (EMPF) technique is examined by conducting battery state estimation and RUL prediction. In general, a battery's internal impedance and its charging capacity are well-accepted indicators to track the battery's aging process, and to approximate the battery's SOH [3,5]. In this work, two degradation models will be used to describe battery degradation in terms of impedance growth and capacity degradation, using common Li-ion battery datasets in this field.

3.2 Battery Datasets of Li-ion Batteries

In this research, the feasibility of the proposed technique will be validated using the well-accepted Li-ion battery prognostic data from the National Aeronautics and Space Administration (NASA) Ames Prognostic Center of Excellence [89]. The related experimental setup to generate these datasets is illustrated in Fig. 3.1. It consists of a set of Li-ion cells, chargers, an EIS, sensors, a load bank, an environment simulation chamber, a data acquisition system, and a computer for test control. The EIS is used to measure battery impedance, and the switching circuitry controls the states of the battery (i.e., charge, discharge and impedance). Each dataset is recorded at three different operating conditions (i.e., charge, discharge and impedance) at constant temperature/humidity conditions, as follows:

1) Charging: A constant current of 1.5A is fed to the battery until its voltage reaches 4.2V; the charging process is then maintained at a constant voltage mode until the charge current decreases by 20mA.

2) Discharging: This process is performed at a constant current of 2.0A until the battery voltage drops to 2.5V.

3) Impedance: This measurement is undertaken using an EIS over the frequency sweeping range between 0.1 Hz and 5.0 kHz.

In the experiment, each battery is repetitively cycled through many iterations of discharging and charging until it reaches the end-of-life criterion (set as losing 30% of its initial capacity).

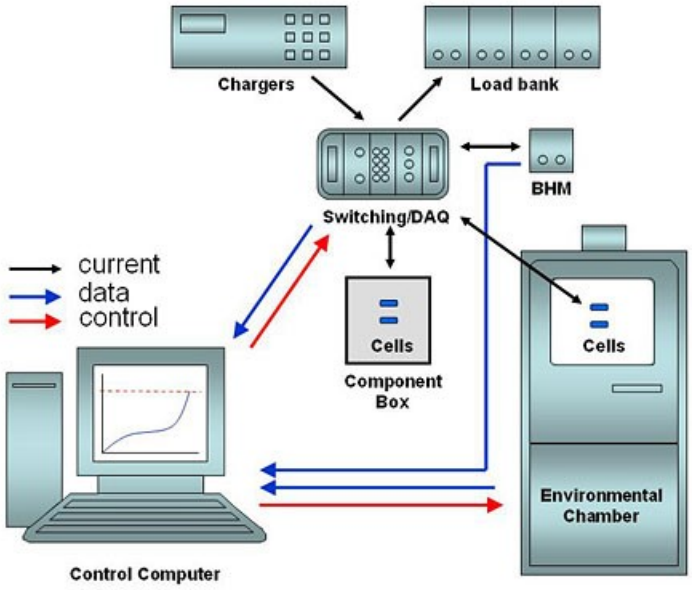

Fig. 3.1. Experimental setup of battery tests [90].

3.3 Performance Evaluation

In general, model-based filtering approach uses a degradation model to describe the evolution of the system state (degradation state) with time, and a filtering/estimation technique to adaptively estimate/update the degradation model parameters [2,9]. The filtering technique aims to propagate the posterior PDF of the current system state using a set of particles to represent the degradation trend at the future time. Then, when the measured data become available, the posterior PDF will be formed (filtered/corrected) based on the likelihood of each particle, given the incoming data at that time instant [5,24]. In this work, a Li-ion battery degradation model is constructed using experimental data described in the previous section. The mathematical model will be identified to characterize battery degradation trends. The proposed EMPF will be applied to conduct parameters estimation in order to capture the battery system's degradation process. Two well-accepted degradation models will be used for comparison.

3.3.1 The exponential model based on the battery internal impedance

A battery's internal impedance is considered as a representative indicator to track the degradation process and to determine the battery's SOH [17,39]. In general, the internal impedance values change with various aging and fault processes such as corrosion, plate sulfation and passivation [91]. Several studies have indicated that an exponential model can characterize the dynamic behavior of a battery's internal impedance over its lifetime, and that the lumped-parameter model can be used to analyze the available impedance data [17,37,67,91,92]. The lumped-parameter model, as illustrated in Fig. 3.2, is used to track battery capacity degradation. The impedance/resistance is usually inversely proportional to the capacity C/1 [17,91,92]; this incorporates the electrolyte resistance (R_E), charge transfer resistance (R_{CT}), Warburg impedance (R_W), and the dual-layer capacitance (C_{DL}). In this testing, the parameters of interest include R_E and R_{CT}, since their values have significant changes over the battery's lifetime due to the degradation/aging process; the R_W is excluded as its change is negligible based on the available data analysis from the EIS tests [91].

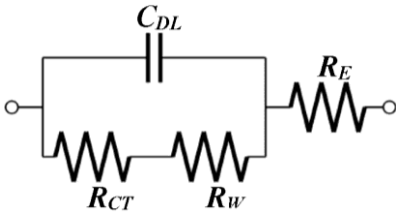

Fig. 3.2. Lumped-parameter model for a Li-ion battery.

The battery dynamic state-space model is built based on the exponential growth model for both electrolyte and charge transfer resistances from EIS measurements [17,91,92]; the state and measurement equations that describe the Li-ion battery degradation model is formulated as:

$$\Omega_k = \Omega_{k-1} + p_k \tag{3.1}$$

$$R_k = R_{k-1} \exp(\Omega_k) + u_k \tag{3.2}$$

$$M_k = R_k + v_k \tag{3.3}$$

where R_k is the state vector (i.e., R_E or R_{CT}) at time instant k (i.e., elapsed cycle), Ω_k is the growth parameter (aging state) to be estimated, and M_k is the measurement vector containing battery parameters inferred from measured data. The state vector R_k at the first-time step took the

initial value of R_E or R_{CT} from the Li-ion battery dataset. The ρ_k, u_k and v_k are additive Gaussian noises at iteration k. Equations (3.1) to (3.3) represent the measurements of R_E, R_{CT} and C in battery #6, which have been smoothed to improve the RUL prediction using the battery model. Fig. 3.3 identifies the approximate linear relationship between $R_E + R_{CT}$ and $C/1$ in battery #6.

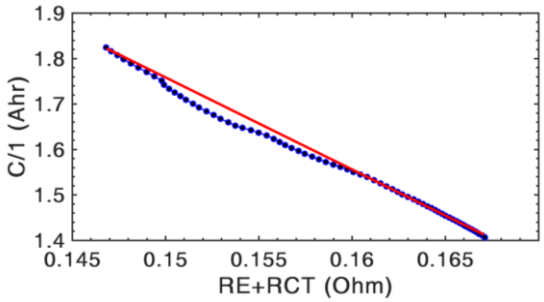

Fig.3.3. The relationship between $R_E + R_{CT}$ and $C/1$ in battery #6 (blue circle line: the measured $R_E + R_{CT}$ versus $C/1$; red solid line: a linear fit).

The performance and reliability of the proposed EMPF technique are examined by conducting an investigation to estimate the performance indices for battery system state tracking (R_E is estimated using the battery model and the Li-ion battery datasets). Figures 3.4-3.6 demonstrate the performance comparison of the related PF techniques (i.e., sampling importance resampling PF (i.e., SIR-PF), regularized PF (i.e., RPF), and mutated PF (i.e., MPF) techniques), corresponding to three different particle numbers (i.e., 50, 200 and 500), over 30 random runs using the same observation datasets. It is seen that the proposed EMPF outperforms other related PF techniques in system state tracking; the other techniques required a large number of particles to deal with sample degeneracy and impoverishment. For example, other research papers such as in [7,37,67] have used 1000-2500 particles with these related PFs to model the battery degradation models, as represented by Eq. (3.1) to (3.3) using the same Li-ion battery dataset.

This is because gaps are generated in the high-likelihood region of the approximated posterior PDF, which have prevented the particle information from being delivered to the subsequent iterations, degrading the estimation accuracy over several iterations in the related PFs. In contrast, the proposed EMPF technique can effectively represent the high-likelihood area of the posterior PDF, and can efficiently track the system state behavior using only a small number of particles. Consequently, the proposed EMPF has great potential to be implemented in real battery health monitoring applications with its higher accuracy and processing efficiency using only a small number of particles.

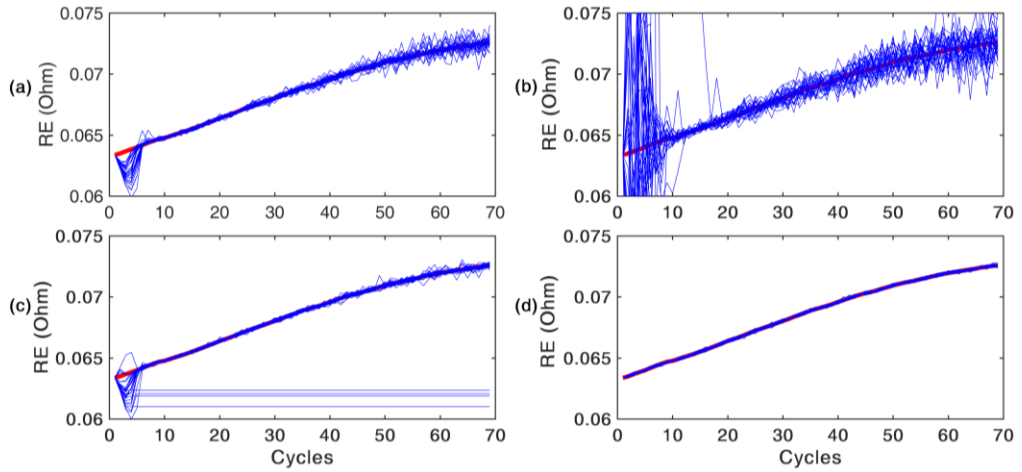

Fig. 3.4. Performance comparison of the related PF techniques, using 50 particles: (a) SIR-PF, (b) RPF, (c) MPF, and (d) EMPF (red solid line: the true states; blue solid lines: the estimated states at different runs).

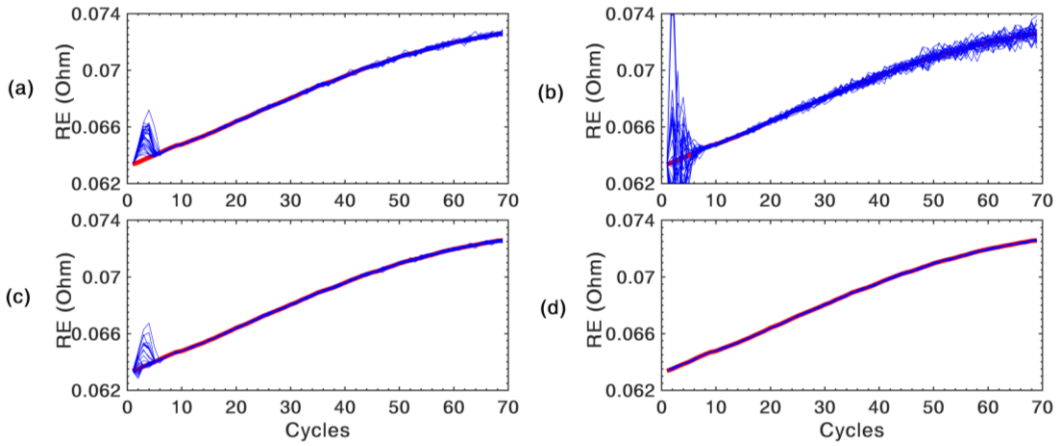

Fig. 3.5. Performance comparison of the related PF techniques, using 200 particles over 30 runs (red solid line: the actual states; blue solid lines: the estimated states at different runs).

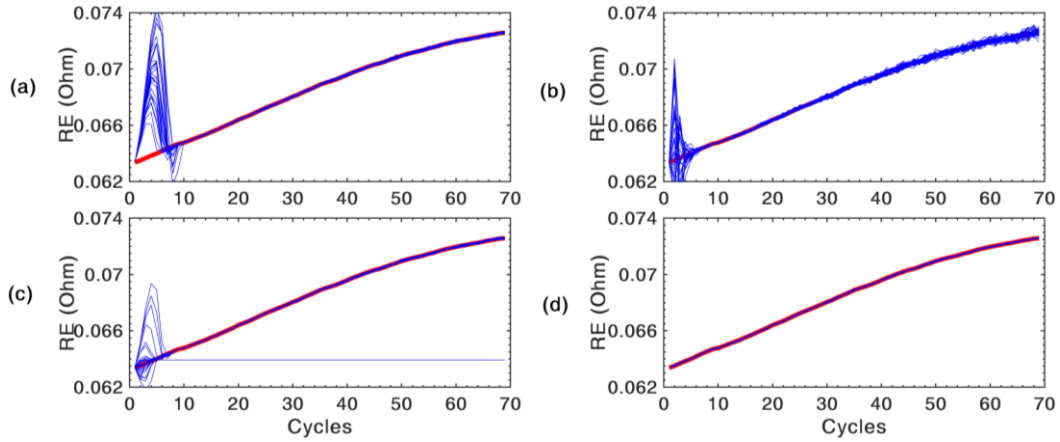

Fig. 3.6. Performance comparison of the related PF techniques, using 500 particles over 30 runs (red solid line: the actual states; blue solid lines: the estimated states at different runs).

To carry out the RUL prediction, the first part of the trajectory (i.e., R_E and R_{CT}) is used to estimate and update the battery's degradation model parameters (growth state). The updated model parameters for each PF technique are then applied to predict the RUL. In each iteration, 1000 particles are generated to estimate the posterior PDF. The time moment to trigger the prediction depends on specific application requirements; in this case, a period of 35 cycles is chosen for long-term prediction (at approximately 85% of actual battery life), as a period of 15 cycles for a short-term prediction (at about 74% of actual battery life). Fig. 3.7 illustrates the long-term prediction of two-state tracking of data R_E and R_{CT}, and the RUL prediction, respectively, using battery #6 data. The forecasting starts at cycle 34 until the battery SOH reaches the failure threshold at cycle 69.

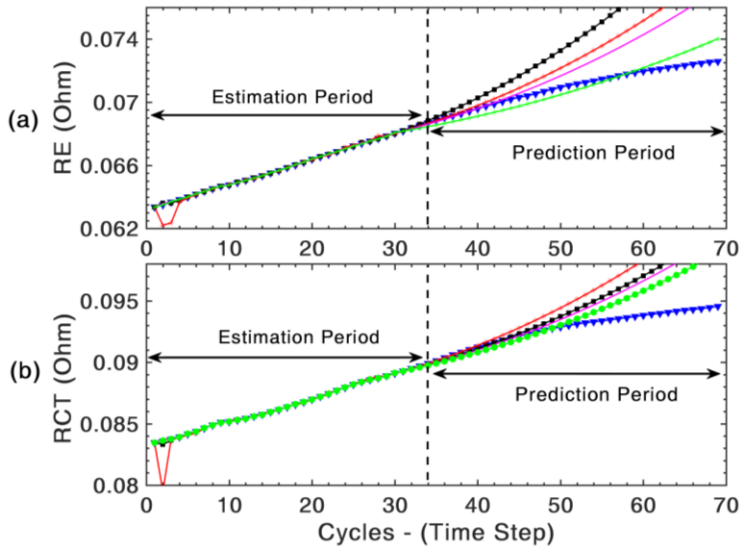

Fig. 3.7. State tracking and future state prediction at cycle 34: (a) for parameter R_E, (b) for parameter R_{CT}, using four PFs: SIR-PF (— black line), RPF(*— red line), MPF (— magenta line), EMPF(◦— green line), and (∇ —blue line) the true states.

It can be seen that the MPF outperforms the SIR-PF and RPF in R_E prediction, while the EMPF provides the best forecasting accuracy for both battery parameters due to its adaptive update of the battery model parameters during estimation. According to the relationship between R_E + R_{CT} and C/1 capacity, the predicted values of R_E and R_{CT} are used to estimate the RUL in terms of the capacity drop [7,73]. The derived capacity is used to calculate the SOH based on the following equation:

$$S_k = \frac{C_k}{C_{\max}} \times 100 \tag{3.4}$$

where C_k is the current capacity at time instant k, and $C_{\max}$ is the initial capacity when the battery is new at time k=1, whereas the estimated values will be compared against the end-of-life threshold (i.e., battery SOH is 70%).

Fig. 3.8 outlines the SOH for the estimation and prediction periods using the four PF techniques, which shows that the proposed EMPF technique can predict an RUL error of only 11 cycles early, and outperforms SIR-PF, RPF and MPF with 22, 19 and 16 cycles early, respectively. Furthermore, the proposed EMPF can be 50%, 40% and 30% more accurate than SIR-PF, RPF and MPF, respectively, in long-term prediction.

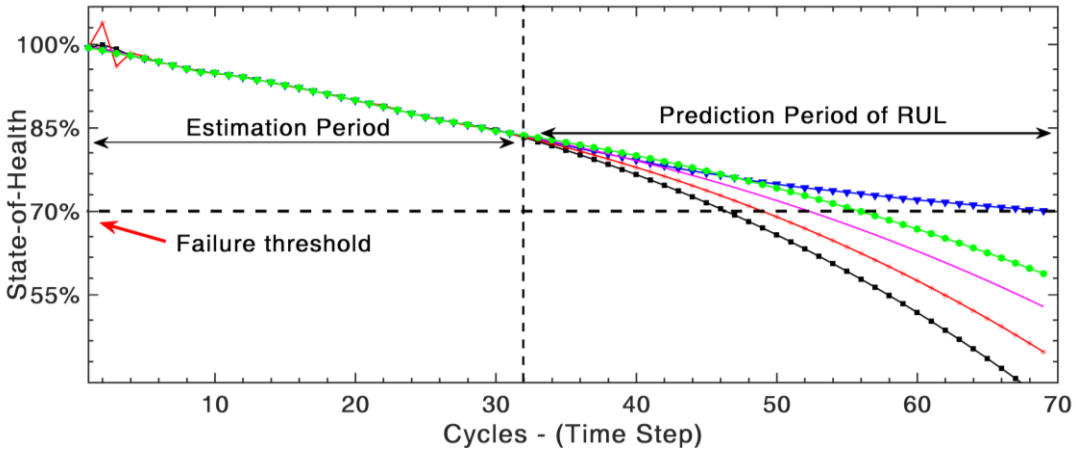

Fig. 3.8. Comparison of the derived capacity using four PFs: SIR-PF (— black line), RPF(*— red line), MPF (— magenta line), EMPF(◦— green line), and true states (∇ —blue line).

In short-term prediction (over 15 cycles in this case), the prediction performance becomes more accurate as more data are used to estimate the battery's model parameters. Fig. 3.9 demonstrates that the proposed EMPF can provide the most accurate forecasting results of R_E and R_{CT} because it can effectively locate the high-likelihood area with its new mutation mechanism.

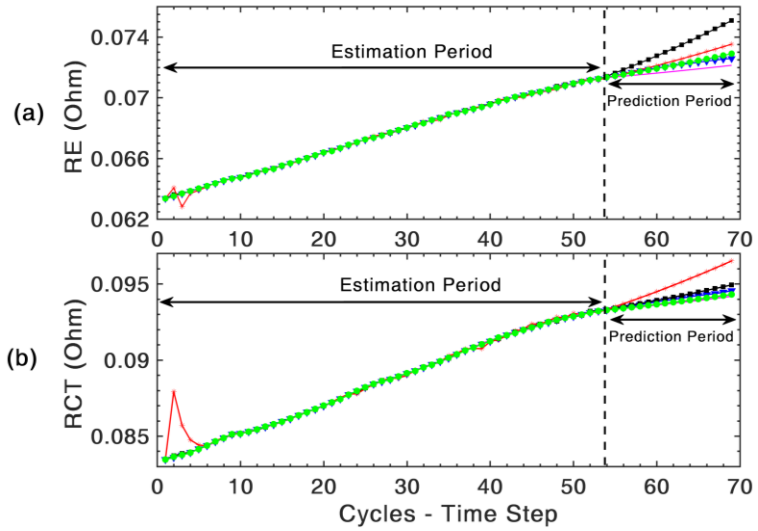

Fig. 3.9. State tracking and future state prediction at cycle 54, (a) for parameter R_E, (b) for parameter R_{CT}, using four PFs: SIR-PF (— black line), RPF(*—red line), MPF (—magenta line), EMPF(◦—green line), and true states (∇ —blue line).

Fig. 3.10 shows zoomed results for the prediction period from cycle 54 to 69 before it reaches the failure threshold. It is clear that the EMPF yields the minimum RUL prediction errors, with only four cycles earlier, due to its ability to explore the entire distribution to diversify the particles and to improve model parameter identification. On the other hand, SIR-PF is incapable of reaching the RUL threshold, with large errors of 0.03 Ah, while MPF and RPF have similar errors with 6.8 and 7 cycles early, respectively.

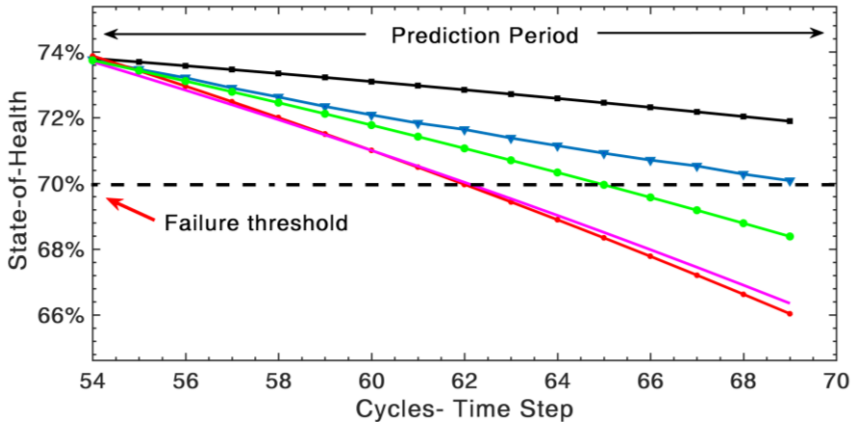

Fig. 3.10. Zoomed prediction period of the derived capacity using four PFs: SIR-PF (— black line), RPF(*—red line), MPF (—magenta line), EMPF(◦—green line), and true states (∇ —blue line).

3.3.2 The empirical degradation model based on the battery capacity

In this section, the empirical degradation model in Eq. (3.5) will be used to characterize the capacity degradation process on the battery system model, which will consider the reduction in capacity with battery use as well as the battery's self-recharge behavior [2,31,40,43].

$$c_{k+1} = \eta_c c_k + b_1 \exp\left(-\frac{b_2}{\Delta t_k}\right) \tag{3.5}$$

where η_c is the Coulombic coefficient (η_c = 0.997 in this case); b_1 and b_2 are the unknown parameters to be estimated; $\Delta_{t_k} = t_{k+1} - t_k$ is the rest time (Δ_{t_k} = 1 in this case); and c_k is the charging capacity at the cycle k^{th}, which has been calculated in the available dataset by integration of the measured current (I) over time from the starting (t_{start}) to the end (t_{end}) of discharging, as in Eq. (3.6).

$$c_k = \int_{t_{start}}^{t_{end}} I(t)\, dt \tag{3.6}$$

In general, the more particles that are used, the higher the estimation accuracy of the unknown model parameters b_1 and b_2, but the larger the computational costs. Our systematic investigation has concluded that the related PFs require at least 200 particles to be able to represent the posterior PDF space and model the system state behavior, while the proposed EMPF technique can work effectively using only a small number of particles. For example, Fig. 3.11 shows the performance of all PFs for SOH estimation and RUL prediction using only 25 particles, where the prediction starts at cycle 106. However, other PFs have lost tracking of the system state within the first few cycles (indicated by black arrows), since their working mechanism rely on the particles' normalized weights to estimate the model parameters. In this demonstration, when all particles fall into the regions with low posterior probability, their normalized weights would misguide the resampling process, which will lead to gaps in the high-likelihood region of the approximated posterior PDF, as previously discussed.

Thus, those related PFs will have to use a large number of particles to capture the high posterior probability region. For example, most research papers use 200-500 particles to characterize this capacity degradation model in Eq. (3.5), using the same Li-ion battery datasets

[22,40,93]. This confirms that the proposed EMPF is capable of dealing with sample degeneracy with a small number of particles. On the other hand, using the particles' normalized weights to identify and process the low-weight particles may not be a reliable measure to reflect the real importance of the particles to the actual state. More importantly, since the proposed EMPF can use only small number of particles, it would require lower computational costs, which is a benefit in real battery health monitoring applications. The SIR-PF technique is excluded from comparison due to its poor performance in this simulation test.

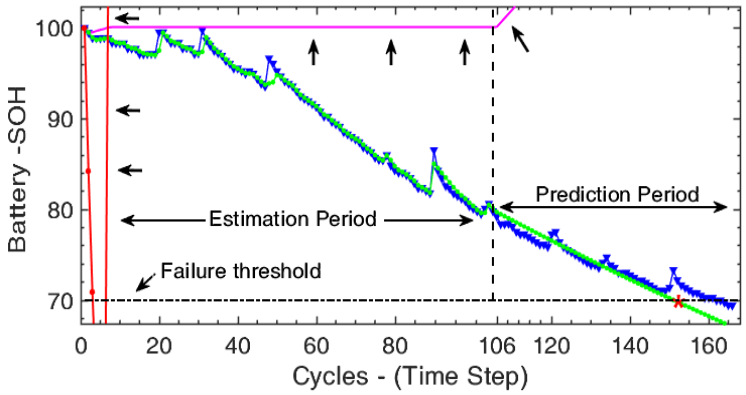

Fig. 3.11. Performance comparison of the estimated and predicted SOH using 25 particles: RPF(■—red line), MPF (—magenta line), EMPF(◦—green line), and actual states (∇—blue line).

In this testing, to carry out the RUL prediction, each PF will be utilized to track battery degradation and to identify the unknown model parameters during the estimation period using 200 particles. The battery model with the identified parameters is then used to predict the capacity states, and to estimate the RUL for the battery to reach the failure threshold. Battery #5 data is used in this test, which can reach its end-of-life criterion at the cycle 162. The time instants to trigger the prediction are selected as 60, 40, and 20 cycles for long-term, medium-term and short-term prediction, respectively. Table 3.1 summarizes the prediction results, which also include the starting point of each prediction period, as well as the relative error for each technique. Figures 3.12-3.13 show the zoomed results for the medium-term and long-term predictions, starting at 126 and 106 cycles, respectively. The relative error can be calculated by Eq. (3.7) [43], where (RUL_{true} = 162 in this case).

$$R_{error} = \frac{\left| RUL_{true} - RUL \right|}{RUL_{true}} \times 100 \tag{3.7}$$

Table 3.1. Summary of the prediction results of the related PFs.

Prediction starting point	PF technique	Prediction result (cycle)	Error (cycle)	Relative error
146	**RPF**	150.2	11.8	7.28%
	MPF	152	10	6.17%
	EMPF	153.1	8.9	5.49%
126	**RPF**	134.8	29.2	16.79%
	MPF	149.5	12.5	7.72%
	EMPF	151.2	10.8	6.67%
106	**RPF**	144.7	17.3	10.61%
	MPF	147.1	14.9	9.09%
	EMPF	148.8	13.2	6.82%

Test results show that EMPF outperforms other related PF in the long-term prediction with RUL relative error of 6.82%, while RPF and MPF have a higher relative error of 9.09% and 10.61%, respectively. Although the forecasting accuracy can be improved for all PF techniques with a shorter prediction period, the proposed EMPF technique provides the best performance for SOH estimation and RUL prediction under all testing conditions. It can capture a battery's dynamics, track its capacity degradation during the estimation period, and effectively predict its RUL. In contrast, other PFs cannot adapt themselves to recognize the characteristics of battery capacity degradation, which could degrade the accuracy of state estimation and RUL prediction.

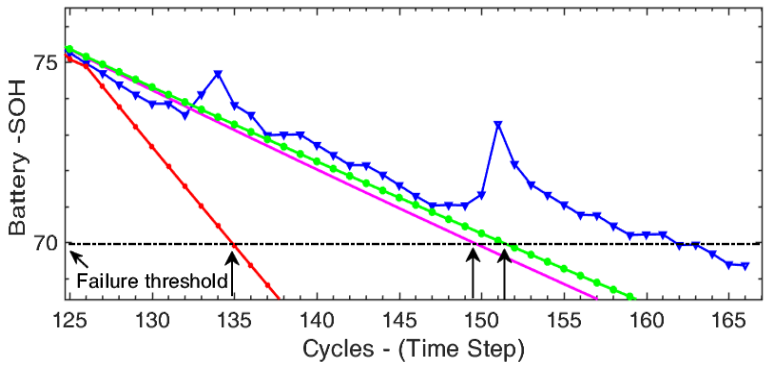

Fig. 3.12. Zoomed performance comparison for prediction period of the medium-term prediction (over 40 cycles) using three PFs: RPF(■—red line), MPF (—magenta line), EMPF(◦—green line), and actual states (∇—blue line).

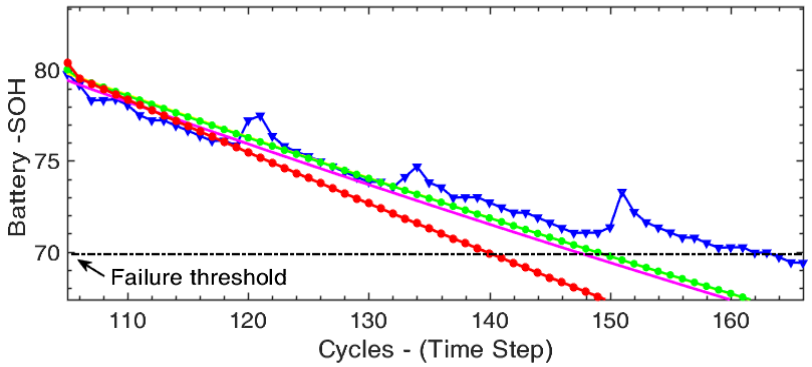

Fig. 3.13. Zoomed performance comparison for prediction period of the long-term prediction (over 60 cycles) using three PFs: RPF(*—red line), MPF (—magenta line), EMPF(◦—green line), and actual states (∇—blue line).

The uncertainty of the PFs techniques can be characterized using the PDF of the estimated state (i.e., RUL prediction), where the PDFs with narrower and taller distributions have more precise results in predictions [7]. Fig. 3.14 illustrates the PDFs for the short-term prediction of the related PF techniques at the point when the related PF techniques have reached the determined end-of-life criterion (i.e., battery SOH of 70%). It is clear that the EMPF has the least uncertainty with its taller PDF and reasonable distribution compared to other PF techniques, due to its ability to effectively represent the high probability region of the posterior PDF. This is because its unique enhanced mutation method and selection scheme work to provide a higher adaptive capability to locate the high-likelihood region on the posterior PDF using a dynamic feedback strategy.

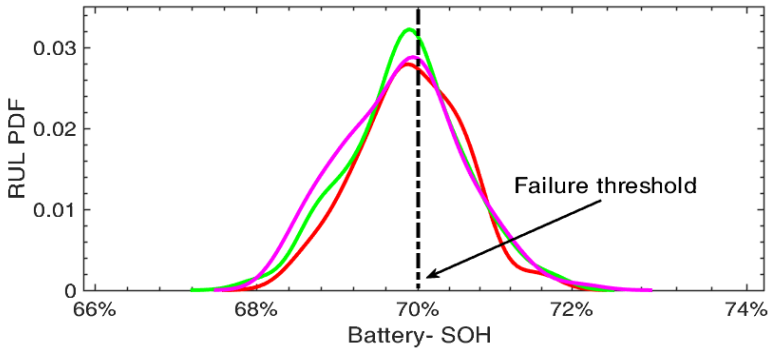

Fig. 3.14. Comparison of the uncertainty of the RUL prediction for short-term prediction: RPF (red line), MPF (magenta line), EMPF (green line), and true states (black line).

3.4 Chapter Conclusion:

In this Chapter, the proposed EMPF has applied two well-accepted degradation models for Li-ion battery SOH monitoring and RUL prediction using the battery's internal impedance and capacity measurements. Test results have concluded that EMPF can accurately track the system characteristics with fewer particles, and provide better results for SOH monitoring and RUL prediction compared to other related PF techniques. However, since no new measurements are available during the prediction period, the parameters of the degradation-prediction model will be fixed during this period, which can degrade the prognostic performance, especially for long-term prediction. To tackle this problem, an adaptive evolving fuzzy (AEF) technique (predictor) will be proposed in the next Chapter for long-term time series forecasting, which will be used to forecast the battery degradation indicator values (e.g., capacity and impedance) so as to improve the accuracy of model-based EMPF prognostics.

CHAPTER 4

AN ADAPTIVE EVOLVING TECHNIQUE FOR LONG-TERM TIME SERIES PREDICTION

4.1 Overview

A reliable long-term time series prediction technique is critically needed in various domains, such as the financial market [94,95], environmental sciences [96,97], and industrial engineering [98,99]. For example, time series forecasting is applied to identify system characteristics based on the current and past data (training data) in order to predict the evolution of the monitored feature, which will be very useful for system health monitoring and prognostics in industrial applications. Many data-driven soft-computing techniques have been proposed in literature for this purpose such as neural networks [50,58,100], fuzzy logic [60,101], and their synergistic schemes [65,98,102,103]. However, those soft-computing techniques usually suffer from limitations related to training efficiency and parameter-setting. Moreover, these data-driven models usually have limited adaptive capability to accommodate the variable environmental and operating conditions due to their fixed structures, especially in nonlinear systems [45,69,104]. In recent years, evolving fuzzy systems (eFS) have been introduced to tackle some of the aforementioned data-driven limitations related to the fixed reasoning architectures.

4.2 Brief Background of Evolving Fuzzy Systems

The evolving fuzzy technique is a recent development in soft-computing, which can be defined as a self-constructing and self-learning system with self-adapting capability for its parameters and structure. An eFS can gradually evolve its reasoning structure to deal with the time-varying system dynamics, and uses incremental learning algorithms to update its parameters to enhance performance [69]. Among the different types of fuzzy models, the Takagi-Surgeon (TS) fuzzy model is commonly applied as the reasoning platform due to its high degree of modeling flexibility [70]. The properties of these eFS techniques are summarized as follows:

1) *Structure-evolving:*

The process of fuzzy clustering is usually undertaken without prior knowledge about how many clusters/rules are required to characterize the system's input/output spaces. A number of criteria have been suggested in the literature to control the fuzzy cluster evolving process [104].

For instance, Angelov *et al*. [105-107] have proposed some evolving TS (eTS) fuzzy models based on the potential of incoming datasets using Cauchy functions. By comparing the new data potential with the potentials of existing clusters, a decision is made for cluster/rule generation and updating. Several publications use distance-based measures to generate and modify fuzzy clusters, for example, using the Euclidean distance [108-111] and the Mahalanobis distance [112,113]. The distance is measured between the new data point and the existing cluster centers to determine if the existing clusters can characterize the properties of the new data point. Another criterion is based on the firing strength (activation degree) of the new data point with respect to existing clusters [70,104,114,115]; for instance, if the firing strength of all existing clusters is below a certain threshold, a new cluster will be generated.

Although some promising results of those evolving mechanisms can be achieved in applications such as control, classification and short-term prediction, their speed of fuzzy cluster/rule generation is sensitive to the distribution of incoming data points. This will be a challenge, especially in long-term forecasting operations of nonlinear systems where the spread of the incoming data (inputs) would be wider as the prediction horizon becomes longer. This would result in the generation of many extra clusters/rules during the evolving process and could lead to problems such as over-fitting and high computational costs.

2) *Incremental learning:*

Typically, eFS uses some incremental learning algorithms, where the antecedent and/or the consequent parameters are updated on a per-sample basis in each evolution pass [114]. Although the antecedent parameters (i.e., the centers and spreads of the clusters) are usually determined in the evolving process on the input space [116,117], they are usually not updated after all fuzzy clusters are formulated. In general, most eFS techniques use a certain measure to update the cluster center; for example, a higher potential data point should fall close to the existing cluster center in order to replace it. However, in some other cases, although a new data point is more related to system dynamics, its potential may not always be high enough to be selected to update the cluster/rule base if the new data point is contaminated by noise. This may degrade the modeling efficiency, resulting in under-fitting, and could reduce its adaptive capability in handling variations in operating conditions.

In addition, our investigation has concluded that the eFS consequent parameters could be dependent, to some degree, on the estimation of antecedent parameters. This means that the coupling error will degrade the training process. Therefore, a new approach is needed to guide antecedent parameter training in order to provide the eFS with more adaptive capability to handle changes in system dynamics and operating conditions. Although some derivative-based methods (e.g., Levenberg–Marquardt, gradient descent and KF) have been applied to optimize the antecedent parameters [110,111,118], the optimization processes are usually undertaken offline due to their high computational costs.

To tackle these aforementioned problems in structure-evolving and incremental learning, an adaptive evolving fuzzy (AEF) technique is proposed in this Chapter to control the fuzzy cluster/rule generation and to enhance incremental learning, with the goal of improving modeling efficiency for long-term time series forecasting.

4.3 Proposed AEF Predictor

The proposed AEF predictor has the following novel aspects: 1) an error assessment method is suggested to monitor the trend of training errors based on a queue data buffer to control the fuzzy cluster/rule evolving process. 2) An adaptive particle filter (aPF) technique is proposed to explore the fuzzy rule space and to adjust/optimize the fuzzy cluster centers in order to improve the modeling flexibility and adaptive capability. In the proposed AEF predictor, the fuzzy rules are the TS-1 type to describe the input-output mapping for *r*-steps-ahead prediction. Consider *n* inputs $\{x_k, x_{k-r}, x_{k-2r}, ..., x_{k-(n-1)r}\}$, where x_k represents the current k^{th} data point, and *r* is the step. The fuzzy reasoning is described as follows:

Rule j: If (x_k is A_1^j) and (x_{k-r} is A_2^j) and ... and ($x_{k-(n-1)r}$ is A_n^j), then:

$$f_j = a_0^j + a_1^j x_k + a_2^j x_{k-r} .... + a_n^j x_{k-(n-1)r} \tag{4.1}$$

where j denotes the j^{th} fuzzy rule, $j \in [1, N]$; N is the total number of rules; A_n^j are the fuzzy sets for the n^{th} input; and $\{a_0^j, a_1^j, ...a_n^j\}$ are the consequent parameters.

To facilitate the input/output partitioning, the membership functions (MFs) of all fuzzy sets are in Gaussian form [118]. The MF grade (i.e., premise parameter) of the n inputs at the time instant k in the set A_n^j is computed by:

$$\mu_{A_i^j}(x_{k-(i-1)r}) = \exp\left(-\frac{(x_{k-(i-1)r} - c_{ij})^2}{2\sigma_{ij}^2}\right) \tag{4.2}$$

where c_{ij} and σ_{ij} are the center and spread of the j^{th} fuzzy cluster for i^{th} input. For simplicity, they will be denoted as c_j and σ_j, respectively, in the remainder of this Chapter. Using a T-norm operator, the firing strength of the j^{th} fuzzy rule can be computed by:

$$W_j = \prod_{i=1}^{n} \mu_{A_i^j}(x_{k-(i-1)r}) \tag{4.3}$$

After normalization, the overall output $\hat{Y}$, which is the r-steps-ahead prediction x_{k+r}, can be computed by:

$$\hat{Y} = \sum_{j=1}^{N} \overline{W}_j f_j = \sum_{j=1}^{N} \overline{W}_j \ (a_0^j + a_1^j x_k + a_1^j x_{k-r} ... + a_n^j x_{k-(n-1)r}) \tag{4.4}$$

where f_j is the consequent part (e.g., the model output) of the rule j, and $\overline{W_j} = \dfrac{W_j}{\sum_{j=1}^{N} W_j}$ is normalized MF degrees. Linear consequent parameters a_n^j are to be updated using the recursive least squares estimator or its variations [117].

4.3.1 The proposed error-assessment method

In inference structure evolution, the potential criteria [118] is used for illustration. The input vector is $X_k \in \{x_k, x_{k-r}, ..., x_{k-(n-1)r}\}$, $Y_k \in \{x_{k+r}\}$ is the actual output, and $\hat{Y}_k$ is the output computed by the proposed AEF predictor. The first data sample $z_k = [X_k, Y_k]$ at the time instant $k = 1$ is used to initialize the rule parameters; the number of clusters $N := 1$, the center of the first

cluster $c_1 := z_k$. The spread will be initialized as $\sigma_1 := 0.25$, the initial potential of this data point $P_k(z_k) := 1$, and the potential of this first cluster $P_k(c_j) := 1$.

As the next data point $z_k = [X_k, Y_k]$ arrives, its potential is calculated by Eq. (4.5), and the potential of all existing clusters will be updating recursively by Eq. (4.6):

$$P_k(z_k) = \frac{k-1}{(k-1)(\theta_k + 1)\sigma_k - 2v_k} \tag{4.5}$$

$$P_k(c_j) = \frac{(k-1)P_{k-1}(c_j)}{k - 2 + P_{k-1}(c_j) + P_{k-1}(c_j)\sum_{i=1}^{n+1}(z_{k-1}^j)^2} \tag{4.6}$$

where $\theta_k = \sum_{i=1}^{n+1}(z_k^j)^2$, $\sigma_k = \sigma_{k-1} + \sum_{i=1}^{n+1}(z_{k-1}^j)^2$, $v_k = \sum_{j=1}^{n+1} z_k^j \beta_k^j$, $\beta_k^j = \beta_{k-1}^j + z_{k-1}^j$, $j \in [1, N]$ denotes the number of fuzzy clusters/rules.

Typically, a new fuzzy cluster is formulated if the potential of the new data point is higher than the potential values of all existing clusters, or if:

$$P_k(z_k) > P_k(c_j), \text{ then:}$$

$$N := N + 1, c_N := z_k, \sigma_N := 0.25, P_k(c_N) := P_k(z_k) \tag{4.7}$$

However, this condition may be satisfied successively over several incoming data points in case of long-term prediction operation. This is because the input horizon of a dynamic system will have a broader distribution pattern due to its nonlinear and non-stationary nature. Fig. 4.1 shows a simulation example of the fuzzy cluster/rule growth of a 10-steps-ahead prediction using the Mackey-Glass benchmark data [104]. It can be seen that it has 5 clusters/rules at data sample 237, which continuously increases until it reaches 19 clusters/rules at time instant 251. This is because the potential of the data sample keeps increasing, and will always be higher than those of all existing cluster centers.

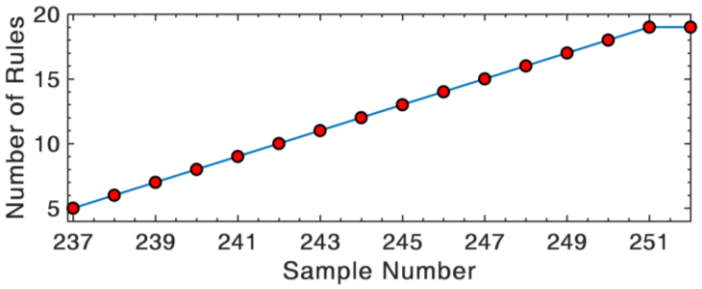

Fig. 4.1. Fuzzy cluster/rule generation process.

The high number of clusters/rules would not only result in higher computational costs, but would also make the system prone to over-fitting. Furthermore, it would degrade processing accuracy, as illustrated in Fig. 4.2, whereby the training error keeps increasing over several steps.

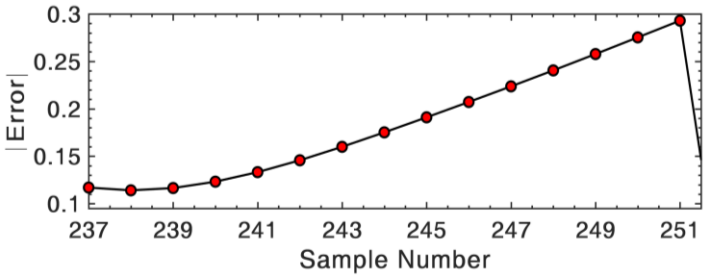

Fig. 4.2. Increase in training errors.

The proposed error assessment method aims to track the trend of training errors (i.e., monotonically decreasing or increasing) to control the cluster formulation process. Since the recent data point usually has a higher impact on the future behavior of the dynamic system, a queue data structure buffer is adopted to keep only the most recent training errors. Based on the determined trend of the recent training errors, a decision will be made to either update the properties of existing cluster/rule to accommodate the new data sample with higher potential, or a new cluster/ rule will be formulated and added to the cluster/rule base.

The proposed error-assessment method is conducted by using a $f(\alpha)$ function, as shown in Eq. (4.8):

$$f(\alpha) = \begin{cases} e^{\alpha} > 1, \text{ if } \alpha > 0 & \text{monotonic increase} \\ e^{\alpha} < 1, \text{ if } \alpha < 0 & \text{monotonic increase} \end{cases} \tag{4.8}$$

where $f(\alpha)$ is monotonically increasing if $\alpha > 0$, and monotonically decreasing if $\alpha < 0$.

The trend of recent training errors held in the queue buffer is estimated by:

$$\alpha_k = E_k - E_{k-1} \tag{4.9}$$

$$E_k = \sum_{i=k-R+1}^{k} e_i \tag{4.10}$$

$$e_k = \left| Y_k - \hat{Y}_k \right| \tag{4.11}$$

where E_k and E_{k-1} are the cumulative training errors for the recent data points at the k^{th} and the $(k\text{-}1)^{\text{th}}$ time instants, respectively.

α in Eq. (4.9) is an indicator that assesses the error trend in the queue buffer: $\alpha > 0$ if the current cumulative errors are increasing, or $\alpha < 0$ if errors are decreasing.

e_k in Eq. (4.11) is the training error at the k^{th} time instant, which is used to update the queue data structure in the buffer, as illustrated in Fig. 4.3. The queue buffer length R can be determined by the prediction step r. In this case, $R = r + 1$ is selected based on the training error patterns.

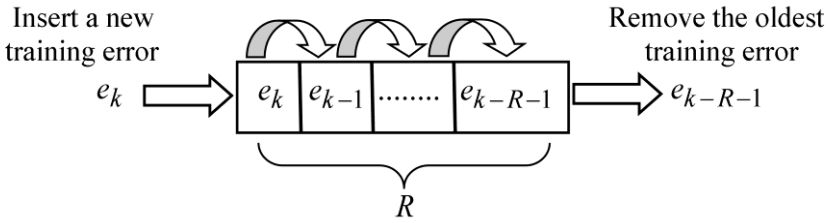

Fig. 4.3. Queue buffer updating mechanism.

The proposed error-assessment method is summarized as follows:

1) Adding a new cluster/rule scenario: A new cluster/rule will be added only if both conditions in Eq. (4.7) and Eq. (4.12) are satisfied simultaneously. This means that the potential of the new data point is higher than the potentials of all existing cluster centers, and the cumulative errors are monotonically increasing:

$$f(\alpha_{k-1}) > 1 + \eta \tag{4.12}$$

where η is a small real number that represents the data bias associated with cluster sensitivity, it can be used to provide some degree of freedom in the threshold of the condition.

2) Updating the existing cluster/rule scenario: If only the condition in Eq. (4.7) is satisfied, but the cumulative error is monotonically decreasing, the new data point with a higher potential will replace the closest existing cluster center, or:

$$I = \arg\min_{j=1}^{N} \left| z_k - c_j \right| \tag{4.13}$$

The cluster center and potential will be updated by:

$$c_I := z_k \tag{4.14}$$

$$P_k(c_I) := P_k(z_k) \tag{4.15}$$

where I is the index of the cluster (with the center c_I), closest to this new data point with a higher potential.

Fig. 4.4 demonstrates how the proposed error-assessment method can tackle the aforementioned problems in Figures 4.1 and 4.2. As illustrated in Fig. 4.4(a), when the error-assessment method recognizes a monotonic increase of the cumulative error at time instant 240, and the following data point (i.e., at 241) has a higher potential, a new cluster will be added, as shown in Fig. 4.4(b), as conditions in Eq. (4.7) and Eq. (4.12) are satisfied simultaneously. Consider another case for the incoming data point at time instant 242, whereby both conditions are satisfied, another new cluster is generated to model the new system characteristics. This demonstrates that the proposed error-assessment method can capture the new characteristics of the system by adding only two clusters/rules instead of 14 clusters/rules, as illustrated in Fig. 4.2. Fig. 4.4(c) outlines how the proposed error-assessment method can prevent the over-fitting problem by reducing training errors and improving modeling efficiency.

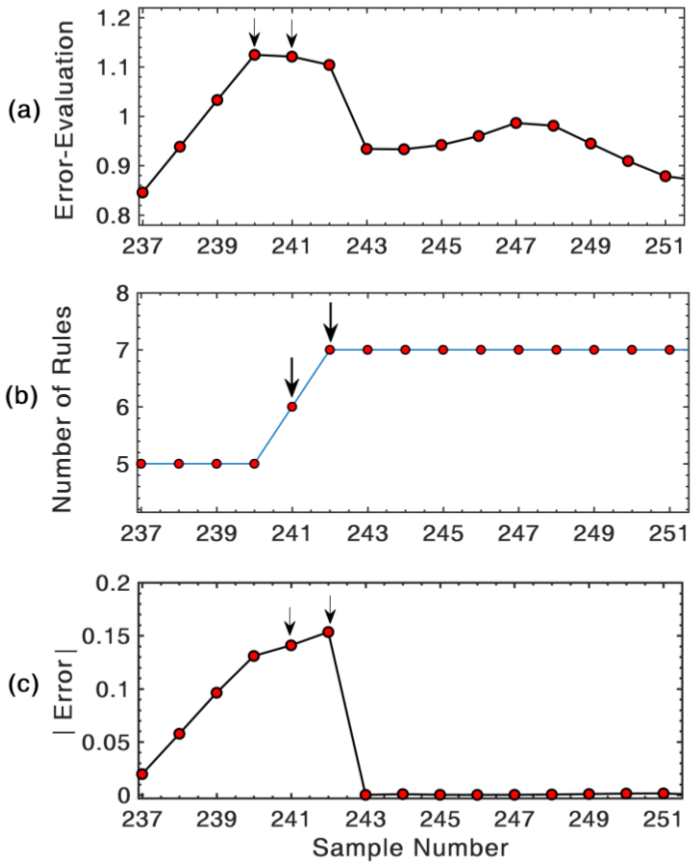

Fig. 4.4. Proposed method mechanism to add rules.

The recognized evolving system will be optimized by using the proposed training approach, (to be discussed in the following section).

4.4. Adaptive Particle Filter Technique for Optimization

Although the fuzzy cluster centers are defined based on an evolving approach, those clusters may not be updated after all clusters have been formulated. Fig. 4.5 illustrates an example of the cluster generation over 1600 data samples for 6-steps-ahead prediction. Two fuzzy clusters are generated within the first few data samples; rule #1 is not updated after data sample 29, which may prevent the eFS from handling variations in operating conditions; it will also degrade forecasting accuracy if the cluster parameters are defined or updated based on noisy data.

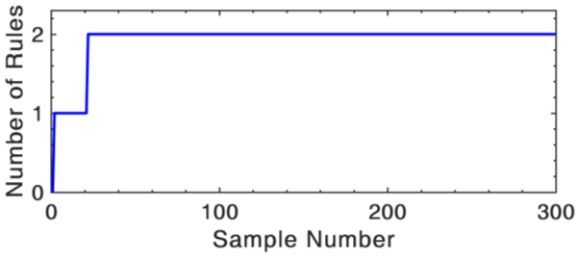

Fig. 4.5. Generated fuzzy clusters/rules progress.

In this work, an adaptive PF (aPF) training technique is proposed to adaptively explore the fuzzy rule space and optimize fuzzy cluster centers. The objectives are to minimize the impact of uncertainties in cluster formulation and improve modeling flexibility. As stated in Subsection 2.2, the PF is a Bayesian estimation method based on the Monte Carlo simulation, whereby posterior PDF is represented by a set of random samples (particles). The associated weights of these particles are computed based on the conditional likelihood of each particle [119]. However, it is difficult to use the general PF algorithm in eFS due to the high computational costs of its resampling process. In addition, it is difficult to properly characterize the high-likelihood area of the estimated posterior PDF due to sample degeneracy.

A new adaptive approach will be suggested in the proposed aPF to generate particles on the high-probability regions of posterior density to improve estimation accuracy. A unique implementation strategy will also be proposed to accelerate the optimization process. The proposed aPF training technique will be executed only if the error-assessment method recognizes monotonically-increasing training errors due to reasons such as poor modeling performance. Unlike the existing PF techniques, the proposed aPF does not require parameter-setting and resampling. Correspondingly, it can reduce computation time for real-time monitoring applications.

As the parameter optimization is related to nonlinear filtering, the respective dynamic state-space model and the measurement model of the proposed aPF technique can be described by Eq. (4.16) and Eq. (4.17):

$$m_j = f(c_j, u_k) \tag{4.16}$$

$$Y_k = h_k(m_j, v_k) \tag{4.17}$$

where m_j is the hidden state to be estimated, which will be the optimal location for the fuzzy cluster center c_j; Y_k is the actual output at the k^{th} time instant; $h(\bullet)$ denotes the proposed AEF predictor; u_k and v_k are random noise.

The posterior PDF of the state m_j can be represented by T particles $\{m_j^1, m_j^2, ..., m_j^T\}$, which will be used in Eq. (4.2) to compute the MFs. The associated weights $\{\pi_j^1, \pi_j^2, ..., \pi_j^T\}$ will be computed based on the conditional likelihood of each particle with respect to the target output. The posterior density at time instant *k* can be approximated as:

$$p(m_j \mid Y_k) \approx \sum_{t=1}^{T} \pi_j^t \delta(m_j - m_j^t) \tag{4.18}$$

where $\delta(.)$ is the Dirac function, and the weight π_j^t can be recursively updated using the principle importance sampling [119].

In initialization, the weight of the current cluster center c_j is computed and denoted as ξ, which is initially considered as the optimal location C_{best} with the highest weight $\pi_{best} := \zeta$.

The proposed aPF training technique will generate a set of T particles $\{m_j^1, m_j^2, ..., m_j^T\}$ using the following steps:

1) Define the respective upper (U) and lower (L) boundaries of the fuzzy cluster/rule space with the searching region:

$$U = C_{best} + \lambda_R \tag{4.19}$$

$$L = C_{best} - \lambda_R \tag{4.20}$$

where λ_R is the standard deviation of the R most recent data points to recognize the optimal location. C_{best} is the optimal location so far.

2) Derive the T particles $\{m_j^1, m_j^2, ..., m_j^T\}$ from the determined high-likelihood region:

$$m_j^t = L + (U - L)\phi \tag{4.21}$$

where $t \in [1, T]$ is the particles index, and $\phi \in [0, 0.5]$ is a random number to explore these boundaries with an approximately uniform distribution for optimization, by minimizing the training error in Eq. (4.17).

3) Compute the weight π_j^t of the driven particles. For each particle, if $\pi_j^t > \pi_{best}$, both C_{best} and π_{best} will be updated by: $C_{best} := m_j^t$, $\pi_{best} := \pi_j^t$. The j^{th} fuzzy cluster center c_j will be updated using the particle value with the highest weight, or $c_j := C_{best}$.

The proposed adjustment approach, as discussed above, can evaluate the modeling performance of each specified location, and adjust a fuzzy cluster/rule center to a new location only to achieve a better performance. This will ensure that the AEF predictor can gradually make the necessary update to maintain high modeling efficiency. Fig. 4.6(a) illustrates high training errors due to the impact of static cluster centers that cannot properly deal with variations in operating conditions. Fig. 4.6(b) demonstrates how the proposed error-assessment method and aPF training technique can recognize and process training errors.

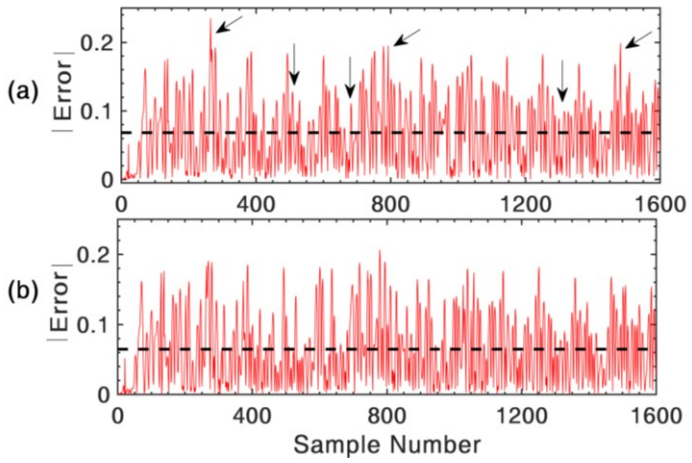

Fig. 4.6. Training errors during 1600 data samples: (a) without using the proposed aPF technique, (b) using the aPF technique.

Fig. 4.7(a) shows a MF grade without updating cluster centers. Fig. 4.7(b) illustrates how the proposed aPF training technique can adjust the fuzzy cluster centers in order to re-capture the system's new dynamics. Fig. 4.8 shows the training error distribution, where the proposed aPF training technique in Fig. 4.8 (b) can generate lower error standard deviation and higher modeling accuracy.

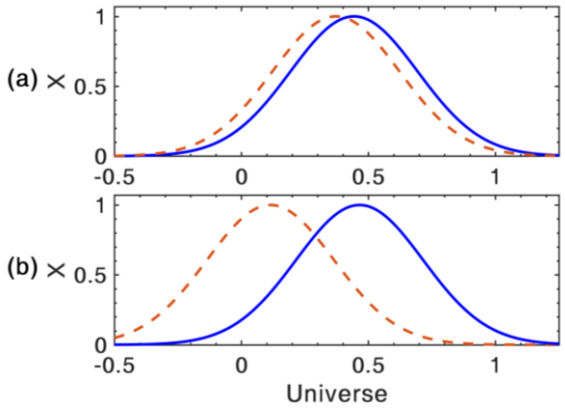

Fig. 4.7. Comparison of the MF grade of the input space: (a) without using the proposed aPF technique, (b) effects using the proposed aPF technique.

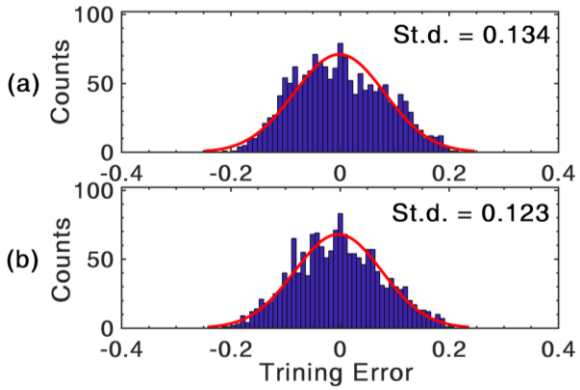

Fig. 4.8. Fitting training error distribution in a histogram: (a) without using the proposed aPF technique, (b) using the aPF technique.

4.5. Performance Evaluation

The effectiveness of the proposed AEF technique and aPF algorithm is evaluated in this section by simulation tests using the Mackey-Glass data series, which is chaotic, non-convergence, and non-periodic in nature. It is a benchmark dataset that has been widely used in many publications in this research and development field [70,98,101,104-110]. The Mackey-Glass data equation is:

$$\frac{dx(t)}{dt} = \frac{0.2x(t-\tau)}{1+x^{10}(t-\tau)} - 0.1x(t) \tag{4.22}$$

In this testing, 10000 data points are generated with the following conditions: $x(0) = 1.2$, $dt = 1$, $\tau = 30$ (which is more nonlinear than the commonly-used $\tau = 17$). The aPF training algorithm will use 15 particles. The test is undertaken using the Matlab R2017a. For

simplicity, the threshold η in Eq. (4.12) is selected as the standard deviation of the data in this testing. Four input variables $\{x_k, x_{k-r}, x_{k-2r}, x_{k-3r}\}$ will be used for the *r*-steps-ahead prediction x_{k+r}, where x_k represents the data point at the k^{th} time instant, and x_{k+r} is the predicted output Y_k.

4.5.1. Performance evaluation for long-term predictions

In this subsection, the proposed AEF predictor is evaluated in terms of modeling performance and the number of fuzzy clusters/rules. Two well-accepted evolving techniques are used for comparison: the evolving eTS technique, based on potential criteria [106,111,116,118], and eFS technique, based on distance criteria [110]. Table 4.1 summarizes the simulation results for the *r*-steps-ahead prediction using 1600 data samples in terms of root-mean-squares error (RMSE) between the actual output and the computed output. Results show that the proposed AEF predictor can provide higher prediction accuracy with fewer clusters/rules, especially for long-term prediction (e.g., 8~14 steps-ahead). When r = 13, although the eFS technique has generated the same number of clusters/rules as the proposed AEF predictor, the AEF predictor is 20% more accurate than the eFS due to its efficient clustering approach.

Table 4.1. Performance comparison of the related predictors in terms of RMSE and number of rules.

No. of Steps	**eTS**		**eFS**		**AEF**	
	RMSE	No. of Rules	RMSE	No. of Rules	RMSE	No. of Rules
1	0.003	4	0.002	1	0.002	2
2	0.007	2	0.008	1	0.007	2
3	0.022	3	0.023	1	0.022	3
4	0.041	3	0.046	1	0.041	3
5	0.063	4	0.057	8	0.063	4
6	0.086	2	0.066	11	0.080	2
7	0.093	5	0.065	11	0.077	4
8	0.077	13	0.057	13	0.055	6
9	0.068	15	0.059	14	0.051	6
10	0.054	31	0.057	12	0.045	7
11	0.056	22	0.060	11	0.045	11
12	0.057	14	0.064	13	0.043	8
13	0.073	12	0.072	9	0.059	9
14	0.081	9	0.073	9	0.071	7

Fig. 4.9 illustrates the test results of those techniques in terms of RMSE, and Fig. 4.10 compares the number of generated clusters/rules. It is clear that the proposed AEF predictor can generate a smaller number of clusters/rules to map the fuzzy input and output spaces with higher modeling accuracy (or lower RMSE). For example, although the eTS and eFS techniques have generated 4 and 2 times more clusters/rules, respectively, than the proposed AEF predictor for 10-steps-ahead prediction, the AEF predictor can effectively capture the system's dynamic characteristics and provide higher modeling accuracy (with lower RMSE (0.045 vs. 0.054 and 0.057)) while using fewer clusters/rules (7 vs. 31 and 12). This is because its error-assessment method can effectively accommodate the high potential data point instead of adding new rules if the training errors follow a decreasing monotonic trend. The proposed aPF training technique can adaptively adjust the fuzzy cluster centers in order to improve the modeling performance. In general, the more clusters/rules are generated, the higher the computational cost to update and estimate the related antecedent and consequent parameters. Since the proposed AEF predictor uses fewer rules to reach high prediction accuracy, it will be more computationally efficient, which is a key for real-time health monitoring and prognostics applications.

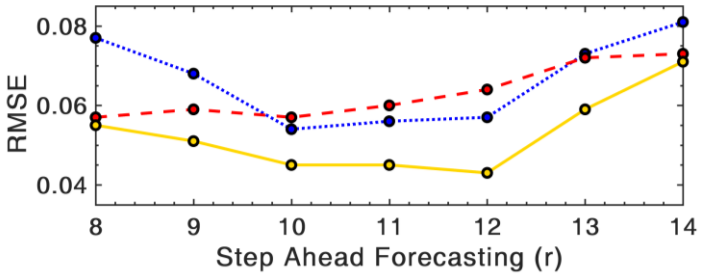

Fig. 4.9. Performance comparison in terms of RMSE using: eTS (blue dotted line), eFS (red dashed line), and AEF (yellow solid line).

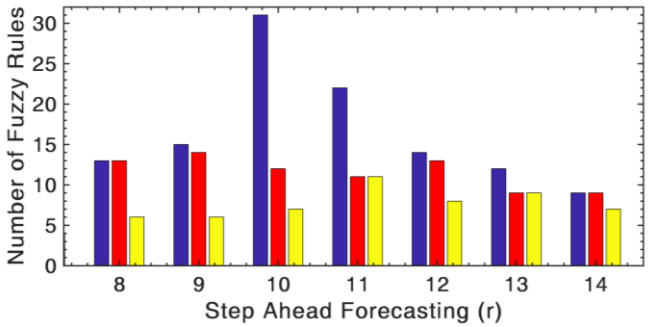

Fig. 4.10. Comparison of the generated rules using: eTS (blue column), eFS (red column), and AEF (yellow column), respectively.

4.5.2. Performance evaluation for the aPF algorithm

To examine the efficiency of the proposed aPF training algorithm, its performance will be compared with two classical training algorithms, such as the gradient descent (GD) and decoupled extended Kalman filter (DEKF) methods [111,120]. The goal is to optimize the antecedent parameters (i.e., the centers of the clusters) of the resulted AEF predictor models from the previous section. The training is performed offline over one epoch using 1600 data points, followed by the testing of 1000 data points to evaluate the recognized models. The learning rate for the GD is determined by trial-and-error (learning rate = 0.01 in this case), which is similar to that in [120] for the same data. Table 4.2 summarizes the performance over five runs of the training and testing stages in terms of RMSE for long-term predictions (i.e., 8, 9…. and 14 steps ahead). Figures 4.11 and 4.12 illustrate the training and testing error distribution as well as the standard deviation examples corresponding to 8-, 11- and 14-steps-ahead prediction, respectively. Figures 4.13 and 4.14 demonstrate the training and testing performance comparison of the related training techniques for 8-steps-ahead prediction, respectively.

Table 4.2. Comparison in terms of the averaged mean for the training RMSE, and testing RMSE.

No. of Steps	**GD**		**DEKF**		**aPF**	
	Training RMSE	Testing RMSE	Training RMSE	Testing RMSE	Training RMSE	Testing RMSE
8	0.046	0.053	0.042	0.051	0.039	0.044
9	0.041	0.084	0.028	0.033	0.026	0.031
10	0.037	0.048	0.044	0.070	0.037	0.047
11	0.036	0.049	0.032	0.041	0.033	0.040
12	0.037	0.047	0.035	0.057	0.029	0.034
13	0.054	0.099	0.054	0.112	0.049	0.063
14	0.084	0.108	0.070	0.092	0.059	0.074

It is clear that the proposed aPF training algorithm has the lowest RMSE during the training stage, in most cases. For example, it has a lower RMSE than DEKF, with about 10%, 15%, 20%, and 15% for 8-, 10-, 12-, and 14-steps-ahead predictions, respectively. In addition, RMSE values are approximately 15%, 40%, 20%, and 30% lower than the GD, for 8-, 9-, 12-, and 14-steps-ahead predictions, respectively. Similarly, the proposed aPF training algorithm outperforms related algorithms such as DEKF and GD under these testing conditions.

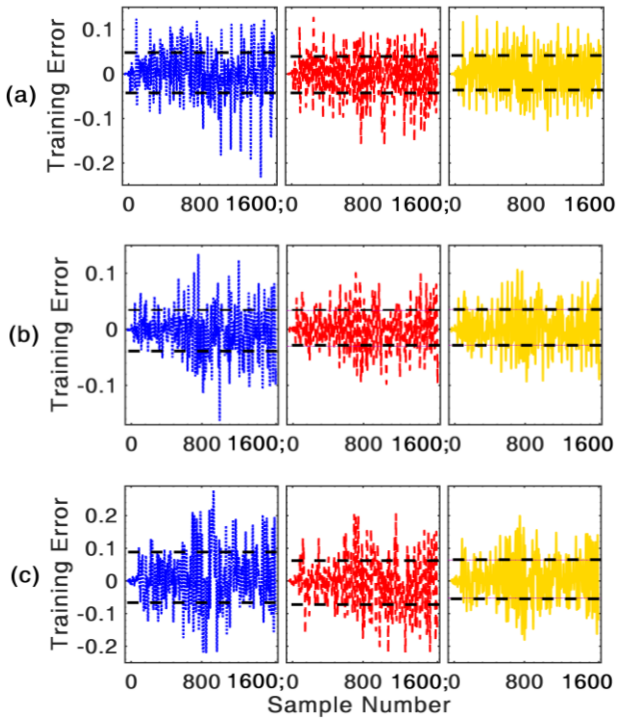

Fig. 4.11. Performance comparison in terms of training errors corresponding to: (a) 8-steps-ahead prediction, (b) 11-steps-ahead prediction, (c) 14-steps-ahead prediction. GD (blue dotted line), DEKF (red dashed line), and aPF (yellow solid line).

Test results conclude that the proposed aPF can maintain high modeling efficiency, and effectively tackle the over-fitting problem; this is because it can effectively explore the fuzzy rule spaces, and capture the high-likelihood region at the posterior PDF in order to reduce the trapping of possible local minima. Furthermore, the working mechanism of the aPF algorithm can effectively recognize the optimal location for fuzzy cluster/rule center, so as to achieve higher modeling efficiency with the current consequent parameters. On the contrary, the GD and DEKF methods perform inconsistently under different testing conditions; for example, the DEKF performs better than the GD under some training and testing condition such as 8-, 9-, and 14-steps-ahead predictions, while the GD outperforms DEKF in predictions with r = 10, and 13. This is due to the fact that the GD usually converges slowly, and is sensitive to training data noise, while the DEKF has limitations related to updating the covariance matrices in a nonlinear dynamic system.

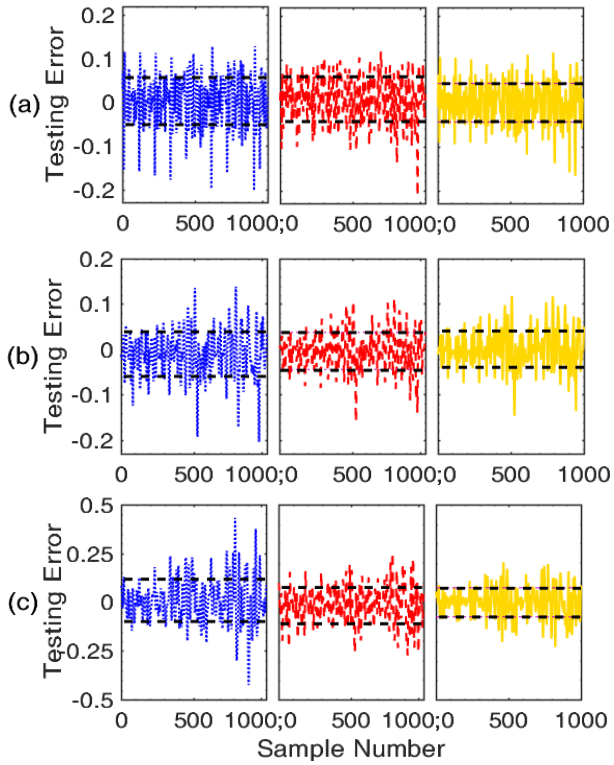

Fig. 4.12. Performance comparison in terms of testing errors corresponding to: (a) 8-steps-ahead prediction, (b) 11-steps-ahead prediction, (c) 14-steps-ahead prediction. GD (blue dotted line), DEKF (red dashed line), and aPF (yellow solid line).

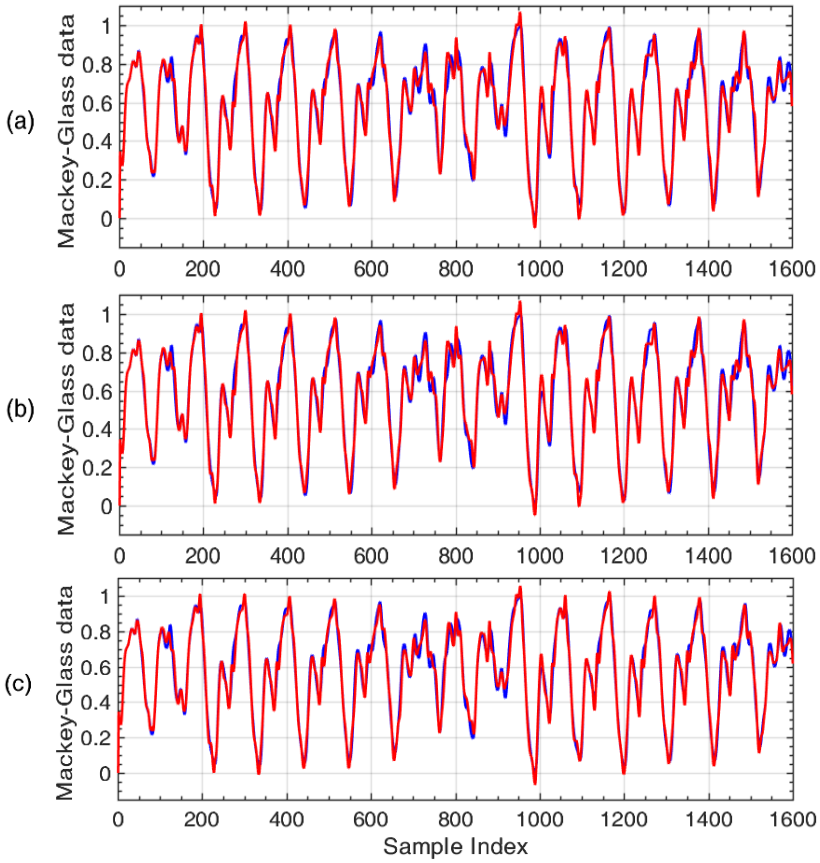

Fig. 4.13. Performance comparison of the related training techniques for 8-steps-ahead prediction training by (a); GD (b) DEKF; and (c) aPF; (blue lines: the actual data; red lines: the prediction performance).

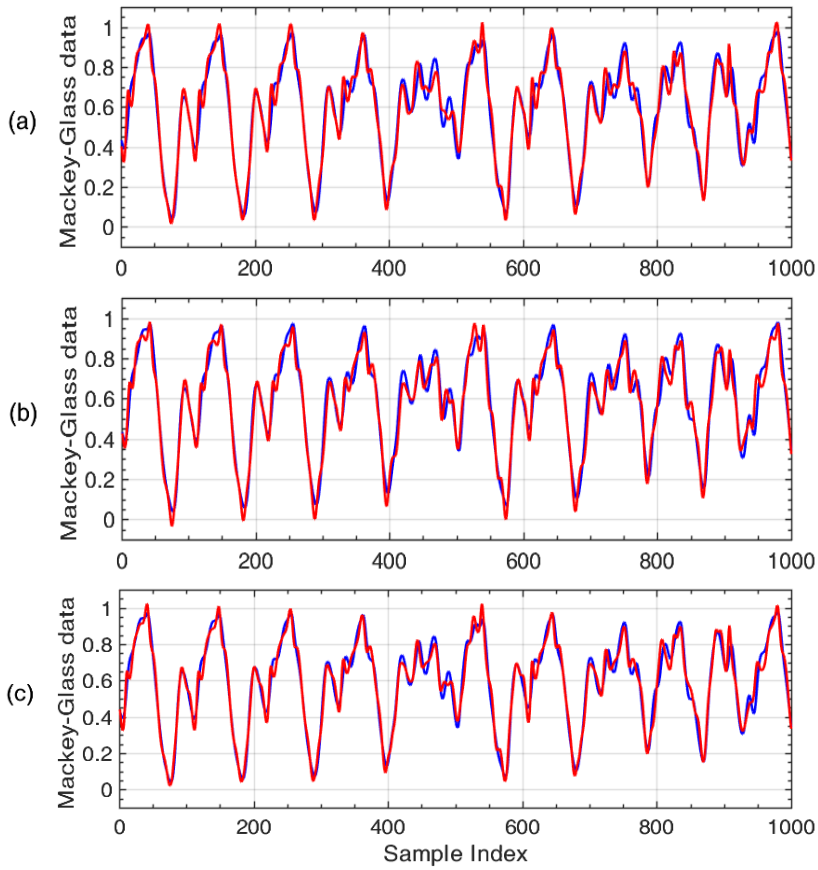

Fig. 4.14. Performance comparison of the related training techniques for 8-steps-ahead prediction testing by (a); GD (b) DEKF; and (c) aPF; (blue lines: the actual data; red lines: the prediction performance).

Furthermore, during the training process, the execution time is used to measure processing efficiency. Table 4.3 summarizes the execution time in seconds of the related training algorithms (i.e., aPF, DEKF, and GD). Test results show that the proposed aPF algorithm has the highest processing efficiency (i.e., the lowest execution time), which is about 15 times faster than other methods on average. This is because the aPF algorithm applies less particles to represent the high-likelihood region at the posterior PDF. In addition, it does not require resampling process at each iteration, which can further reduce computational time and required memory. In contrast, GD and DEKF algorithms have more complex working mechanisms, which require high computational costs at each iteration to update their parameters (i.e., gradient vectors, covariance matrices, observation error covariance matrices, etc.).

Table 4.3. Comparison in terms of training execution time for the related training techniques.

No. of Steps	GD	DEKF	aPF
	Time (sec)	Time (sec)	Time (sec)
8	7.206	6.072	0.401
9	7.149	6.389	0.424
10	7.516	6.436	0.471
11	8.044	7.216	0.626
12	7.689	6.733	0.549
13	7.515	7.498	0.563
14	7.243	7.764	0.535

4.6 Chapter Conclusion:

In this Chapter, an adaptive evolving fuzzy (or AEF) predictor has been proposed for long-term time series forecasting. In this AEF predictor, an error-assessment method is proposed to control the fuzzy cluster/rule generation. A queue data structure buffer is suggested and applied to monitor the trend of cumulative training errors. An adaptive particle filter (or aPF) training algorithm has been proposed to adaptively adjust the fuzzy cluster centers so as to improve modeling accuracy of the proposed AEF predictor. The effectiveness of the proposed AEF and aPF technologies has been verified through simulation tests using a commonly-used benchmark data. Test results have demonstrated that the proposed AEF predictor not only can generate a smaller number of clusters/rules to model the fuzzy rule spaces, but also can reach higher prediction accuracy. Due to its simpler processing mechanism and efficient aPF training, the AEF can be much faster, which is a benefit for online prediction in real-world applications.

In the next Chapter, the proposed AEF predictor will be integrated with the model-based EMPF method to further improve prognostics performance for Li-ion batteries.

CHAPTER 5

A HYBRID PROGNOSTIC FRAMEWORK FOR BATTERY HEALTH MONITORING AND RUL PREDICTION

5.1 Overview

As discussed in Chapter 1, compared with data-driven techniques, a PF-based prognostic method has its own advantages in Li-ion battery prognostics, including 1) modeling the underlying physics of battery SOH degradation processes; 2) making inferences about hidden states; and 3) ability to represent the uncertainty in the estimated state with less sensitivity to noise [1,5,10,25,26,123]. However, PF methods have limitations, such as: 1) sample degeneracy and impoverishment, which affect the estimation accuracy of the posterior PDF and RUL prediction [7,22,24,37,38]; and 2) difficulty in updating the posterior PDF during the prognostic period since no new measurement data are available [1,9,22,44,71,72]. To solve some of these PF problems, a model-based EMPF technique has been proposed in Chapters 2 and 3 for battery health prognosis. The EMPF applies a novel mutation approach to characterize the underlying physics of battery degradation. It can properly represent prediction uncertainty with its posterior PDF, and provide better state estimation than other related PF techniques. However, due to the lack of battery measurement information during the prognostic process, its RUL prediction errors increase as the prediction horizon becomes longer.

To deal with the lack of battery measurements during the prognostic process, a data-driven AEF predictor has been proposed in Chapter 4 for long-term time series prediction, which will gradually evolve its reasoning structure and tune its related parameters. Test results have demonstrated that the AEF predictor can effectively capture the characteristics of a dynamic system and has sufficient adaptive capability to deal with variations in operating conditions. However, it also has some shortcomings as a data-driven method, for example, it cannot make inferences about hidden states that are inaccessible to the sensors for measurement, and cannot properly model uncertainty associated with its predicted future values [1,23,121,122].

In general, both a model-based technique and a data-driven predictor have their own merits and unpreventable limitations. Their performance depends on the complexities of battery system dynamics, noise and uncertainties in operation, prediction horizon, and measurement availability [9,20]. A new hybrid prognostic framework will be developed in this Chapter to

integrate the merits of both model-based EMPF and data-driven AEF techniques, but will reduce their respective limitations. Specifically, the AEF will be used to predict the values of the battery degradation trend, and the EMPF will be applied to reduce modeling uncertainty and improve the accuracy of SOH and RUL prediction.

5.2 The Proposed Hybrid Prognostic Framework

The developed hybrid prognostics framework consists of two phases in processing, as illustrated in Fig. 5.1. In Phase 1, the model-based EMPF will be used to describe the evolution of the system state and to model battery degradation trend with time for battery SOH estimation; its model parameters are adaptively updated using the available battery measurement indicator values (e.g., capacity and impedance). On the other hand, the AEF predictor will be evolved using the available measured indicator values in a gradual but online manner, which will be used in Phase 2. The battery RUL will be predicted in Phase 2, during which there will be no new measurements. The formulated AEF in Phase 1 will be used to forecast measurement indicator values beyond the available window, which will be used by the model-based EMPF to track the battery's degradation trend. By this methodology, the EMPF will keep updating its posterior PDF to reduce uncertainty and forecast the degradation trend for RUL prediction. The details methodology of the proposed hybrid prognostic framework will be discussed in the following subsections.

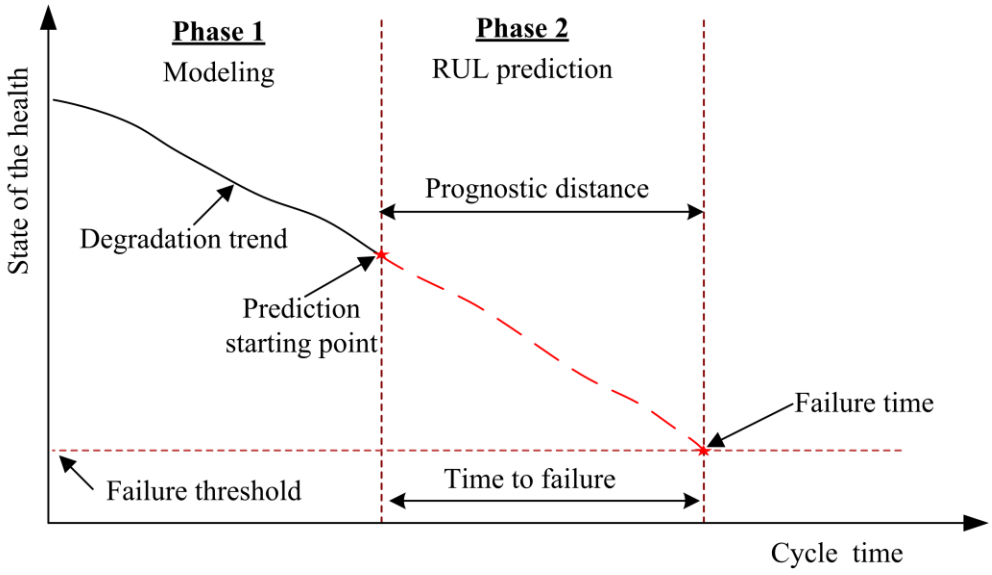

Fig. 5.1. Schematic diagram of the prognostics framework phases.

5.2.1 Phase 1: Degradation modeling (battery health monitoring):

The block diagram of degradation modeling processes is illustrated in Fig. 5.2. The monitoring data are available during Phase 1 period. The goal of the prognostic framework is to capture and track the battery degradation characteristics based on the available measurements so far. The model-based EMPF will use a degradation-prediction model (i.e., diagnosis model) to represent the battery's degradation progression during the battery's lifetime. It models the battery's health as a function of battery use condition (i.e., SOH), time duration (elapsed cycle), and model parameters (damage/aging behavior). The EMPF conducts state estimation based on the state transition and measurement (observation) models that can define the evolution of the system degradation behavior with time. The system state transition model as in Eq. (5.1) and the measurement or observation model in Eq. (5.2) will represent the mapping relation between the measured degradation indicator values and the degradation model parameters:

$$x_k = f_k(x_{k-1}, u_{k)} \tag{5.1}$$

$$y_k = h_k(x_k, v_k) \tag{5.2}$$

where x_k are the model parameters to be estimated; y_k are the battery degradation indicators (i.e., capacity and impedance) at k^{th} time instant; u_k and v_k are Gaussian white noise signals with zero mean.

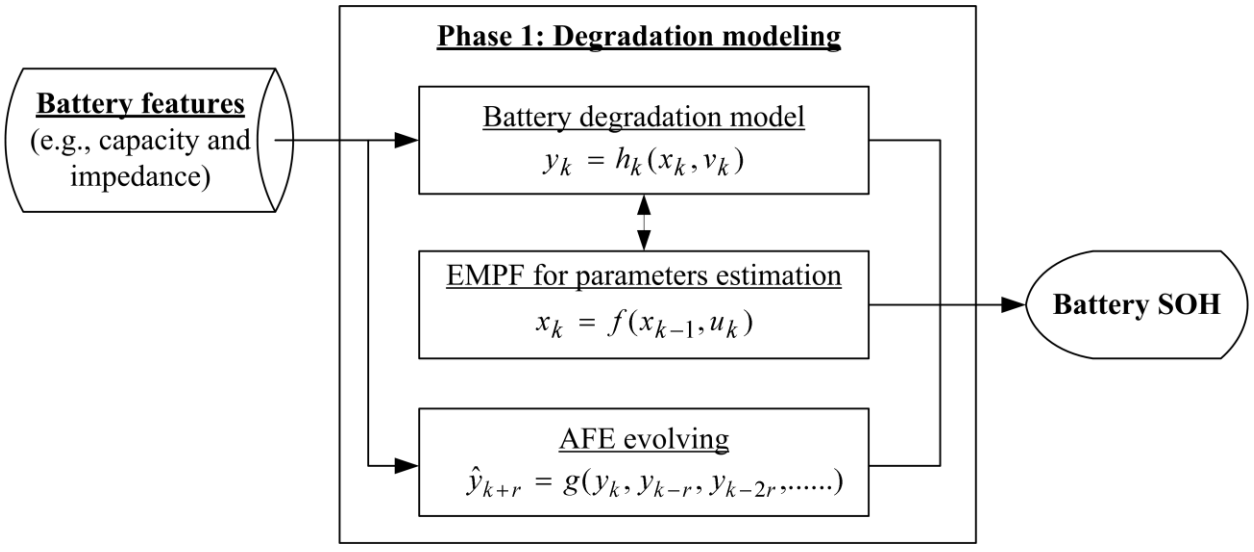

Fig. 5.2. Schematic diagram of degradation modeling phase in the prognostics framework.

The objective of the model-based EMPF is to perform battery state estimation with model parameters identified recursively as new observation becomes available. The EMPF can estimate the posterior PDF of the hidden state (i.e., model parameters) through some random samples (particles), where particle weights are continuously adjusted according to the likelihood of each particle from the new observation at that time instant. The updated/estimated posterior PDF can represent the high probability region for the system state whose PDF can characterize the expected uncertainty in the estimated result. The goal of this process is to use these available battery degradation indicator values to recognize the high-likelihood area on the system space in order to track the battery degradation trajectories and model the fault propagation with time.

Furthermore, the AEF predictor will be evolved in Phase 1 using the available battery measured indicator values (e.g., capacity and impedance) for long-term time series prediction. As discussed in subsection 4.3, the AEF predictor will be gradually evolved to describe the input-output mapping for *r*-steps-ahead prediction, and its related antecedent and consequent parameters will be recursively updated to enhance performance. The *r*-steps-ahead predicted value can be described as:

$$\hat{y}_{k+r} = g(y_k, y_{k-r}, y_{k-2r}, ...) \tag{5.3}$$

where $\hat{y}_{k+r}$ is the forecasted indicator value at the $(k+r)^{\text{th}}$ time instant; $\{ y_k, y_{k-r}, y_{k-2r}, ... \}$ are the available battery degradation indicator values in Phase 1; and $g(\bullet)$ denotes the AEF predictor.

Unlike other data-driven techniques used in the related hybrid prognosis frameworks such as [17,22,44,67,71-72], the AEF predictor in this work cannot only evolve its reasoning structure online to deal with the time-varying system dynamics and update its related parameters to improve modeling flexibility and accuracy. It can, however, maintain sufficient adaptive capability to capture and track the battery's degradation characteristics. In contrast, other related data-driven techniques apply fixed reasoning structures, and their parameters are usually trained offline using some historical data that may not reflect the current operating conditions. This can degrade the modeling efficiency by resulting in under-fitting, and reduce their adaptive capability in handling variations in operating conditions.

5.2.2 Phase 2: RUL prediction

Fig. 5.3 shows the processing procedures in Phase 2. The moment to trigger the battery RUL prediction is referred to as the starting point (Fig. 5.1). Then the recognized EMPF degradation-prediction model from Phase 1 will be used to forecast the battery RUL, or the time duration for the battery state to reach its threshold (i.e., 70% of the original battery SOH state). The formulated AEF predictor in Phase 1 will be applied to forecast the future measurement indicator values $(\hat{y}_{k+1}, \hat{y}_{k+2}, \hat{y}_{k+3}, ...\hat{y}_{k+r})$ in order to tackle the problem of lack of battery measurements during the prognostic process. Therefore, the EMPF can continuously update its posterior PDF to reduce modeling uncertainty and improve the accuracy of SOH and RUL prediction.

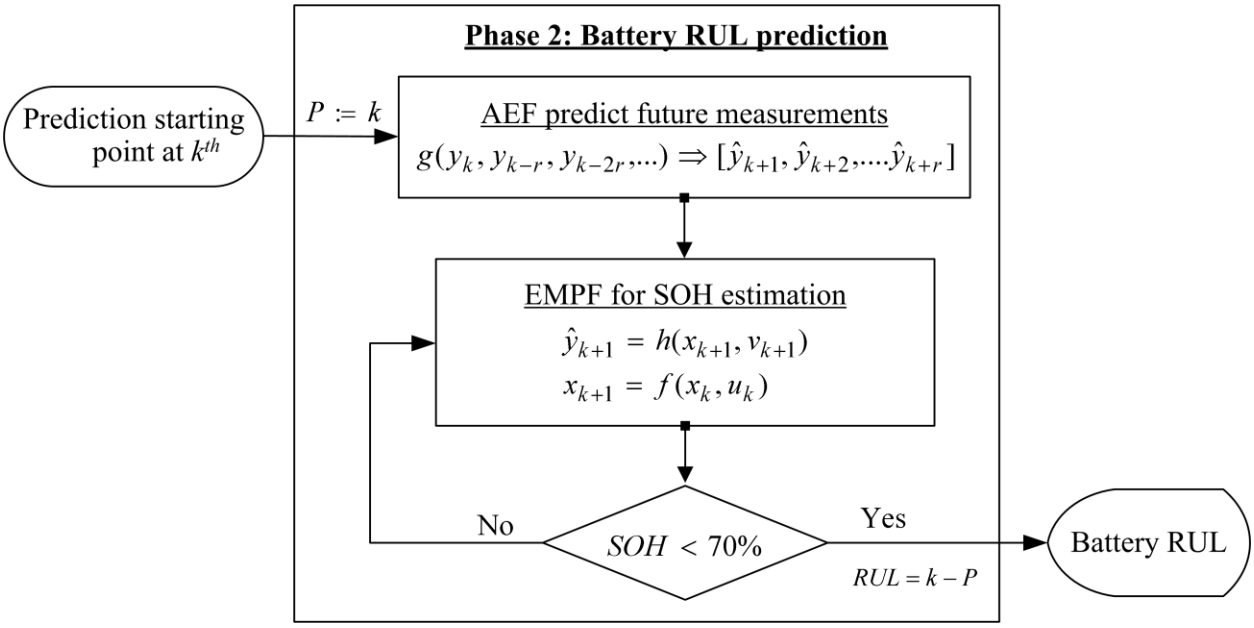

Fig. 5.3. Schematic diagram of the battery RUL prediction in the hybrid prognostics framework.

System RUL is usually conducted by modeling the fault propagation trend to estimate the time before failure. In Phase 2, the model-based EMPF will firstly perform a one-step-ahead prediction to forecast the degradation state distribution (i.e., the predicted PDF) of the next time step or $(k+1)$, using the posterior PDF of the current state (i.e., the initial PDF). The particles that shape the current posterior PDF will be propagated using the state transition model in Eq. (5.1) to form the predicted PDF. Then, as discussed in subsection 2.3, the unique mutation

approach in the EMPF will recursively update the new posterior PDF (i.e., predicted PDF) based on the likelihood of each particle, as illustrated in Fig. 5.4.

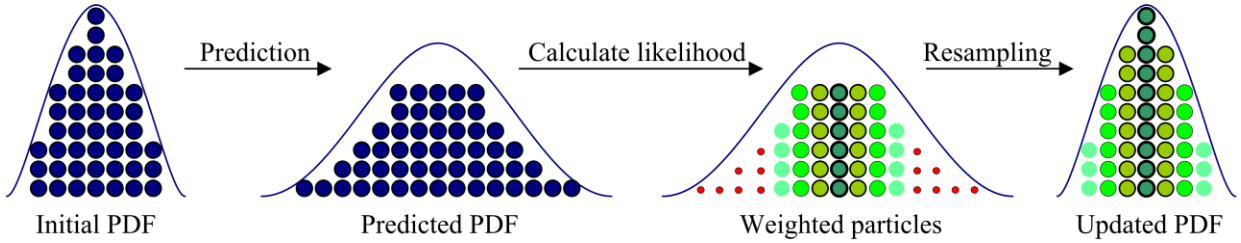

Fig. 5.4. Illustration of the EMPF operations for updating the posterior PDF.

The propagation operation in Fig. 5.4 will be repeated a number of times to forecast the degradation trend and identify the moment when the battery SOH reaches its end-of-life threshold for RUL prediction. In general, the posterior PDF of the current state (related to the initial PDF) is considered to be the core element in this prognostic process. Using the predicted indicator values by the AEF predictor to update the posterior PDF at each time step in Phase 2 will force particles to shift/focus to areas with high-likelihood, which could reduce modeling uncertainty and result in more accurate predictions. In general, a PDF with a narrower and taller distribution would have more precise predictions [1,7,20,23]. Fig. 5.5 illustrates a comparison of the PDF properties using this developed hybrid prognostics framework versus that using a single model-based EMPF.

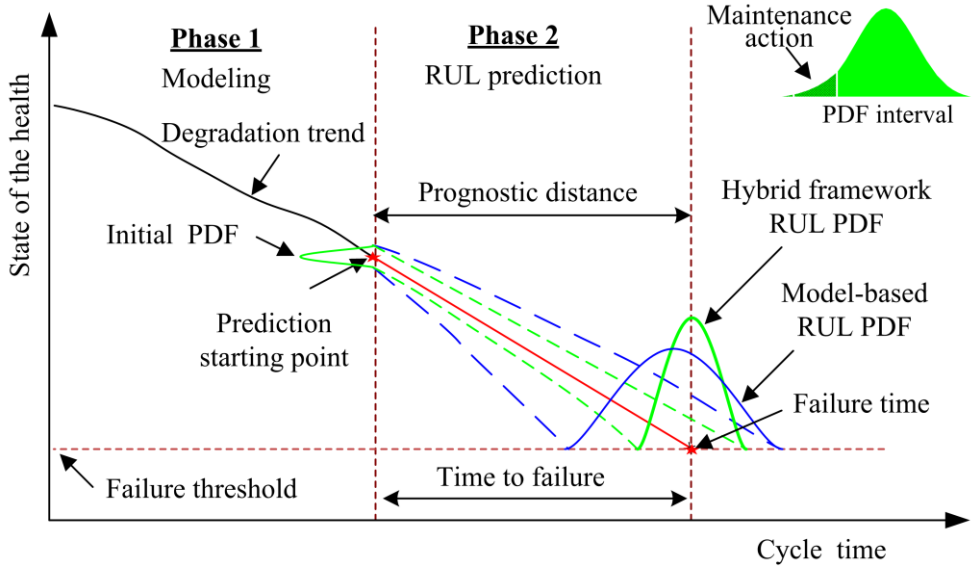

Fig. 5.5. Illustration of uncertainty in the form of the PDF in the phase of RUL prediction.

5.3 Performance Evaluation for Battery RUL Prediction

The effectiveness of the developed EMPF and AEF hybrid prognosis framework, denoted as EMPF-AEF, will be examined in this section for battery SOH monitoring and RUL prediction. This testing will be conducted using the same datasets as used in Chapter 3 (i.e., battery datasets and prediction starting points). It will investigate the framework's reliability to deal with the problem of no measurements during the prognostic process in Phase 2, and the uncertainty associated with its RUL prediction in the form of PDF distribution. Its performance will be compared with the related PF methods:

1) the quantum particle swarm optimization-based PF (QPSO), which is a population-based swarm intelligence algorithm [43].

2) the hybrid method of QPSO integrated with a data-driven technique: adaptive neuro-fuzzy inference system (ANFIS) [124], denoted as QPSO-ANFIS in this test.

Since the AEF predictor is a data-driven technique that cannot express uncertainty associated with its processing result in the form of probability as discussed in subsection 1.3.3, it will be excluded from the comparison as an individual method.

In investigating battery SOH for RUL prediction, the battery capacity is usually used as a degradation indicator in many studies [10,21,22,31-33,35], which can be calculated by integrating the battery current over time. In this test, the empirical degradation model in Eq. (5.4) will be used to model the Li-ion battery physics, which can consider the reduction in battery capacity as well as the battery's self-recharge behavior [2,31,40,43]. The battery capacity can be converted to the SOH in a unified form in Eq. (5.5) :

$$C_{k+1} = \eta_c C_k + b_1 \exp\left(-\frac{b_2}{\Delta t_k}\right) \tag{5.4}$$

$$S_{k+1} = \frac{C_{k+1}}{C_0} \times 100 \tag{5.5}$$

where η_c is the Coulombic coefficient ($\eta_c = 0.997$ in this case); C_k is the charging capacity at the k^{th} cycle; C_0 is the initial capacity at the time $k = 1$; b_1 and b_2 are the parameters to be estimated; S_k is the battery SOH at the k^{th} cycle; and $\Delta_{t_k} = t_{k+1} - t_k$ is the rest time interval from the k^{th} cycle to the $(k+1)^{\text{th}}$ cycle ($\Delta_{t_k} = 1$ in this case).

In this test, the number of particles is selected to be 200, which is similar to that in the QPSO-PF in [43] to ensure a fair comparison. To compare the performance of the related methods, testing is performed over 50 times, using data of battery #5 from the NASA battery prognostic data [89], which reaches its failure threshold at cycle 162. The test comparison is in terms of the accuracy of modeling and RUL forecasting. The time moments to trigger the prediction are selected at 86, 106, 126, and 146 cycles, respectively, which will cover different battery SOH conditions and represent long-term, medium-term, and short-term predictions. Table 5.1 summarizes the average mean and standard deviation values of RMSE over 50 test runs. Fig. 5.6 shows the comparison of the related techniques, corresponding to different prediction starting points (i.e., 86, 106,126, and 146) over 50 random runs.

Table 5.1 Average mean and standard deviation of RMSE over 50 runs.

Prediction starting point	Method	Averaged mean of RMSE	Standard deviation of RMSE
86	**QPSO-PF**	0.035	0.003
	QPSO-ANFIS	0.017	4.827×10^{-5}
	EMPF-AEF	0.015	4.596×10^{-5}
106	**QPSO-PF**	0.019	0.002
	QPSO-ANFIS	0.014	5.117×10^{-5}
	EMPF-AEF	0.013	4.311×10^{-5}
126	**QPSO-PF**	0.016	0.001
	QPSO-ANFIS	0.013	3.688×10^{-5}
	EMPF-AEF	0.008	3.532×10^{-5}
146	**QPSO-PF**	0.012	4.584×10^{-4}
	QPSO-ANFIS	0.006	7.003×10^{-5}
	EMPF-AEF	0.004	3.246×10^{-5}

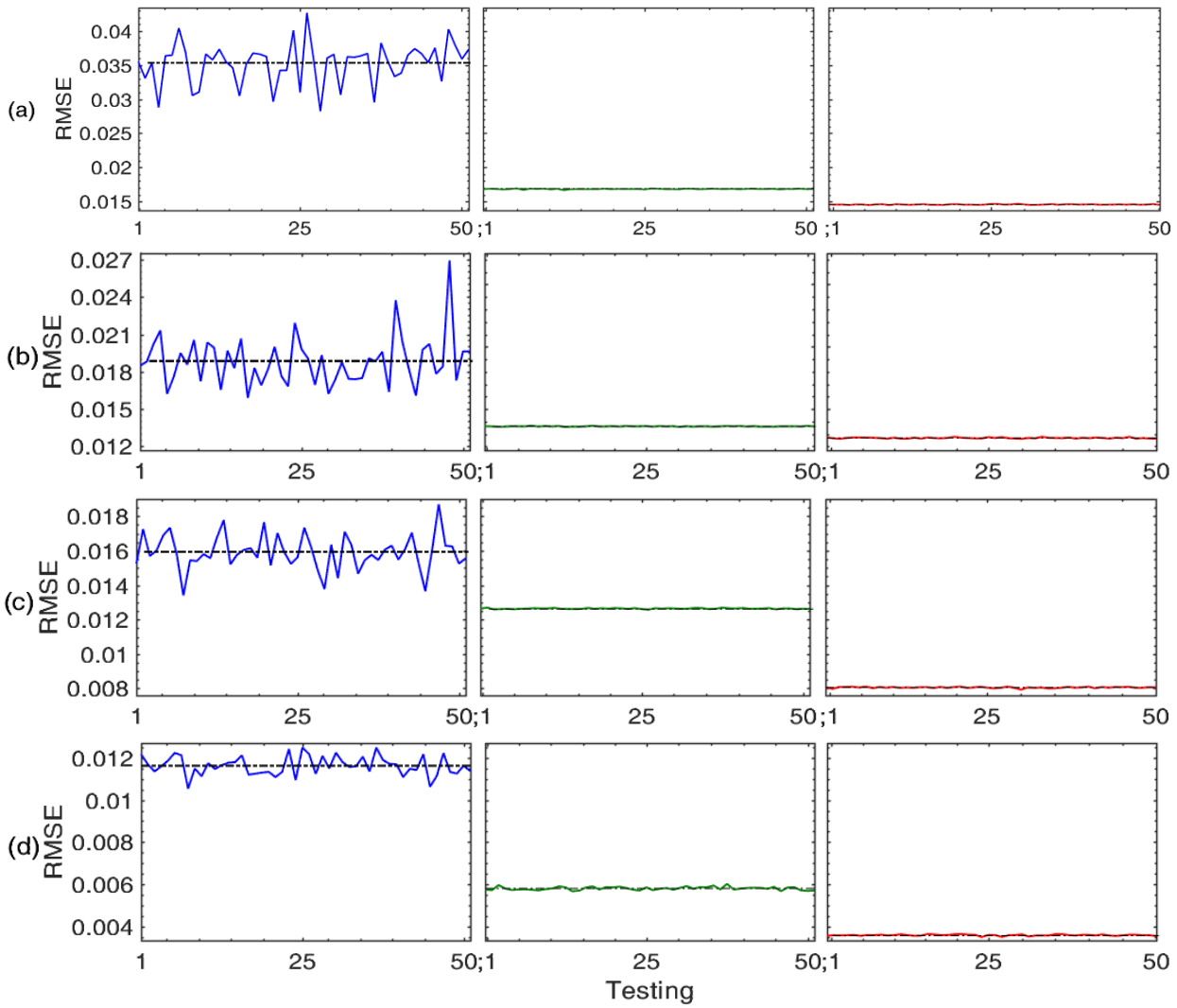

Fig. 5.6. Performance comparison (the average RMSE over 50 runs) corresponding to different prediction starting point: (a) 86, (b) 106, (c) 126, and (d) 146, using QPSO-PF (blue line), QPSO-ANFIS (green line), and EMPF-AEF (red line).

The RMSE can be reduced as the prediction period becomes shorter using all related techniques. The QPSO-ANFIS outperforms the QPSO-PF, because the ANFIS predictor keeps updating the model parameters during the prediction period. The developed EMPF-AEF framework performs best under all testing conditions; for example, it is approximately 60%, 30%, 50%, and 65% lower in RMSE than QPSO-PF, as well as 10%, 8%, 40%, and 30% lower than the QPSO-ANFIS, corresponding to prediction starting points at 86, 106, 126 and 146, respectively. This is because the proposed EMPF-AEF framework can effectively integrate the strengths of both the EMPF and AEF techniques in modeling the underlying physics of battery health degradation.

In this case, the EMPF can alleviate the impact of sample degeneracy and impoverishment for better system state estimation. In addition, it can properly represent the high-likelihood region of the posterior PDF to track battery dynamic behavior and to forecast the degradation state distribution, which is the key aspect to achieve high-performance prediction. The unique evolving mechanism of the AEF predictor can effectively capture the battery dynamic characteristics even using the limited available battery data in Phase 1, due to its adaptive capability to adjust its reasoning structures and parameters to minimize the impact of uncertainties. The model-based EMPF in Phase 2 can properly update its posterior PDF using the predicted indicator values by the AEF and improve RUL prediction performance under all testing conditions. Furthermore, the small standard deviation of the RMSE using the proposed EMPF-AEF framework can demonstrate its robustness under different operating conditions.

Processing efficiency (i.e., execution time) plays a key role in real-time system monitoring applications, which can be an indicator of the computing complexity of the related techniques. Table 5.2 summarizes the average execution time using the related techniques, which are measured under the same testing conditions over 50 random runs using the same observation datasets. Fig. 5.7 schematically compares the average execution time using the related methods, corresponding to different prediction starting points (i.e., 86, 106,126 and 146), over 50 random runs. It is seen that execution time increases significantly for both the QPSO-PF and the QPSO-ANFIS as the prediction period becomes shorter; it is because the extra available data have to be processed for modeling and forecasting. In addition, the QPSO-PF duplicates its particle numbers using a wave function to reduce sample degeneracy and impoverishment, which takes longer time for processing.

The QPSO-ANFIS framework takes even longer execution time than the QPSO-PF in modeling and ANFIS training. In contrast, the developed EMPF-AEF framework uses the shortest execution time, or it is about 4 times faster than the QPSO-PF (1.309 sec vs. 5.794 sec, 1.598 sec vs. 7.469 sec, 1.678 sec vs. 8.600 sec, 1.739 sec vs. 9.813 sec), and almost 7 times faster than the QPSO-ANFIS framework (1.309 sec vs. 10.579 sec, 1.598 sec vs. 11.196 sec, 1.678 sec vs. 11.720 sec, 1.739 sec vs. 13.404 sec). This is because the EMPF uses a dynamic feedback mechanism to guide the search of the high-likelihood region at the posterior PDF, as discussed in subsection 2.3.1; its selection scheme can also accelerate the recognition of low-weight particles to reduce sample degeneracy as discussed in subsection 2.3.2. In addition, the

AEF predictor can map the input-output spaces with fewer clusters/rules, which in turn can speed up the training process.

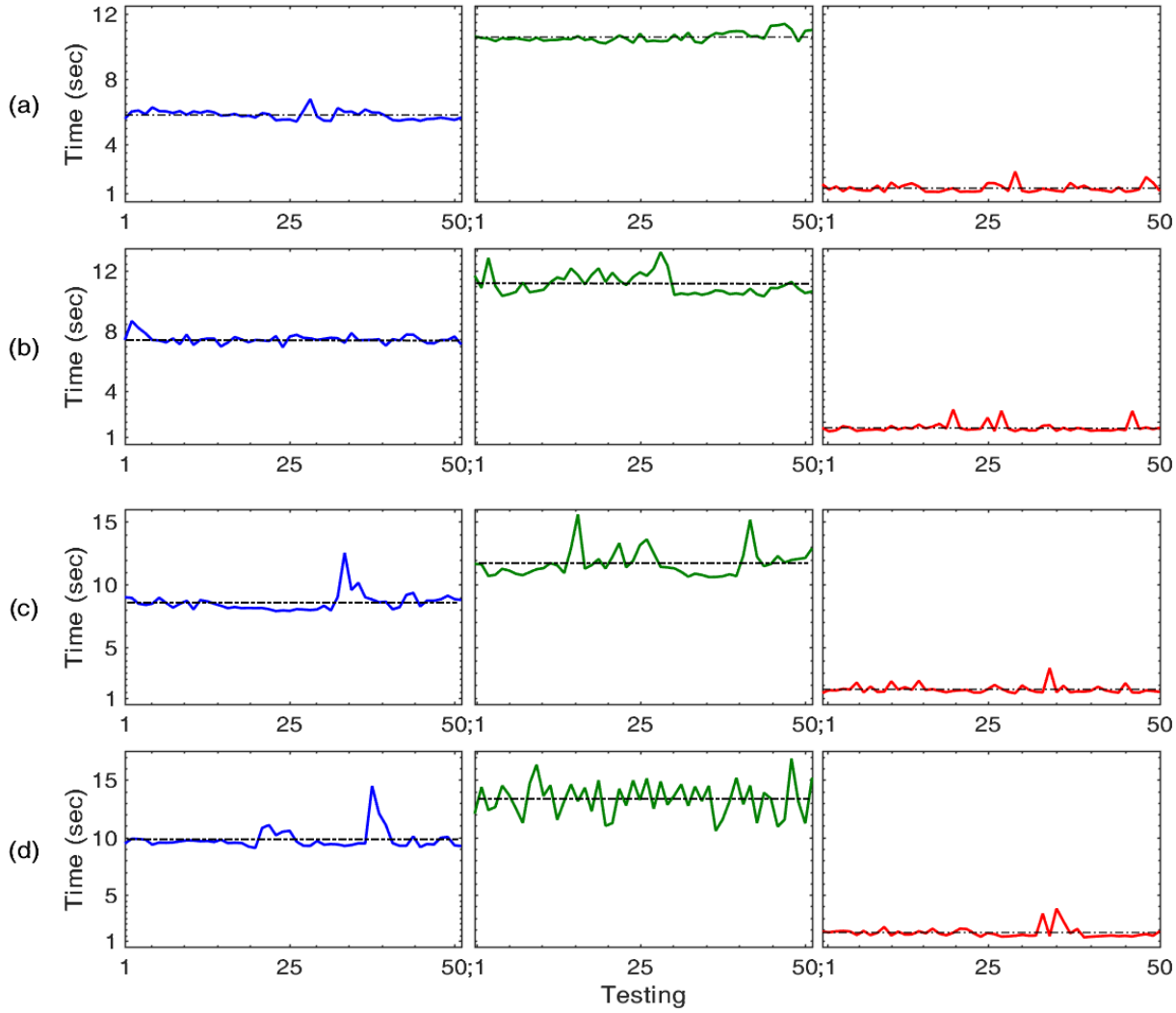

Fig. 5.7. Comparison of the average execution time over 50 runs corresponding to different prediction starting point: (a) 86, (b) 106, (c) 126, and (d) 146, using QPSO-PF (blue line), QPSO- ANFIS (green line), and EMPF-AEF (red line).

Table 5.2 The average execution time of the related methods over 50 runs.

Prediction starting point	Method	Time (sec)
86	**QPSO-PF**	5.794
	QPSO-ANFIS	10.579
	EMPF-AEF	1.309
106	**QPSO-PF**	7.469
	QPSO-ANFIS	11.196
	EMPF-AEF	1.598
126	**QPSO-PF**	8.600
	QPSO-ANFIS	11.720
	EMPF-AEF	1.678
146	**QPSO-PF**	9.813
	QPSO-ANFIS	13.404
	EMPF-AEF	1.739

Table 5.3 summarizes the results for the battery RUL prediction using the related techniques, which also includes the RUL PDF interval, relative errors, and prediction starting points. Fig. 5.8 outlines the performance of the related methods for SOH estimation and RUL prediction with prediction starting at cycle 86 (over 80 cycles). Figures 5.9 and 5.10 show the zoomed results for the medium-term and short-term predictions, starting at 106 and 126 cycles, respectively. It is seen that the QPSO-PF has the lowest prediction accuracy (with the highest errors) under all testing conditions because it cannot update model parameters during the prediction operation, even though its performance can be improved for short-term predictions. The QPSO-ANFIS framework performs better than the QPSO-PF because the ANFIS can adaptively predict the degradation indicator values during the prognostic process (Phase 2) to update the degradation model in RUL prediction. On the other hand, the QPSO-ANFIS could not

generate clear improvement as the prediction length becomes shorter and more data are used in modeling in Phase 1, when the prediction starts at cycle 106 and 126, respectively. This is because the ANFIS predictor has limited adaptive capability due to its fixed reasoning structure, which could limit its ability to deal with electro-chemical battery system conditions.

Table 5.3 Summary of the prediction results of the related methods

Prediction starting point	Method	Prediction result (cycle)	RUL-PDF interval	Absolute error (cycles)	Relative error
86	**QPSO-PF**	140	92-166	22	13.58%
	QPSO-ANFIS	152	151-153	10	6.17%
	EMPF-AEF	159	158-162	3	1.85%
106	**QPSO-PF**	146	109-166	16	9.88%
	QPSO-ANFIS	155	154-156	7	4.32%
	EMPF-AEF	159	158-161	3	1.85%
126	**QPSO-PF**	148	123-166	14	8.64%
	QPSO-ANFIS	154	156-161	8	4.94%
	EMPF-AEF	155	153-157	7	4.32%
146	**QPSO-PF**	152	139-166	10	6.17%
	QPSO-ANFIS	164	163-165	2	1.24%
	EMPF-AEF	162	161-163	0	0.00%

In contrast, the developed EMPF-AEF framework performs the best in RUL prediction under all testing conditions, which is approximately 30%, 40%, and 10% more accuracy than QPSO-ANFIS with prediction starting points at 86, 106, and 126, respectively. The AEF predictor in the proposed EMPF-AEF framework has advanced adaptive capability to accommodate dynamic battery conditions, by updating not only its parameters like the ANFIS,

but also its reasoning architectures. Therefore, it can model battery dynamics and track its degradation characteristics more accurately.

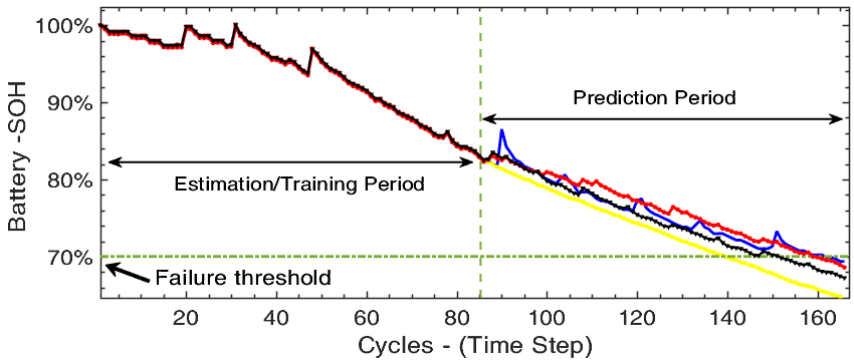

Fig. 5.8. Performance comparison of the estimated and predicted SOH for long-term prediction (over 80 cycles) using: QPSO-PF (■—yellow line), QPSO-ANFIS (▽—black line), EMPF-AEF (•—red line), and actual states (blue line).

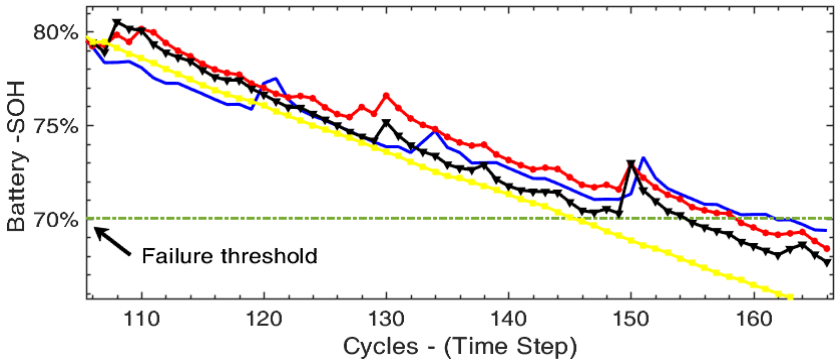

Fig. 5.9. Zoomed performance comparison for prediction period of medium-term prediction (over 60 cycles) using: QPSO-PF (■—yellow line), QPSO-ANFIS (▽—black line), EMPF-AEF (•—red line), and actual states (blue line).

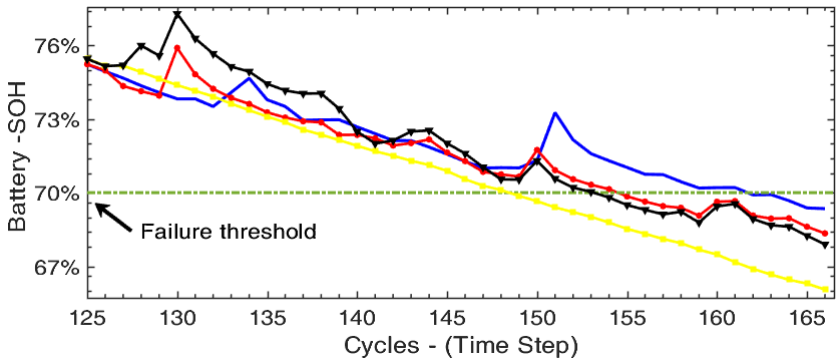

Fig. 5.10. Zoomed performance comparison for prediction period of short-term prediction (over 40 cycles) using: QPSO-PF (■—yellow line), QPSO-ANFIS (▽—black line), EMPF-AEF (•—red line), and actual states (blue line).

In machinery health management and prognostics, the reliable RUL prediction information can be used to schedule the predictive maintenance and repair operations [23,121,122]. In this work, the confidence interval associated with the RUL estimation will be represented in the form of the PDF distribution (i.e., PDF interval), where a lower interval indicates less uncertainty and more reliability [7,121,122]. In other words, the more accurate RUL prediction (with less uncertainty) corresponds to a PDF with a narrower and taller distribution, as illustrated in Fig. 5.5. The processing uncertainty of each technique can be characterized by using the PDF in the RUL prediction as the state reaches the battery's end-of-life threshold. Table 5.3 above summarizes the RUL PDF intervals of the upper and lower bounds of the posterior PDF distributions. Figures 5.11 and 5.12 illustrate the PDFs of the related techniques for predictions starting at cycle 106 and 146, respectively, which are approximated using the kernel density method [43]. It can be seen that the PDF of the proposed EMPF-AEF framework has narrower and taller distributions than other related techniques, which can attest to its better robustness and modeling efficiency to represent the region of the posterior PDF due to its enhanced mutation approach, as discussed in subsection 2.3.1.

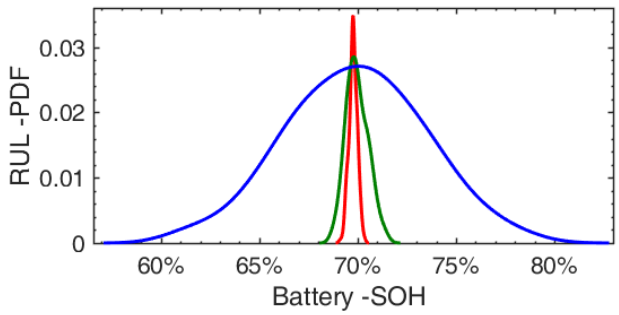

Fig. 5.11. Comparison of the uncertainty of the RUL prediction for medium-term prediction (over 60 cycles) using: QPSO-PF (black line), QPSO-ANFIS (blue line), EMPF-AEF (red line).

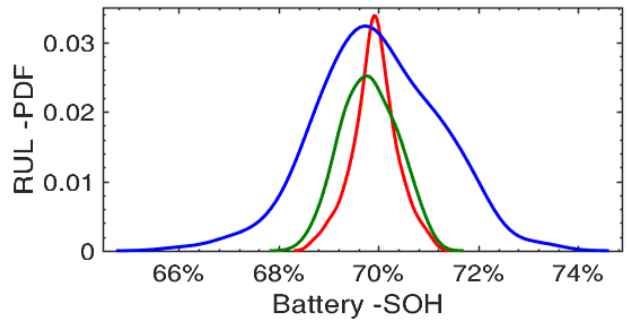

Fig. 5.12. Comparison of the uncertainty of the RUL prediction for short-term prediction (over 20 cycles) using: QPSO-PF (black line), QPSO-ANFIS (blue line), EMPF-AEF (red line).

In comparison, the QPSO-PF method has a wider PDF distribution, which becomes even wider as the prediction horizon becomes longer. This is because it duplicates particles to represent a wider area of the posterior PDF, without a mechanism to guide its particles to the high-probability area of the posterior PDF. Although the QPSO-ANFIS framework has a narrower PDF distribution than that of QPSO-PF, its distribution is slightly skewed because the resampling process would select particles with high weights many times, resulting in more particles concentration to some area. This degraded diversity on the PDF distribution could affect the RUL prediction when the mean values are used.

5.4 Chapter Conclusion

In this Chapter, a new hybrid prognostic framework has been developed to integrate the model-based EMPF and the data-driven AEF to improve modeling accuracy and RUL prediction reliability. The developed hybrid prognostics framework involves two phases of operation. In Phase 1, the battery health degradation is modeled by the EMPF, and the AEF predictor is formulated using the available battery measurement indicator values. The RUL prediction is undertaken in Phase 2, where the EMPF will perform successive one-step prediction by propagating the posterior PDF of the current state to forecast the state distribution at the future time. The forecast indicator values by the AEF predictor will then be used by the EMPF to recursively update its posterior PDF to reduce modeling uncertainty. This process is repeated a number of times to describe the evolution of the battery degradation state to predict when the battery SOH will reach the end-of-life threshold. The effectiveness of the proposed framework has been examined through simulation tests in terms of convergence, modeling accuracy and processing efficiency.

CHAPTER 6

CONCLUSIONS AND FUTURE WORK

6.1 Conclusions

The Li-ion battery is one of the greatest advances in energy-storage technology, which has been commonly used in engineering applications, such as electric vehicles. However, the Li-ion battery's performance degrades over time due to problems such as aging-related capacity degradation and impedance growth. These consequences affect the battery's performance, and may result in system breakdowns as well as safety issues in applications such as passenger vehicles. Although many techniques have been developed in the literature for Li-ion battery health monitoring and RUL prediction, it is still challenging to accurately capture and model the electro-chemical behaviors of the Li-ion battery, whose properties vary with environmental (e.g., humidity and temperature) and operating (e.g., load and speed) conditions. Besides, its nonlinear degradation features are almost inaccessible to measure using general sensors. Therefore, the uniqueness of a Li-ion battery system makes it difficult to achieve reliable prognostics performance using these existing methods, which may have succeeded in other health assessment and prognostics fields (e.g., machinery).

For example, the PF-based prediction methods are applied to battery health monitoring and RUL prediction in many studies due to the capability of the PF algorithm to properly deal with the battery nonlinear degradation features, and because it is less sensitive to noise and model complexity. However, these methods have suffered from limitations related to sample degeneracy and impoverishment, which can prevent these methods from properly representing the posterior PDF to capture the battery degradation dynamics. Another limitation is that the posterior PDF cannot be updated during the prognostic period since no new measurements are available, which can degrade the prognostic performance, especially for long-term predictions. Therefore, it is extremely important to effectively eliminate the impact of these limitations to have more reliable and robust performance to diagnose the battery's SOH and predict the RUL.

To tackle these aforementioned challenges, in this PhD work, a model-based EMPF technique has been proposed to tackle some limitations of the current PF methods such as being

unable to effectively recognize low-weight particles in the posterior PDF (sample degeneracy), lack of particle diversity in the posterior PDF space, and inability to deal with possible outlier particles on the posterior PDF distribution. A new mutation approach has been proposed to process low-weight particles and reduce sample degeneracy. A new selection mechanism has been suggested to improve particles diversity and guide the mutation approach to locate the high-likelihood area in the posterior PDF space, while an outlier detection method is introduced to identify and process outlier particles. Test results have shown that the EMPF technique can enhance the posterior PDF representation, and alleviate the impact of sample degeneracy and impoverishment. In addition, it can effectively capture the battery SOH degradation dynamics and track system characteristics for RUL prediction. Furthermore, the EMPF technique can also characterize the uncertainty of RUL prediction in the form of PDF instead of a single value as is the case in data-driven techniques.

Also, in this PhD work, an AEF technique has been developed for long-term time series forecasting, to deal with the lack of battery measurements during the prognostic period in the model-based EMPF. The AEF is new in two aspects: 1) An error-assessment method is suggested to control the fuzzy cluster evolving process; 2) an adaptive particle filter optimization algorithm is proposed to enhance incremental learning and improve modeling efficiency. Its effectiveness has been examined by simulations using the common benchmark dataset in this research and development field (i.e., Mackey-Glass). Test results have demonstrated that the AEF predictor can generate a smaller number of clusters/rules to map the input-output spaces, and can provide more flexibility in fuzzy modeling to deal with the time-varying system dynamics.

In general, both a model-based technique and a data-driven predictor have their own merits and unpreventable limitations. For example, the EMPF technique cannot update its posterior PDF during the prognostic period since no new measurements are available to compute the battery's degradation feature/indicator. Therefore, its RUL prediction errors increase as the prediction horizon becomes longer. On the other hand, the AEF predictor has some drawbacks as a data-driven technique: 1) it cannot make inferences about hidden states that are inaccessible to the sensors for measurement; 2) it cannot properly model uncertainty associated with its predicted future values. To bridge the gap between both techniques and tackle these

aforementioned drawbacks. In this PhD work, a new hybrid prognostic framework for battery health monitoring and RUL prediction has been developed to provide a more reliable tool for battery health prognosis and management in electric vehicles. It has integrated the merits of both model-based EMPF and data-driven AEF techniques, and attempts to reduce their respective limitations.

The developed hybrid prognostics framework consists of two phases in processing. In Phase 1, the EMPF is used to model the evolution of the system degradation state for battery SOH estimation. At the same time, the AEF predictor is gradually evolved using the available measured indicator values. The RUL prediction is performed in Phase 2, in which the formulated AEF in Phase 1 is used to forecast measurement indicator values beyond the available window to tackle the lack of measurements during the prediction stage. The model-based EMPF will propagate the posterior PDF of the current state to forecast the state distribution in the future. The EMPF will then use the forecasted indicator values by the AEF to update the EMPF posterior PDF. This propagated procedure will be repeated several times to forecast the degradation trend and identify the RUL of the battery. The effectiveness of the developed hybrid prognostic framework has been examined by simulation tests using NASA battery prognostic data under different conditions over 50 runs. Test results reveal that the developed hybrid prognostic framework can effectively deal with the lack of measurements during the prognostic process in Phase 2. It can properly solve some limitations of the current prognostic techniques such as the effect of sample degeneracy in the SOH estimation accuracy, fixed reasoning architectures, and reduce the level of uncertainty associated with the prediction results. Besides its improved reliability in SOH and RUL prediction, it can clearly improve the computation efficiency with low computational costs, and has great potential to be used for battery health monitoring and prognosis in electric vehicles.

6.2 Future Work

Advanced research can be undertaken to cover the following topics:

1) Develop new Li-ion batteries datasets when the battery research facility will be available at Dr. Wang's research lab. The tests will be undertaken corresponding to battery cells

and modules under different operating conditions in terms of load and speed for advanced research and development in order to further improve battery performance.

2) Develop new data-driven intelligent classifiers and efficient machine learning algorithms to improve SOC and SOH analysis accuracy and to further improve the adaptive capability to accommodate different electric vehicle operating conditions.

3) Develop new soft-computing tools that can fuse battery system information received from various sources to capture the characteristics of the system's dynamic. For example, the principal component analysis can be used to decompose multidimensional extracted features (e.g., voltage, current and impedance) into several independent source signals. Then some soft-computing tools will be used to model these multi-source signals, which can enrich the input-output mapping process for accurately capturing the battery degradation characteristics.

4) Implement the developed hybrid prognostic framework in real battery applications at both the cell and module levels.

REFERENCES

[1] H. Meng and Y.-F. Li, ‘‘A review on prognostics and health management (PHM) methods of lithium-ion batteries,’’ *Renew. Sustain. Energy Rev*., vol. 116, pp. 1–12, 2019.

[2] H. Tian, P. Qin, K. Li, and Z. Zhao, “A review of the state of health for lithium-ion batteries: Research status and suggestions,” *J. Cleaner Prod*., vol. 261, Art. no 120813, 2020.

[3] M. S. H. Lipu, M. A. Hannan, A. Hussain, M. M. Hoque, P. J. Ker, M. H. M. Saad, and A. Ayob, ‘‘A review of state of health and remaining useful life estimation methods for lithium-ion battery in electric vehicles: challenges and recommendations,” *Journal of Cleaner Production*, vol. 205, pp. 115-133, 2018.

[4] Y. Wang, B. Liu, Q. Li, S. Cartmell, S. Ferrara, Z.D. Deng, and J. Xiao, “Lithium and lithium-ion batteries for applications in microelectronic devices: review,” *J. Power Sources.*, vol. 286, pp. 330-345, 2015.

[5] J. Zhang and J. Lee, “A review on prognostics and health monitoring of Li-ion battery,” *J. Power Sources*, vol. 196, no. 15, pp. 6007–6014, 2011.

[6] C. Lin, A. Tang, H. Mu, W. Wang and C. Wang, “Aging Mechanisms of Electrode Materials in Lithium-Ion Batteries for Electric Vehicles,” *Journal of Chemistry,* vol. 2015, pp. 1-11, 2015.

[7] D. Li, W. Wang and F. Ismail, “A mutated particle filter technique for system state estimation and battery life prediction,” *IEEE Trans. Instrum. Meas*., vol. 63, no. 8, pp. 2034-2043, 2014.

[8] Z. Zhang, X. Si, C. Hu and M. Pecht, “A Prognostic Model for Stochastic Degrading Systems with State Recovery: Application to Li-Ion Batteries,” *IEEE Trans. Reliab.*, vol. 66, no.4, pp.1293–1308, 2017.

[9] M. Kordestani, M. Saif, M. Orchard, R. Razavi-Far, and K. Khorasani, “Failure prognosis and applications–a survey of recent literature,” *IEEE transactions on relaiability*, (in press), 2019.

[10] X. Hu, L. Xu, X. Lin, and M. Pecht, “Battery lifetime prognostics,” *Joule.*, vol. 4, no.2, pp.310–346,2020.

[11] T. Horiba, “Lithium-ion battery systems,” *Proc. IEEE.,* vol. 102, no. 6, pp. 939–950, 2014.

[12] C. Julien, A. Mauger, A. Vijh, and K. Zaghib, “Lithium Batteries: Science and Technology,” Springer, New York, 2015.

[13] C. Liu, Z.G. Neale, and G. Cao, “Understanding electrochemical potentials of cathode materials in rechargeable batteries,” *Materials.Today*., vol. 19, no.2, pp.109-123, 2016.

[14] X. Han, L. Lu, Y. Zheng, X. Feng, Z. Li, J. Li, and M. Ouyang “A review on the key issues of the lithium ion battery degradation among the whole life cycle,” *eTransportation*., vol. 1, Art. no 100005, 2019.

[15] V. Agubra and J. Fergus, "Lithium-ion battery anode aging mechanisms," *Materials*, vol. 6, no. 4, pp. 1310–1325, 2013.

[16] A. Barré, B. Deguilhem, S. Grolleau, M. Gérard, F. Suard, and D. Riu, "A review on lithium-ion battery aging mechanisms and estimations for automotive applications," *J. Power Sources*., vol. 241, pp. 680–689, 2013.

[17] L. Liao and F. Köttig, "A hybrid framework combining data-driven and model-based methods for system remaining useful life prediction," *Appl. Soft Comput*., vol. *44*, pp.191-199, 2016.

[18] X. Hu, S. Li, and H. Peng, "A comparative study of equivalent circuit models for Li-ion batteries," *J. Power Sources.*, vol. 198, pp. 359–367, 2012.

[19] A. Seaman, T.-S. Dao, and J. McPhee, "A survey of mathematics-based equivalent-circuit and electrochemical battery models for hybrid and electric vehicle simulation," *J. Power Sources*., vol. 256, no. 15, pp. 410–423, 2014.

[20] C. Wu, C. B, Zhu, and Y. W. Ge, "A review on fault mechanism and diagnosis approach for Li-Ion batteries," *J. Nanomater.*, vol. 2015, p. 631263, 2015.

[21] A. El Mejdoubi, H. Chaoui, H. Gualous, P. Van Den Bossche, N. Omar, and J. Van Mierlo, "Lithium-ion batteries health prognosis considering aging conditions," *IEEE Trans. Power Electron*., vol. 34, no. 7, pp. 6834–6844, Jul. 2019.

[22] D. Liu, Y. Luo, J. Liu, Y. Peng, L. Guo, and M. Pecht, "Lithium-ion battery remaining useful life estimation based on fusion nonlinear degradation AR model and RPF algorithm," *Neural Comput. Appl*., vol. 25, no. 3-4, pp. 557–572, 2014.

[23] D. An, J. H. Choi, and N. H. Kim, "Prognostics 101: A tutorial for particle filter-based prognostics algorithm using Matlab," *Rel. Eng. Syst. Safety*, vol. 115, no. 1, pp. 161–169, 2013.

[24] M. Jouin, R. Gouriveau, D. Hissel, M. Pera, and N. Zerhouni, "Particle filter-based prognostics: Review, discussion and perspectives," *Mech. Syst. Signal Process*., vols. 72-73, pp. 2–31, 2016.

[25] D. Simon, "Optimal State Estimation: Kalman, Nonlinear Approaches," Wiley Publisher, 2006.

[26] M. Arulampalam, S. Maskell, N. Gordon and T. Clapp, "A tutorial on particle filters for online nonlinear /non-Gaussian Bayesian tracking," *IEEE Trans. Signal Process*., vol. 50, no. 2, pp. 174–188, 2002.

[27] S. Sivaraman and M.M. Trivedi, "A general active-learning framework for on-road vehicle recognition and tracking," *IEEE Trans. Intell. Transp*., vol. 11, no. 2, pp. 267–276, 2010.

[28] S. Sutharsan, T. Kirubarajan, T. Lang, and M. McDonald, "An optimization-based parallel particle filter for multitarget tracking," *IEEE Trans. Aerosp. Electron. Syst*., vol. 48, no. 2, pp. 1601–18, 2012.

[29] W. Xian, B. Long, M. Li, and H. Wang, "Prognostics of lithium-ion batteries based on the Verhulst model, particle swarm optimization and particle filter," *IEEE Trans. Instrum. Meas*., vol. 63, no. 1, pp. 2–17, 2013.

[30] B. Saha, K. Goebel, S. Poll, and J. Christophersen, "An integrated approach to battery health monitoring using Bayesian regression and state estimation," *in Proc IEEE Autotestcon*, pp. 646–653,2007.

[31] B. Saha and K. Goebel, "Modeling Li-ion battery capacity depletion in a particle filtering framework," in Proc. Annu. Conf. Prognost. Health Manage. Soc., San Diego, CA, USA, pp. 1–10, 2009.

[32] E. Walker, S. Rayman, and R. E. White, "Comparison of a particle filter and other state estimation methods for prognostics of lithium-ion batteries," *J. Power Sour*., vol. 287, pp. 1–12, 2015.

[33] Y. Xing, E. W. M. Ma, K.-L. Tsui, and M. Pecht, "An ensemble model for predicting the remaining useful performance of lithium-ion batteries," *Microelectron. Rel., vol. 53*, no. 6, pp. 811–820, 2013.

[34] D. Wang, F. Yang, Y. Zhao, and K.L Tsui, "Battery Remaining Useful Life Prediction at Different Discharge Rates," *Microelectronics Reliability*, vol. 78, pp. 212-219, 2017.

[35] G. Dong, Z. Chen, J. Wei and Q. Ling, "Battery health prognosis using Brownian motion modeling and particle filtering," *IEEE Trans. Ind. Electron*., vol. 65, no. 11, pp. 8645-8655, 2018.

[36] T. Li, S. Sun, T. Sattar, and J. Corchado, "Fight sample degeneracy and impoverishment in particle filters: A review of intelligent approaches," *Expert Syst. Appl*., vol. 41, no. 8, pp. 3944–3954, 2014.

[37] J. Liu, W. Wang, and F. Ma, "A regularized auxiliary particle filtering approach for system state estimation and battery life prediction," *Smart Mater. Struct*., vol. 20, no. 7, pp. 1–9, 2011.

[38] Q. Miao, L. Xie, H. J. Cui, W. Liang, and M. Pecht, "Remaining useful life prediction of lithium-ion battery with unscented particle filter technique," *Microelectron. Rel*., vol. 53, no. 6, pp. 805–810, 2013.

[39] H. Dong, X. Jin, Y. Lou, and C. Wang, "Lithium-ion battery state of health monitoring and remaining useful life prediction based on support vector regression-particle filter," *Power Sources*, vol. 271, pp. 114–123, 2014.

[40] Y. Tian, C. Lu, Z. Wang and L. Tao, "Artificial Fish Swarm Algorithm-Based Particle Filter for Li-Ion Battery Life Prediction," *Mathematical Problems in Engineering*, vol. 2014, pp. 1-10, 2014.

[41] Peng, X., Zhang, C., Yu, Y., and Zhou, Y, "Battery Remaining Useful Life Prediction Algorithm Based on Support Vector Regression and Unscented Particle Filter," IEEE, Prognostics and Health Management (ICPHM), 2016 IEEE International Conference, pp. 1-6, 2016.

[42] D. Wang, F. Yang, K.-L. Tsui, Q. Zhou, and S. J. Bae, "Remaining useful life prediction of lithium-ion batteries based on spherical cubature particle filter," *IEEE Trans. Instrum. Meas*., vol. 65, no. 6, pp. 1282–1291, 2016.

[43] J. Yu, B. Mo, D. Tang, H. Liu and J. Wan, "Remaining Useful Life Prediction for Lithium-Ion Batteries Using a Quantum Particle Swarm Optimization-Based Particle Filter," *Quality Engineering*, vol. 29, no. 3, pp. 536-546, 2017.

[44] Y. Chang and H. Fang, ''A hybrid prognostic method for system degradation based on particle filter and relevance vector machine,'' *Rel. Eng. Syst. Saf*., vol. 186, pp. 51–63, 2019.

[45] T. Sutharssan, D. Montalvao, Y.K Chen, W.C. Wang, C. Pisac, and H. Elemara, "A review on prognostics and health monitoring of proton exchange membrane fuel cell," *Renewable and Sustainable Energy Reviews*, vol. 75, pp.440–450, 2017.

[46] H. Li, D. Pan, and C. Chen, "Intelligent prognostics for battery health monitoring using the mean entropy and relevance vector machine," *IEEE Trans. Syst., Man, Cybern., Syst*., vol. 44, no. 7, pp. 851–862, 2014.

[47] X. S. Si, W. Wang, C. H. Hu, and D. H. Zhou, "Remaining useful life estimation-A review on the statistical data driven approaches," *European Journal of Operational Research*, vol. 213, no. 1, pp. 1–14, 2011.

[48] D. Wang, Q. Miao, and M. Pecht, "Prognostics of lithium-ion batteries based on relevance vectors and a conditional three-parameter capacity degradation model," *J. Power Sources*, vol. 239, pp. 253–264, 2013.

[49] A. Nuhic, T. Terzimehic, T. Soczka-Guth, M. Buchholz, and K. Dietmayer, "Health diagnosis and remaining useful life prognostics of lithium-ion batteries using data-driven methods," *J. Power Sour*., vol. 239, pp. 680–688, 2013.

[50] Y. Zhou, Y. Huang, J. Pang, and K. Wang, "Remaining useful life prediction for supercapacitor based on long short-term memory neural network," *Journal of Power Sources*, vol. 440, Art. no 227149, 2019.

[51] X. Liu, D. Liu, Y. Zhang, Q. Wang, H. Wang, and F. Zhang, "Least squares support vector machine based lithium battery capacity prediction," in Mechatronics and Control (ICMC), International Conference on, pp. 1148–1152, 2014.

[52] D. Yang, X. Zhang, R. Pan, Y. Wang, and Z. Chen, "A novel Gaussian process regression model for state-of-health estimation of lithium-ion battery using charging curve," *J. Power Sources*, vol. 384, pp. 387–395, 2018.

[53] R. R. Richardson, M. A. Osborne, and D. A. Howey, "Gaussian process regression for forecasting battery state of health," *J. Power Sources*, vol. 357, pp. 209–219, 2017.

[54] X. Lu, W. Liu, C. Zhou and M. Huang, "Robust Least-Squares Support Vector Machine With Minimization of Mean and Variance of Modeling Error," *IEEE transactions on neural networks and learning systems*, vol. pp, no. 99, pp.1–12, 2017.

[55] Li Y, Liu K, Foley AM, Zülke A, Berecibar M, Nanini-Maury E, Van Mierlo J, and Hoster HE, "Data-driven health estimation and lifetime prediction of lithium-ion batteries: a review," *Renew Sustain Energy Rev*, vol. 113, Art. no. 109254, 2019.

[56] D. Yang, Y. Wang, R. Pan, R. Chen, and Z. Chen, "A neural network-based state-of-health estimation of lithium-ion battery in electric vehicles," Energy Procedia105, pp.2059-2064. 2017.

[57] A. Eddahech, O. Briat, N. Bertrand, J.-Y. Delé- tage, and J.-M. Vinassa, "Behavior and state-of-health monitoring of Li-ion batteries using impedance spectroscopy and recurrent neural networks," *Int. J. Electr. Power Energy Syst*., vol. 42, pp. 487–494, 2012.

[58] J. Liu, A. Saxena, K. Goebel, B. Saha, and W. Wang, "An adaptive recurrent neural network for remaining useful life prediction of lithium-ion batteries," in Proc. Annu. Conf. Prognostics Health Manag. Soc., pp. 1–9, 2010.

[59] F. Yang, D. Wang, Y. Xing, and K.-L. Tsui, ''Prognostics of Li(NiMnCo)O2-based lithium-ion batteries using a novel battery degradation model,'' *Microelectron. Rel*., vol. 70, pp. 70–78, 2017.

[60] P. Singh, R. Vinjamuri, X.Q. Wang, and D. Reisner, ''Fuzzy logic modeling of EIS measurements on lithium-ion batteries," *Electrochim. Acta*, vol. 51 (8-9), pp. 1673-1679, 2006.

[61] M. Landi and G. Gross, "Measurement techniques for online battery state of health estimation in vehicle-to-grid applications," *IEEE Trans. Instrum. Meas*., vol. 63, no. 5, pp. 1224–1234, 2014.

[62] T. Ming-Fa, P. Yi-Yuan, T. Chung-Shi, and L. Nan-Sin, "Modeling and estimation of state of charge for Lithium-ion batteries using ANFIS architecture," in Industrial Electronics (ISIE), IEEE International Symposium on, Hangzhou, pp. 863-868,2012.

[63] H. Dai, P. Guo, X. Wei, Z. Sun, and J. Wang, "ANFIS (adaptive neuro-fuzzy inference system) based online SOC (State of Charge) correction considering cell divergence for the EV (electric vehicle) traction batteries," *Energy*, vol. 80, pp. 350–360, 2015.

[64] Rahbari, O., Mayet, C., Omar, N., and Van Mierlo, J, "Battery Aging Prediction Using Input-Time-Delayed Based on an Adaptive Neuro-Fuzzy Inference System and a Group Method of Data Handling Techniques,". *Applied Sciences*, vol. 8, no. 8, Art. no 1301, 2018.

[65] C. Fleischer, W. Waag, Z. Bai, and D. U. Sauer, "On-line self-learning time forward voltage prognosis for lithium-ion batteries using adaptive neuro-fuzzy inference system," *J. Power Sources*, vol. 243, pp. 728–749, 2013.

[66] T. Zahid, K. Xu, W. Li, C. Li, H. Li, and P. Singh, "State of charge estimation for electric vehicle power battery using advanced machine learning algorithm under diversified drive cycles,". *Energy*, vol. 162, pp. 871–882, 2018.

[67] J. Liu, W. Wang, F. Ma, Y. Yang, and C. Yang, "A data-model-fusion prognostic framework for dynamic system state forecasting," *Engin. Appl. Artif. Intell.*, vol. 25, pp. 814–823, 2012.

[68] C. Chen, B. Zhang, G. Vachtsevanos, and M. Orchard, "Machine condition prediction based on adaptive neuro–fuzzy and high-order particle filtering," *IEEE Trans. Ind. Electron*., vol. 58, no. 9, pp. 4353–4364, 2011.

[69] I. Skrjanc, J. Iglesias, A. Sanchis, D. Leite, E. Lughofer, and F. Gomide, "Evolving fuzzy and neuro-fuzzy approaches in clustering, regression, identification, and classification: A survey," *Information. Sciences*., vol. 490, pp. 344–368, 2019.

[70] D. Ge, and X. J. Zeng, "A self-evolving fuzzy system which learns dynamic threshold parameter by itself," *IEEE Trans. Fuzzy Syst*., vol. 27, no. 8, pp. 1625–1637, 2019.

[71] Y. Chang, H. Fang and Y. Zhang, "A new hybrid method for the prediction of the remaining useful life of a lithium-ion battery," *Appl. Energy*, vol. 206, pp. 1564-1578, 2017.

[72] Y. Song, C. Yang, T. Wang, D. Liu, and Y. Peng, "Hybrid approach of iterative updating for lithium-ion battery remaining useful life estimation," In Prognostics and System Health Management Conference (PHM-Chengdu), pp. 1-6, 2016.

[73] J. Wei, G. Dong and Z. Chen, "Remaining Useful Life Prediction and State of Health Diagnosis for Lithium-ion Batteries Using Particle Filter and Support Vector Regression," *IEEE Transactions on Industrial Electronics*, vol. PP, No.99, pp. 1-1, 2017.

[74] Y. Ma, Y. Chen, X. Zhou, and H. Chen, ''Remaining useful life prediction of lithium-ion battery based on gauss-hermite particle filter,'' *IEEE Trans. Control Syst. Technol*., vol. 27, no. 4, pp. 1788-1795, 2019.

[75] N. J. Gordon, D. J. Salmond, and A. F. Smith, "Novel approach to nonlinear/non-Gaussian Bayesian state estimation," *Proc. Inst. Elect. Eng. Radar Signal Process*., vol. 140, no. 2, pp. 107–113, 1993.

[76] R. Van Der Merwe, A. Doucet, N. De Freitas and E. Wan, "The unscented particle filters," *Advances in Neural Information Processing Systems*, pp. 584-590, 2001.

[77] C. Musso, N. Oudjane, and F. LeGland, "Improving Regularized Particle Filters," New York, NY, USA: Springer-Verlag, 2001.

[78] A. Murangira, C. Musso, and K. Dahia, "A mixture regularized raoblackwellized particle filter for terrain positioning," *IEEE Trans. Aerosp. Eletron. Syst*., vol. 52, no. 4, pp. 1967–1985, 2016.

[79] S. Yin and X. Zhu, "Intelligent particle filter and its application on fault detection of nonlinear system," *IEEE Trans. Ind. Electron*., vol. 62, no. 6, pp. 3852–3861, 2015.

[80] K. Deep and M. Thakur, "A new crossover operator for real-coded genetic algorithm," *Appl. Math. Comput*., vol. 188, no. 1, pp. 895–911, 2007.

[81] L. Martino, V. Elvira, and F. Louzada, "Effective sample size for importance sampling based on the discrepancy measures," *Signal Process*., vol. 131, pp. 386–401, 2017.

[82] C.P. Robert, G. Casella, "Introducing Monte Carlo Methods with R," Springer, New York, 2010.

[83] M.-H. Chen, Q.-M. Shao, and J.G. Ibrahim, "Monte Carlo Methods in Bayesian Computation," Springer Science & Business Media, 2012.

[84] L. Devroye and G. Lugosi, “Combinatorial Methods in Density Estimation,” New York: Springer-Verlag, 2001.

[85] Liu H., Shah S., Jiang W., “On-line outlier detection and data cleaning,” *Computers and Chemical Engineering*, vol. 28, pp.1635–1647, 2004.

[86] R. Domingues, M. Filippone, P. Michiardi, and J. Zouaoui, “A comparative evaluation of outlier detection algorithms: Experiments and analyses,” *Pattern Recognit*., vol. 74, pp. 406–421,2018.

[87] P. J. Rousseeuw and M. Hubert, “Robust statistics for outlier detection,” *Wiley Interdisc. Rew: Data Mining and Knowledge Discovery*, vol. 1, no. 1, pp. 73–79, 2011.

[88] L. Li, P. Wang, K.-H. Chao, Y. Zhou, and Y. Xie, “Remaining useful life prediction for lithium-ion batteries based on Gaussian processes mixture,” *PLoS ONE.*, vol. 11, no. 9, Art. no. e0163004, 2016.

[89] B. Saha and K. Goebel. (2007). Battery Data Set NASA Ames Prognostics Data Repository, NASA Ames, CA, USA [Online]: https://ti.arc.nasa.gov/tech/dash/groups/pcoe/prognostic-data-repository/

[90] NASA Prognostics Center of Excellence, Battery Prognostics, Laboratory Setup [Online]. Available: https://ti.arc.nasa.gov/tech/dash/groups/pcoe/battery-prognostics/lab-setup/.

[91] B. Saha, K. Goebel, S. Poll, and J. Christophersen, “Prognostics methods for battery health monitoring using a Bayesian framework,” *IEEE Trans. Instrum. Meas*., vol. 58, no. 2, pp. 291–296, 2009.

[92] K. Goebel, B. Saha, A. Saxena, J. R. Celaya, and P. Christophersen, “Prognostics in battery health management,” *IEEE Instrum. Meas. Mag*., vol. 11, no. 4, pp. 33–40, 2008.

[93] H. Zhang, Q. Miao, X. Zhang, and Z. Liu, ‘‘An improved unscented particle filter approach for lithium-ion battery remaining useful life prediction,’’ *Microelectron. Reliab.*, vol. 81, pp. 288-298, 2018.

[94] S. M. Chen and C. D. Chen, “TAIEX forecasting based on fuzzy time series and fuzzy variation groups,” *IEEE Trans. Fuzzy Syst*., vol. 19, no. 1, pp. 1-12, 2011.

[95] S. H. Cheng, S. M. Chen, and W. S. Jian, “Fuzzy time series forecasting based on fuzzy logical relationships and similarity measures,” *Inf. Sci*., vol. 327, pp. 272-287, 2016.

[96] X. Qing and Y. Niu, “Hourly day-ahead solar irradiance prediction using weather forecasts by LSTM,” Energy, vol. 148, pp. 461–468, Apr. 2018.

[97] N. Safari, C. Y. Chung, and G. C. D. Price, “Novel multi-step short-term wind power prediction framework based on chaotic time series analysis and singular spectrum analysis,” *IEEE Trans. Power Syst*., vol. 33, no. 1, pp. 590–601, 2018.

[98] A. Soualhi, K. Medjaher, G. Celrc, and H. Razik, “Prediction of bearing failures by the analysis of the time series,” *Mech. Syst. Signal Process*., vols. 139, Art.no.106607, 2020.

[99] L. Yang, Y. Cai, Y. Yang, and Z. Deng, “Supervisory long-term prediction of state of available power for lithium-ion batteries in electric vehicles,” *Appl Energy*., vol. 257, Art. no. 114006, 2020.

[100] R. Liu, B. Yang, and A. G. Hauptmann, "Simultaneous bearing fault recognition and remaining useful life prediction using joint-loss convolutional neural network," *IEEE Trans. Ind. Inform*., vol. 16, no. 1, pp. 87–96, 2020.
[101] L. Chao and W. Haiyue, "Fuzzy forecasting for long-term time series based on time-variant fuzzy information granules," *Appl. Soft Comput*., vol. 88, Art.no.106046, 2020.
[102] D. Li, W. Wang, and F. Ismail, "Fuzzy neural network technique for system state forecasting," *IEEE Trans. Cybern*., vol. 43, no. 5, pp. 1484–1494, 2013.
[103] K. T. Chau, K. C. Wu, and C. C. Chan, "A new battery capacity indicator for lithium-ion battery powered electric vehicles using adaptive neuro-fuzzy inference system," *Energy Convers. Manage*., vol. 45, no. 11/12, pp. 1681-1692, 2004.
[104] D. Ge, and X. J. Zeng, "Learning data streams online- an evolving fuzzy system approach with self-learning/adaptive thresholds," *Information. Sciences*., vol. 507, pp. 172–184, 2020.
[105] P. Angelov and R. Buswell, "Identification of evolving rule-based models," *IEEE Trans. Fuzzy Syst*., vol. 10, no. 5, pp. 667–677, 2002.
[106] P. Angelov, and D. P. Filev, "An Approach to Online Identification of Takagi-Sugeno Fuzzy Models," *IEEE Trans. Syst. Man Cybern. B*., vol. 34, no. 1, pp. 484–498, 2004.
[107] P. Angelov, "Fuzzily connected multimodel systems evolving autonomously from data streams," *IEEE Trans. Syst. Man Cybern. B*., vol. 41, no. 4, pp. 898–910, 2011.
[108] N.K. Kasabov and Q. Song, "DENFIS: dynamic evolving neural-fuzzy inference system and its application for time-series prediction," *IEEE Trans. Fuzzy Syst*., vol. 10, no. 2, pp. 144–154, 2002.
[109] E.D. Lughofer, "FLEXFIS: A robust incremental learning approach for evolving Takagi–Sugeno fuzzy models," *IEEE Trans. Fuzzy Syst*., vol. 16, no. 6, pp. 1393–1410, 2008.
[110] W. Wang, and J. Vrbanek, "An evolving fuzzy predictor for industrial applications," *IEEE Trans. Fuzzy Syst*., vol. 16, no. 6, pp. 1439–1449, 2008.
[111] D. Li, W. Wang, and F. Ismail, "An evolving fuzzy neural predictor for multi-dimensional system state forecasting," *Neurocomputing*, vol. 145, pp. 381-391, 2014.
[112] E. Lughofer, C. Cernuda, S. Kindermann, and M. Pratama, "Generalized smart evolving fuzzy systems," *Evolving. Syst*, vol. 6, no. 4, pp.269–292, 2015.
[113] L. Maciel, R. Ballini, and F. Gomide, "An evolving possibilistic fuzzy modeling approach for value-at-risk estimation," *Appl. Soft Comput*., vol. 60, pp. 820–830, 2017.
[114] E. Lughofer, and M. Pratama, "Online active learning in data stream regression using uncertainty sampling based on evolving generalized fuzzy models," *IEEE Trans. Fuzzy Syst*., vol. 26, no. 1, pp.292–309, 2018.
[115] N.N. Nguyen, W.J. Zhou, and C. Quek, "GSETSK: a generic self-evolving tsk fuzzy neural network with a novel Hebbian-based rule reduction approach," *Appl. Soft Comput*., vol. 35, pp. 29–42, 2015.
[116] R. Dutta Baruah and P. Angelov, "Evolving fuzzy systems for data streams: A survey," in Wiley Interdisciplinary Reviews: Data Mining and Knowledge Discovery, Wiley, New York, USA, vol. 1, pp.461–476, 2011.

[117] P. Angelov, “Evolving Fuzzy Systems,” in Computational Complexity, R. A. Meyers, Ed. Springer New York, pp. 1053–1065, 2012.
[118] W. Wang, D. Z. Li, and J. Vrbanek, “An evolving neuro-fuzzy technique for system state forecasting,” *Neurocomputing*, vol. 87, pp. 111–119, 2012.
[119] D. An, N. H. Kim, and J.-H. Choi, “Practical options for selecting data-driven or physics-based prognostics algorithms with reviews,” *Rel. Eng. Syst. Safety*., vol. 133, pp. 223–236, 2015.
[120] I. Eyoh, R. John, G. D. Maere, and E. Kayacan, “Hybrid learning for interval type-2 intuitionistic fuzzy logic systems as applied to identification and prediction problems,” *IEEE Transactions on Fuzzy Systems*, vol. 26, no. 5, pp. 2672–2685, 2018.
[121] J. Sun, H. Zuo, W. Wang, and M. Pecht, “Prognostics uncertainty reduction by fusing on-line monitoring data based on a state-space-based degradation,” *Mech. Syst. Signal Process*., vol. 45, no. 2m, pp. 396–407, 2014.
[122] S. Sankararaman, “Significance, interpretation, and quantification of uncertainty in prognostics and remaining useful life prediction,” *Mech. Syst.Signal Process*., vol. 52–53, pp. 228–247, 2015.
[123] P. Baraldi, F. Mangili, and E. Zio, “Investigation of uncertainty treatment capability of model-based and data-driven prognostic methods using simulated data,” *Rel. Eng. Syst. Safety*, vol. 112, no. 1, pp. 94–108, 2013.
[124] X. Wang, H. Hu, and A. Zhang, “Concentration measurement of three-phase flow based on multi-sensor data fusion using adaptive fuzzy inference system,” *Flow Meas. Instrum*., vol. 39, pp. 1–8, 2014.